



CIVIL ENGINEERING STUDIES
Illinois Center for Transportation Series No. 09-053
UIIU-ENG-2009-2034
ISSN: 0197-9191

PERFORMANCE OF CONCRETE PAVEMENTS WITH OPTIMIZED SLAB GEOMETRY

Prepared By
Victor Cervantes
Jeffery Roesler
University of Illinois at Urbana-Champaign

Research Report ICT-09-053

August 2009

Technical Report Documentation Page

1. Report No. ICT-09-053	2. Government Accession No.	3. Recipient's Catalog No.	
4. Title and Subtitle PERFORMANCE OF CONCRETE PAVEMENTS WITH OPTIMIZED SLAB GEOMETRY		5. Report Date August 2009	
		6. Performing Organization Code	
		8. Performing Organization Report No. ICT-09-053 UILU-ENG-2009-2034	
7. Author(s) Victor Cervantes and Jeffery Roesler		10. Work Unit (TRAIS)	
9. Performing Organization Name and Address University of Illinois at Urbana-Champaign Department of Civil and Environmental Engineering 205 North Matthews Ave. Urbana, IL 61801		11. Contract or Grant No.	
		13. Type of Report and Period Covered Final Report May 2007 to August 2009	
		14. Sponsoring Agency Code	
12. Sponsoring Agency Name and Address Comercial TCPavements Ltda. Teatians 500 Santiago, Chile		15. Supplementary Notes	
16. Abstract The typical slab dimensions for a concrete pavement are 12 ft wide by 15ft long with slab thicknesses ranging from 6 to 14 inches depending on the level of traffic. The required thickness is primarily dependent on the axle weight and number of load repetitions, concrete strength, slab length, and curling stresses. A new methodology for designing concrete pavements has recently been proposed to optimize the slab dimensions, e.g., 6 ft by 6 ft panel sizes, which concurrently decreases the load and curling induced tensile stresses in the slab. This concomitant reduction in stresses enables a thinner concrete slab and subsequently the economical viability of concrete pavements is improved. It has also been proposed that these pavement systems don't need any man-made load transfer devices across the transverse contraction joints. This new way of designing concrete pavements has been referred to as "Thin Concrete Pavements (TCP)" or concrete slabs with optimized geometry. Full-scale test sections of this new concrete pavement system have been constructed and tested under accelerated pavement loading conditions. The design and concrete material factors that have been subjected to repeated loading in this research are the following: concrete thickness of 4, 6, and 8 inches; aggregate base or asphalt concrete base; plain concrete or fiber reinforced concrete; and edge versus wheel path loading. The accelerated pavement testing showed that these thinner concrete slabs with reduced slab sizes could sustain a significant number of ESALs before cracking. The 8 inch concrete slabs on granular base did not experience fatigue cracking until 51 million ESALs. The 6 inch concrete slabs on granular began cracking on average at 12 million ESALs. The concrete slabs on asphalt base resisted a significant larger number of ESALs than the same concrete thickness on granular base. The cracking performance of the 3.5 inch concrete slabs varied with the stiffness of the soil. In all cases for the 3.5 inch slab thickness, structural fibers provided a longer fatigue life, extended service life, and high load transfer efficiency across the transverse joint relative to the plain concrete slabs. Trafficking tests indicated that the fibers may also be able to serve as a replacement for the lateral restraint pins. Finally, the shorter slabs sizes maintained a medium to high load transfer efficiency over the accelerated loading period for all slab thicknesses. Measurements indicated these slab systems have higher deflections as expected and therefore the aggregate base layer and subgrade must be designed and specified to reduce the rate of permanent deformation and minimize the possibility of pumping and erosion. Premature concrete slab cracking may result if improper base material and thickness is not utilized, a geotextile separation layer is not used between the base and subgrade, and inadequate drainage of the slab system is not provided.			
17. Key Words Concrete Pavement, slab thickness, accelerated pavement testing, fibers, fatigue, optimized joints		18. Distribution Statement No restrictions. This document is available to the public through the National Technical Information Service, Springfield, Virginia 22161.	
19. Security Classif. (of this report) Unclassified	20. Security Classif. (of this page) Unclassified	21. No. of Pages	22. Price

EXECUTIVE SUMMARY

The typical slab dimensions for a concrete pavement are 12 ft wide by 15ft long with slab thicknesses ranging from 6 to 14 inches depending on the level of traffic. The required thickness is primarily dependent on the axle weight and number of load repetitions, concrete strength, slab length, and curling stresses. A new methodology for designing concrete pavements has recently been proposed to optimize the slab dimensions, e.g., 6 ft by 6 ft panel sizes, which concurrently decreases the load and curling induced tensile stresses in the slab. This concomitant reduction in stresses enables a thinner concrete slab and subsequently the economical viability of concrete pavements is improved. It has also been proposed that these pavement systems don't need any man-made load transfer devices across the transverse contraction joints. This new way of designing concrete pavements has been referred to as "Thin Concrete Pavements (TCP)" or concrete slabs with optimized geometry.

Full-scale test sections of this new concrete pavement system have been constructed and tested under accelerated pavement loading conditions. The design and concrete material factors that have been subjected to repeated loading in this research are the following: concrete thickness of 4, 6, and 8 inches; aggregate base or asphalt concrete base; plain concrete or fiber reinforced concrete; and edge versus wheel path loading. The accelerated pavement testing showed that these thinner concrete slabs with reduced slab sizes could sustain a significant number of ESALs before cracking. The 8 inch concrete slabs on granular base did not experience fatigue cracking until 51 million ESALs. The 6 inch concrete slabs on granular began cracking on average at 12 million ESALs. The concrete slabs on asphalt base resisted a significant larger number of ESALs than the same concrete thickness on granular base. The cracking performance of the 3.5 inch concrete slabs varied with the stiffness of the soil. In all cases for the 3.5 inch slab thickness, structural fibers provided a longer fatigue life, extended service life, and high load transfer efficiency across the transverse joint relative to the plain concrete slabs. Trafficking tests indicated that the fibers may also be able to serve as a replacement for the lateral restraint pins. Finally, the shorter slabs sizes maintained a medium to high load transfer efficiency over the accelerated loading period for all slab thicknesses.

Measurements indicated these slab systems have higher deflections as expected and therefore the aggregate base layer and subgrade must be designed and specified to reduce the rate of permanent deformation and minimize the possibility of pumping and erosion. Premature concrete slab cracking may result if improper base material and thickness is not utilized, a geotextile separation layer is not used between the base and subgrade, and inadequate drainage of the slab system is not provided.

ACKNOWLEDGEMENTS

The authors would like to acknowledge TCPavements Ltda for their financial support of this research. TCPavements is patented in Chile (44820-2009), the United States (7,571,581), and with the World Organization of Intellectual Property (PCT/EP2006/064732). A special thanks to the following companies for participating in the project: A&R Services Inc. for providing general contracting services during construction, Prairie Materials for the ready-mixed concrete, W.R. Grace for the synthetic macrofibers, ARA, Inc for FWD tests, and Geocon Engineering, Inc. for the geotechnical tests. The contents of this report reflect the view of the authors, who are responsible for the facts and accuracy of the data presented herein.

TABLE OF CONTENTS

LIST OF TABLES.....	vii
LIST OF FIGURES.....	viii
CHAPTER 1. INTRODUCTION	1
1.1 DESIGN CONCEPT OF SLAB WITH OPTIMIZED GEOMETRY	2
1.2 RESEARCH OBJECTIVES	3
CHAPTER 2. DESIGN AND CONSTRUCTION OF FULL-SCALE PAVEMENT	
TEST SECTIONS.....	4
2.1 TEST SECTIONS.....	4
2.2 SITE PLAN AND LAYOUT	6
2.3 MATERIALS.....	7
2.4 GEOTECHNICAL REPORT	9
2.5 THEORETICAL STRESS ANALYSIS	10
2.6 INSTRUMENTATION AND MONITORING.....	10
2.7 CONSTRUCTION	11
CHAPTER 3. PRE-TRAFFIC MONITORING.....	15
3.1 JOINT CRACK DEVELOPMENT	15
3.2 FALLING WEIGHT DEFLECTOMETER	16
CHAPTER 4. ACCELERATED PAVEMENT TESTING RESULTS.....	19
4.1 ACCELERATED TRANSPORTATION LOADING ASSEMBLY (ATLAS).....	19
4.2 IDEALIZED ATLAS TESTING PLAN.....	19
4.3 LOAD AND REPETITION MAGNIFICATION FACTOR.....	20
4.4 SECTION 1 LOADING.....	22
4.4.1 CRACK DEVELOPMENT SECTION 1- SOUTH	22
4.4.2 CRACK DEVELOPMENT SECTION 1 - NORTH	26
4.4.3 VERTICAL LVDTs – SECTION 1 SOUTH	32
4.4.4 VERTICAL LVDTs – SECTION 1 NORTH.....	34
4.4.5 STRAINS – SECTION 1 SOUTH.....	36
4.4.6 STRAINS – SECTION 1 NORTH.....	37
4.5 SECTION 2 LOADING.....	39
4.5.1 CRACK DEVELOPMENT SECTION 2 – SOUTH.....	39
4.5.2 CRACK DEVELOPMENT SECTION 2 – NORTH	42
4.5.3 VERTICAL DEFLECTIONS – SECTION 2 SOUTH.....	46
4.5.4 VERTICAL DEFLECTIONS – SECTION 2 NORTH	48
4.5.5 TENSILE STRAINS – SECTION 2 SOUTH.....	50
4.5.6 TENSILE STRAINS – SECTION 2 NORTH.....	51
4.6 SECTION 3 LOADING.....	52
4.6.1 CRACK DEVELOPMENT SECTION 3 – SOUTH.....	52
4.6.2 CRACK DEVELOPMENT SECTION 3 – NORTH	55
4.6.3 VERTICAL DEFLECTIONS – SECTION 3 SOUTH.....	61
4.6.4 VERTICAL DEFLECTIONS – SECTION 3 NORTH	63
4.6.5 TENSILE STRAINS – SECTION 3 SOUTH.....	65
4.6.6 TENSILE STRAINS – SECTION 3 NORTH.....	66
4.7 JOINT PERFORMANCE AND LOAD TRANSFER EFFICIENCY	67
CHAPTER 5. SIGNIFICANCE OF THE CONCRETE SLAB TESTING RESULTS.....	73
5.1 APPLICATION TO PAVEMENTS WITH SIGNIFICANT OVERLOADING.....	73
5.2 EFFECTS OF SUPPORT LAYER STIFFNESS	73
5.3 EFFECTS OF STRUCTURAL FIBERS ON FATIGUE CRACKING AND SERVICEABILITY	75

5.4 THICKNESS AND SIZE EFFECT ON CONCRETE SLAB FATIGUE LIFE	76
5.5 TEMPERATURE CURLING EFFECTS	76
5.6 LATERAL RESTRAINT PINS	77
CHAPTER 6. CONCLUSIONS	79
REFERENCES	81
APPENDIX A	A-1
A.1 INSTRUMENTATION LAYOUT	A-1
A.2 GEOTECHNICAL REPORT	A-4
A.3 DCP ANALYSIS	A-6
A.4 MAXIMUM THEORETICAL STRAINS	A-12
A.5 TABLES FOR MAGNIFICATION FACTORS	A-14

LIST OF TABLES

Table 1. Slab thickness for a given stress level (after Covarrubias 2008)	2
Table 2. Concrete Mixture Design.....	8
Table 3. Percentage of cracked joints	15
Table 4. Modulus of subgrade reaction (k) values for each section backcalculated from edge loading (except for 3.5 in. over granular – north) and magnification factor	20
Table 5. Load repetitions and cracking summary for Section 1- South (Edge Loading)	26
Table 6. Load repetitions and cracking summary for Section 1 north	31
Table 7. Load repetitions and cracking summary for Section 2 south (6 in.)	41
Table 8. Load repetitions and cracking summary for Section 2 south (8 in.)	42
Table 9. Load repetitions and cracking summary for Section 2 north (6 in.).....	45
Table 10. Load repetitions and cracking summary for Section 2 north (8 in.).....	46
Table 11. Load repetitions and cracking summary for Section 3 south (January 2008).....	55
Table 12. Load repetitions and cracking summary for Section 3 south (April 2008).....	55
Table 13. Wheel path loading and cracking for Section 3 north.....	60

LIST OF FIGURES

Figure 1. ATREL accelerated pavement testing sections (Google Maps)	2
Figure 2. Test Sections for Accelerated Pavement Testing of Thin Concrete Pavement.....	5
Figure 3. Thin Concrete Pavement Cross Section.....	5
Figure 4. Topographic map of test section.....	6
Figure 5. Profile of project site. Test section begins at station 36 (ft).....	7
Figure 6. Mass loss data for TCP	8
Figure 7. Shrinkage data for TCP	9
Figure 8. Schematic of dynamic strain gauge placement.....	10
Figure 9. Strain gauge on steel chair prior to paving.....	11
Figure 10. Milled asphalt concrete	11
Figure 11. Granular base over geotextile.....	12
Figure 12. Compaction of granular base	12
Figure 13. Instrumentation installation	12
Figure 14. Casting day	13
Figure 15. Saw-cutting	13
Figure 16. Manual saw cutting of edges	13
Figure 17. Lateral restraint pins	14
Figure 18. Plot of first observation of crack at a specific joint	15
Figure 19. FWD used for center slab deflections and joint load transfer efficiency.....	16
Figure 20. Center slab 9-kips normalized deflections (mils=0.001 inch).....	16
Figure 21. Load transfer efficiency of transverse contraction joints	17
Figure 22. 9-kip deflection at a given joint location	18
Figure 23. Accelerated Transportation Loading Assembly (ATLAS) device	19
Figure 24. Lateral offset magnification factor for the various concrete test sections.....	22
Figure 25. Section 1 south cracking performance after 5/9/09 testing (7.2 Million ESALs).....	23
Figure 26. Section 1 south cracking performance after 5/11/09 testing (12.7 Million ESALs).....	24
Figure 27. Section 1 south cracking performance after 5/12/09 testing (37.1 Million ESALs).....	24
Figure 28. Section 1 south cracking performance after 5/14/09 testing (44 Million ESALs).....	25
Figure 29. Section 1 south cracking performance after 5/15/09 testing (57.5 Million ESALs).....	25
Figure 30. Section 1 north cracking performance after 4/20/09 testing (2 Million ESALs).....	27
Figure 31. Section 1 north cracking performance after 4/21/09 testing (2.2 Million ESALs).....	28
Figure 32. Section 1 north cracking performance after 4/22/09 testing (6.3 Million ESALs).....	28
Figure 33. Section 1 north cracking performance after 4/23/09 testing (13.2 Million ESALs).....	29
Figure 34. Section 1 north cracking performance after 4/24/09 testing (21.6 Million ESALs).....	29
Figure 35. Section 1 north cracking performance after 4/25/09 testing (30.6 Million ESALs).....	30

Figure 36. Section 1 north cracking performance after 4/26/09 testing (51.6 Million ESALs).....	30
Figure 37. Section 1 north cracking performance after 4/27/09 testing (69.3 Million ESALs).....	31
Figure 38. Description of LVDT nomenclature	33
Figure 39. Rebound deflections of 4 in. concrete slab over 6.5 in. asphalt concrete (Section 1-south).....	33
Figure 40. Rebound deflections of 6 in. concrete slab over 4.5 in. asphalt concrete (Section 1-south).....	34
Figure 41. Wheel path rebound deflection of 4 in. concrete slab over 6.5 in. asphalt concrete (Section 1-noth)	35
Figure 42. Wheel path rebound deflection of 6 in. concrete slab over 4.5 in. asphalt concrete (Section 1-north).....	35
Figure 43. Rebound deflections of 4 in. concrete slab over 6.5 in. asphalt concrete (Section 1-north).....	36
Figure 44. Rebound deflections of 6 in. concrete slab over 4.5 in. asphalt concrete (Section 1-north)	36
Figure 45. Tensile strain responses for 4 in. and 6 in. concrete over asphalt concrete (Section 1-north).....	37
Figure 46. Wheel path tensile strains responses for 4 in. and 6 in. concrete slabs over asphalt concrete (Section 1-north).....	38
Figure 47. Edge loading responses for 4 in. and 6 in. concrete slabs over asphalt concrete (Section 1-north).....	38
Figure 48. Section 2 south cracking performance after 5/5/08 testing (6 inch=16.4 Million ESALs; 8 inch=14 Million ESALs).....	39
Figure 49. Section 2 south cracking performance after 5/9/08 testing (6 inch=20.2 Million ESALs; 8 inch=17.2 Million ESALs).....	40
Figure 50. Section 2 south cracking performance after 5/10/08 testing (6 inch=22.5 Million ESALs; 8 inch=19.2 Million ESALs)	40
Figure 51. Section 2 south cracking performance after 5/12/08 testing (6 inch=22.9 Million ESALs; 8 inch=19.5 Million ESALs)	41
Figure 52. Section 2 north cracking performance after 3/30/09 testing (6 inch = 834,000 ESALs; 8 inch=730,000 ESALs)	43
Figure 53. Section 2 north cracking performance after 4/6/09 testing (6 inch = 9.7 Million ESALs; 8 inch=8.5 Million ESALs).....	43
Figure 54. Section 2 north cracking performance after 4/10/09 testing (6 inch = 16.4 Million ESALs; 8 inch=14.3 Million ESALs).....	44
Figure 55. Rebound deflections of 6 in. concrete slab over granular base (Section 2-south).....	47
Figure 56. Rebound deflections of 8 in. concrete slab over granular base (Section 2-south).....	47
Figure 57. Water pump used to drain Section 2 North.....	48
Figure 58. Wheel path rebound deflection of 6 in. concrete slab over granular base (Section 2-north).....	48
Figure 59. Wheel path rebound deflection of 8 in. concrete slab over granular base (Section 2-north).....	49
Figure 60. Rebound deflections of 6 in. concrete slab over granular base (Section 2-north).....	49
Figure 61. Rebound deflections of 8 in. concrete slab over granular base (Section 2-north).....	50

Figure 62. Maximum tensile strain responses for 6 and 8 in over granular base– (Section 2 – south)	51
Figure 63. Tensile strains in 6 and 8 inch concrete slab over granular base for wheel path loading	51
Figure 64. Tensile strains in 6 and 8 inch concrete slab over granular base for edge loading.....	52
Figure 65. Section 3 south cracking performance after 4/19/08 testing (192,000 ESALs).....	53
Figure 66. Section 3 south cracking performance after 4/21/08 testing (233,000 ESALs).....	54
Figure 67. Section 3 south final cracking performance after 234,000 ESALs.....	54
Figure 68. Wheel path testing of Section 3 north (2,960 ESALs).....	56
Figure 69. Wheel path testing Section 3 north FRC 3/9/09 (3,103 ESALs)	57
Figure 70. Wheel path testing Section 3 north 3/10/09 (4,545 ESALs).....	57
Figure 71. Longitudinal joint loading cracking pattern 3/14/09 (4,700 ESALs).....	58
Figure 72. Cracking pattern for longitudinal joint trafficking on 3/15/09 (48,000 ESALs).....	58
Figure 73. Cracking pattern for longitudinal joint trafficking on 3/16/09 (58,000 ESALs).....	59
Figure 74. Cracking pattern for longitudinal joint trafficking on 3/19/09 (64,000 ESALs).....	59
Figure 75. Rebound deflection of 3.5 in. plain concrete slab over a granular base during January 2008 (Section 3-south).....	61
Figure 76. Rebound deflection of 3.5 in. FRC slab over a granular base during January 2008 (Section 3-south).....	62
Figure 77. Rebound deflection of 3.5 in. plain concrete slab over a granular base (Section 3-south).....	62
Figure 78. Rebound deflection of 3.5 in. FRC slab over a granular base (Section 3-south).....	63
Figure 79. Wheel path rebound deflection of 3.5 in. plain concrete slab over a granular base (Section 3-south).....	64
Figure 80. Wheel path rebound deflection of 3.5 in. FRC slab over a granular base (Section 3-south).....	64
Figure 81. Maximum tensile strain responses for 3.5 in. plain over a granular base during Winter 2008 (Section 3 – south).....	65
Figure 82. Maximum tensile strain responses for 3.5 in. FRC over a granular base during Winter 2008 (Section 3 – south).....	66
Figure 83. Maximum tensile strain responses for 3.5 in. plain and FRC over a granular base (Section 3 – south).....	66
Figure 84. Wheel path maximum tensile strain responses for 3.5 in. plain and FRC over a granular base (Section 3 – north)	67
Figure 85. Deflection load transfer efficiency for edge loading (Section 1 – south)	68
Figure 86. Deflection load transfer efficiency measured at free edge for wheel path loading (Section 1 – North)	68
Figure 87. Deflection load transfer efficiency at free edge (Section 1 – North).....	69
Figure 88. Deflection load transfer efficiency for edge loading (Section 2 – south)	70
Figure 89. Deflection load transfer efficiency measured at free edge for wheel path loading (Section 2 – north).....	70
Figure 90. Deflection load transfer efficiency at free edge loading (Section 2 – north).....	71
Figure 91. Deflection load transfer efficiency for edge loading (Section 3 – south)	72

Figure 92. Deflection load transfer efficiency measured at free edge for wheel path loading (Section 3 – north)	72
Figure 93. Fatigue cracking of 4 in. concrete slab over asphalt base on section 1 north at 20 million ESALs	74
Figure 94. Fatigue cracking of 4 in. concrete slab over asphalt base on section 1 south at 56 million ESALs	75
Figure 95. Slab temperature curling for 8 in. over granular base without loading	76
Figure 96. Effect of temperature change on vertical deflections (Section 2 – south)	77
Figure 97. Longitudinal joint opening on 3.5 inch plain concrete section	78
Figure 98. Longitudinal joint on 3.5 inch FRC section	78

CHAPTER 1 INTRODUCTION

The AASHO Road Test was one of the most influential full-scale pavement test sections ever built. One objective of the Road Test was to develop a relationship between the thickness of rigid pavements and the number of axle load repetitions of varying magnitudes and arrangements (Huang 2004). The main findings of the AASHTO road test were the concept of pavement serviceability and the equations that relate serviceability, load level, and thickness design of rigid pavements. Typical concrete pavements today are designed to have a thickness of approximately 6 to 8 inches for low volume roads and 9 to 14 inches for high volume roads based on the original findings at the AASHO Road Test.

One large factor which has been linked to the favorable performance of concrete pavements is the slab geometry. Currently, jointed plain concrete pavements (JPCP) are the most common rigid pavement type designed and constructed. JPCP are built with contraction joints spaced between 12 and 30 feet depending on many geometric, climatic, and material factors. CRCP were originally design to provide short panel sizes which promoted a much smoother ride. Based on JPCP performance surveys, researchers over the years have settled on approximately 12 to 20 ft as a maximum slab size depending the local materials, base type, and environmental conditions. Many other researchers have shown that longer joint spacing creates premature cracking or other distresses on concrete pavements. Larger slab sizes increase the susceptibility of the pavement system to temperature and moisture curling and excessive joint openings due to normal environmental changes.

In an effort to improve the cost-benefit of rigid pavements, a design concept was proposed that would limit the slab size to minimize the magnitude of curling and still provide the required fatigue life for a given slab thickness. Previous research on ultra-thin whitetopping has shown smaller slab sizes 6'x6' or 4'x4' improve the performance of this concrete rehabilitation option (ACPA 1998; Vandenbossche and Fagerness 2002; Vandenbossche 2003).

In the proposed research, this new concept has been termed Thin Concrete Pavements (TCP or TCPavements) after the name of the company holding the patent on the idea. The most significant variables which will affect the cracking and joint performance of TCP are the concrete slab thickness, panel size, concrete material constituents, and slab support conditions. In order to quantify the performance of TCP, full-scale testing was conducted at the University of Illinois' Advanced Transportation Research and Engineering Laboratory (ATREL) in Rantoul, Illinois.



Figure 1. ATREL accelerated pavement testing sections (Google Maps).

1.1 DESIGN CONCEPT OF SLAB WITH OPTIMIZED GEOMETRY

The general concept of thin concrete pavements is that by reducing tensile stresses in the pavement, a reduction in required slab thickness can be realized. A concrete slab's tensile stresses are a function of the environmental and load conditions. These tensile stresses will be reduced by modifying the slab size from the more common 12 feet by 15 feet to approximately 6 feet by 6 feet slabs. In the current rigid pavement design, the critical tensile stresses can be at the mid-slab edge for a single axle load or at the top of the slab for a steer-drive axle combination sitting on a single slab. Both cases are exasperated with day or night time temperature curling conditions, respectively. With the smaller slab sizes proposed by the TCP design, then only one wheel load is on a slab at any given time.

An example of the TCP design concept is demonstrated next from a recent paper by Covarrubias and Covarrubias (2008). The critical tensile stresses on the top of a slab for a steer-drive axle combination with typical slab dimensions (approximately 12 feet x 15 feet x 10 inches) are calculated first as seen in

Table 1. The slab geometry (slab size and thickness) are then changed to achieve the same tensile stress as seen in

Table 1. By reducing the slab size, the load and curling stresses decrease and thus the required slab thickness for a given tensile stress level is significantly smaller.

Table 1. Slab Thickness for a Given Stress Level (after Covarrubias 2008)

Max Top Stress (psi)	Slab Dimensions		
	Length (ft)	Width (ft)	Thickness (in)
356	14.8	11.8	9.8
350	8.2	5.9	5.5
357	5.9	5.9	6.3
353	4.6	5.9	5.1

With a reduced slab size and thickness, the pavement deflections increase significantly and thus the potential for pumping, erosion, and permanent deformation of

the support layers become more paramount to address. This is similar to the dilemma faced by the PCA method for rigid pavement design which demonstrated that a certain slab thickness could provide an infinite fatigue life but the erosion or pumping could be the controlling factor (Packard 1984). Therefore the smaller slab geometry of the TCP design requires special attention during the design and construction phase with particular attention on the design and specification of the support layers and jointing system.

A characteristic of the TCP system (Covarrubias 2008) is that the aggregate base should be a drainable layer in order to minimize pumping, e.g., an aggregate gradation containing less than 6% fines passing the #200 sieve. A separation layer (non-woven geotextile interlayer) is also required between the subgrade and the granular layers to prevent upward movement of the natural soil fines into the more open graded granular base layer and penetration of the aggregate base into the subgrade.

The characteristics of the TCP joint spacing and design enable the thickness of the slab to be reduced and minimize the initial cost of this pavement type. The shorter slab sizes require more saw-cuts; however, the joints are typically not reinforced. The shorter slab sizes reduces the joint opening thus should maintain a higher joint load transfer over time, which is one objective being evaluated with this research. The joints also are not sealed. The slabs also have to be laterally confined since there is typically no reinforcement to tie the longitudinal contraction joints.

1.2 RESEARCH OBJECTIVES

The objectives of this research is to conduct full-scale accelerated pavement testing of concrete pavements with optimized slab geometry (small panel sizes) and collect response and performance data to assess the viability of these new pavement systems. The collected performance can then be subsequently used to validate a proposed design method for concrete slabs with optimized geometry. The performance data collected includes the type of and severity of slab cracking and joint deterioration for loading near the edge and in the wheel path versus load repetitions for several slab thickness values. The effect of different base stiffness and utilization of macrofibers on the performance of the concrete slabs will also be assessed.

CHAPTER 2 DESIGN AND CONSTRUCTION OF FULL-SCALE PAVEMENT TEST SECTIONS

The details of the concrete pavement with optimize slab geometry test section construction are presented in this chapter. Specifically, a description of each test section, the site plan and layout, materials, a geotechnical report, instrumentation, and the concrete casting day are presented.

2.1 TEST SECTIONS

Three consecutive 132 ft test sections were constructed (396 feet total) to test the effects of thickness, base stiffness, and concrete mixture design on TCP performance, as shown in Figure 2(a), 1(b), and 1(c) below. A total of 14 slabs and joints can be tested during one loading sequence. Each test section in Figure 2 has two variables and therefore 7 slabs and joints will be trafficked for each variable with the accelerated pavement testing device. The pavement cross sections are shown in Figure 3. Figure 3 (a) is the cross section of the first test section supported by a variable thickness asphalt concrete base and Figure 3 (b) is the cross section of the two test sections supported by a 15cm unbound aggregate base. To ensure proper drainage, test sections 2 and 3 have a 0.5% cross slope draining from south to north. The length of the sections was selected based on the dimensions of the accelerated testing device called the ATLAS (Accelerated Transportation Loading ASsembly). The ATLAS is 125 ft long and must be supported by a rigid foundation. The ATLAS can test an 85 ft section length with 65 ft being tested at a constant velocity.

As seen in Figure 2 (a), the first test section will determine the performance difference between the 10 and 15 cm on an asphalt concrete base layer. Figure 2 (b) shows the second test section which will determine the performance of 15 and 20 cm slab thickness on an aggregate base layer. Finally, Figure 2(c) will determine the structural benefit and performance of concrete made with and without discrete fiber reinforcement for a constant slab thickness of 8 cm on an aggregate base layer. A comparison between the three test sections' performances can also be made to later determine the optimal thickness for a given traffic level and also against accepted cracking models such as RiPPER model (Smith et al. 1998) and the M-EPDG (ARA 2007). There are no dowels or tie bars in the test sections and the joints are not sealed.

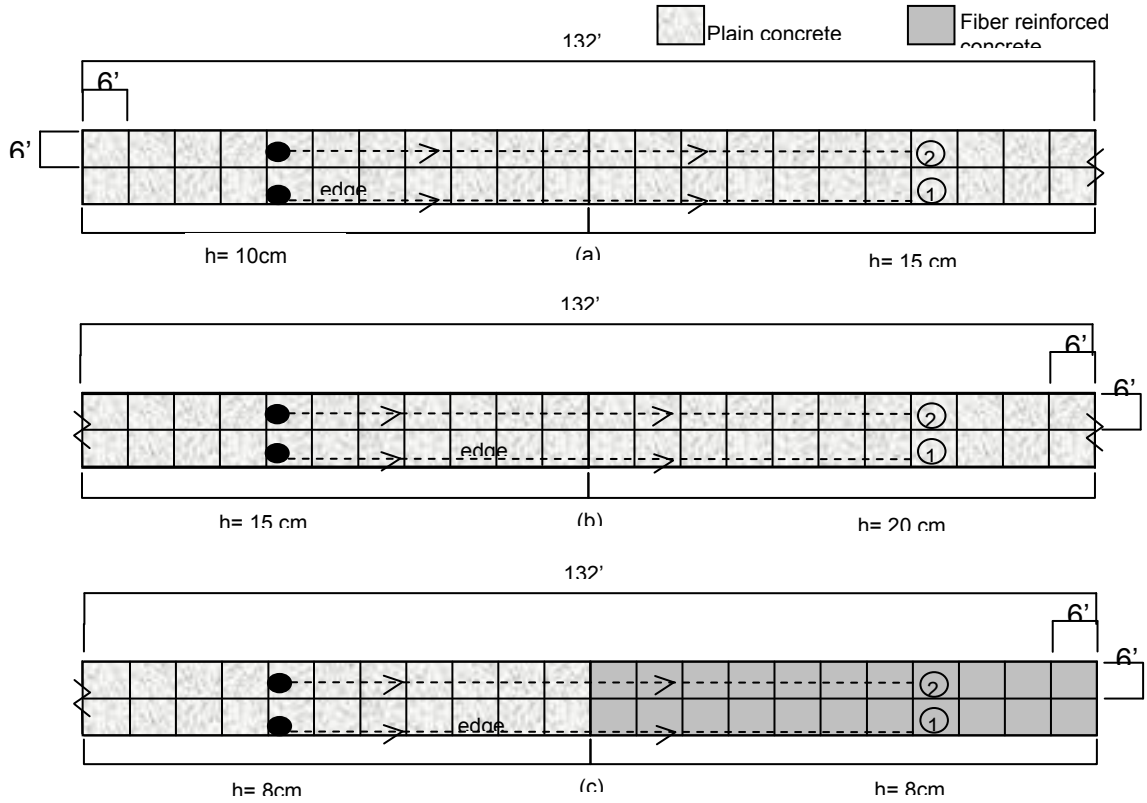


Figure 2. Test Sections for Accelerated Pavement Testing of Thin Concrete Pavement; (a) Section 1 with 10 and 15 cm sections on asphalt concrete base; (b) Section 2 comparison of 15 and 20 cm sections on an aggregate base; (c) Section 3 comparison of 8cm section on aggregate base with and without fiber reinforced concrete.

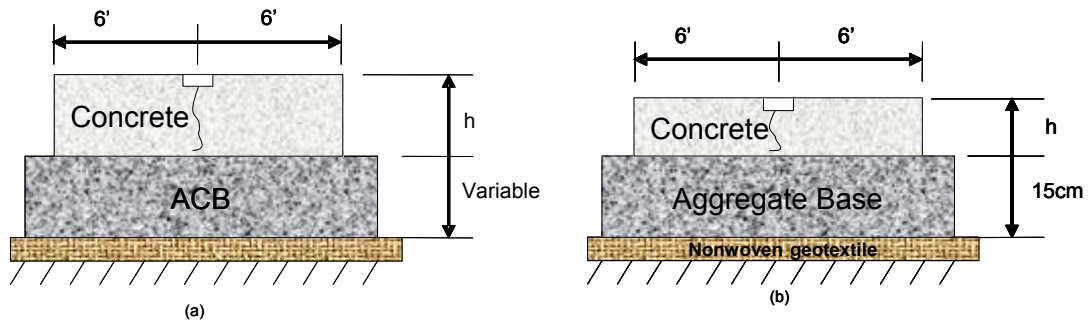


Figure 3. Thin Concrete Pavement Cross Section; (a) Section 1a with 10 cm slab on top of 21.5cm of asphalt concrete base (ACB) and section 1a with 15 cm TCP over 14 cm ACB; (b) Sections 2 and 3 with varying thickness (h) on unbound aggregate base with a geotextile separation layer.

2.2 SITE PLAN AND LAYOUT

During the summer of 2007, the project site was surveyed and the layout for the concrete pavement section was developed. Figure 4 is a topographic map of the TCP project site. As the figure shows, the sites topography slopes to the north and east. Minimal earthwork was done in order to ensure that the pavement would have a smooth transition between the three test sections which have varying concrete depths and to ensure the drainage of the site would not be compromised. The site profile can be seen in Figure 5. This figure shows how the subgrade was altered to meet the specified section thicknesses. This project had approximately 45 yd³ of cut soil and 10 yd³ of fill soil. The contractor was responsible for achieving a minimum of 95% modified proctor in accordance to ASTM D 1557.

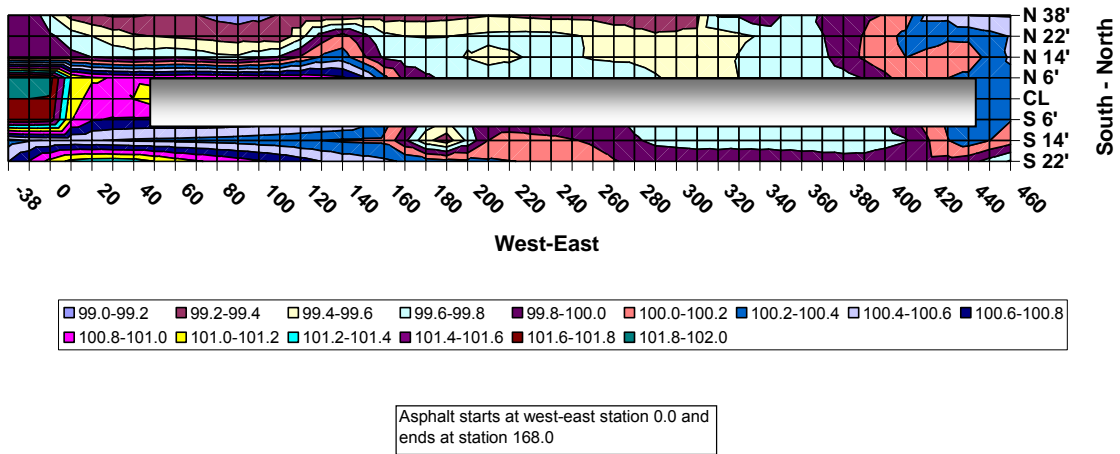


Figure 4. Topographic map of test section.

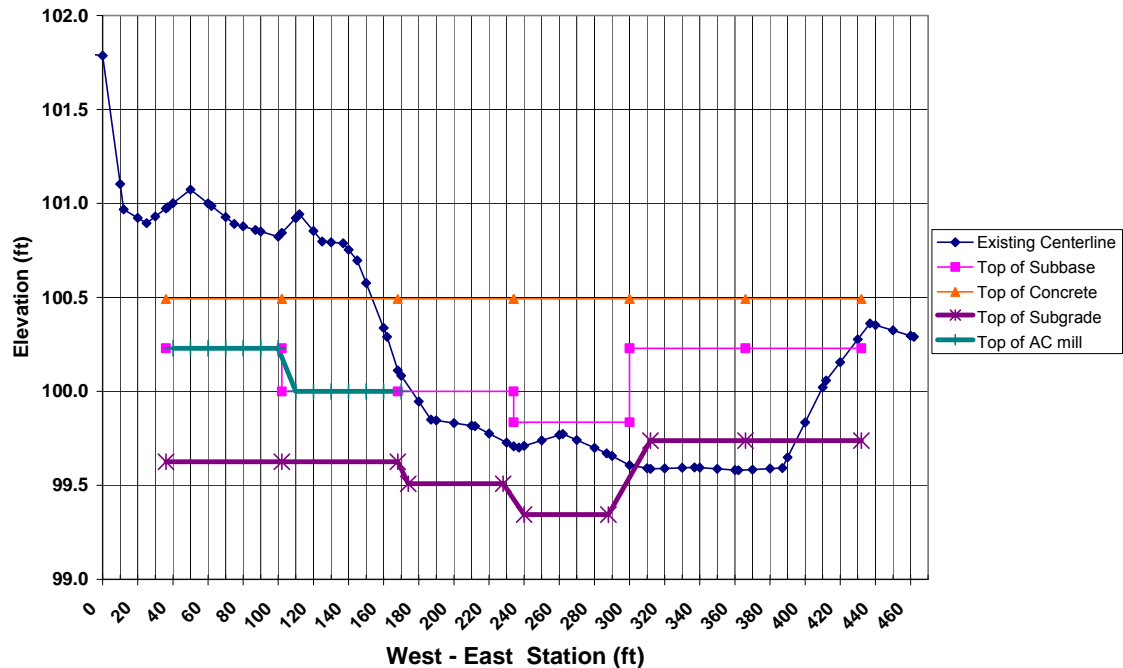


Figure 5. Profile of project site. Test section begins at station 36 (ft).

2.3 MATERIALS

As shown in Figure 3b, the pavement sections (2 and 3) contained compacted subgrade, a non-woven geotextile separator layer (between the aggregate base layer and the subgrade), and 6-inches of compacted granular base. The non-woven geotextile prevents the intrusion of subgrade material into the base layer which could lead to pumping especially under accelerated loading. The aggregate base layer was set to be 12 inches wider on both sides of the slab, resulting in a 14 ft total width. The aggregate base material was specified to contain less than 6% fines passing the #200 sieve (<75 microns). In order to have less 6% fines, a 50/50 weight ratio of CA6 and CA11 aggregate (IDOT specifications) was created by the contractor.

The concrete mixture design utilized for construction of the concrete test sections is shown in Table 2 below. The concrete constituents was proportioned to achieve a minimum design flexural strength of 650 psi at 90 days (4.5 MPa) using ASTM C78. The total cementitious content was approximately 561 lbs/yd³ with 25% replacement with Type C fly ash. The water to cement ratio was 0.42. The coarse aggregate had a maximum aggregate size of 1-inch. The target air content of the mixture was 6 percent. The measured air content on casting day for sections 1, 2, and 3a were 3.2%, 3.8%, and 1.9% respectively. A superplasticizer was added at the site to promote adequate mixing of the fibers. The fiber content (synthetic macro fiber) was 6 lbs/yd³ for the FRC test sections. This level of fibers were added to try and achieve an equivalent flexural strength ratio (R_{150}^{150}) of 30 percent (Roesler et al. 2008), which is a calculated value based on the measured residual strength (f_{150}^{150}) from ASTM C1609-07 and the concrete flexural strength.

Table 2. Concrete Mixture Design

Material	Quantity (lb/yd ³)
Coarse Aggregate	1903
Fine Aggregate	1214
Cement	421
Fly Ash (Type C)	140
Water	236
STRUX 90/40 Fibers	6
Daracem 19*	26 (Fl oz/ yd ³)
Air Entraining Agent	5 to 8%

*As needed

For each of the three sections, six flexural strength beams (21 in x 6 in x 6 in) were cast. Three of the beams are to be tested prior to the loading of the given section and the second three will be tested after testing of that section is complete. For the third section three of the beams have already been tested and the flexural strength was determined to be 969 psi. To determine the elastic modulus, a total of six cylinders measuring 6 in diameter x 12 in high were cast.

Six free shrinkage samples were cast, two for every section. On the third section the fiber reinforced concrete mixture was sampled. The shrinkage data that has been collected is presented in Figure 6 and

Figure 7. At 86 days, the mass loss percentage between the highest and lowest percentage loss varied by only 0.33%. The greatest mass loss was for the fiber mix.

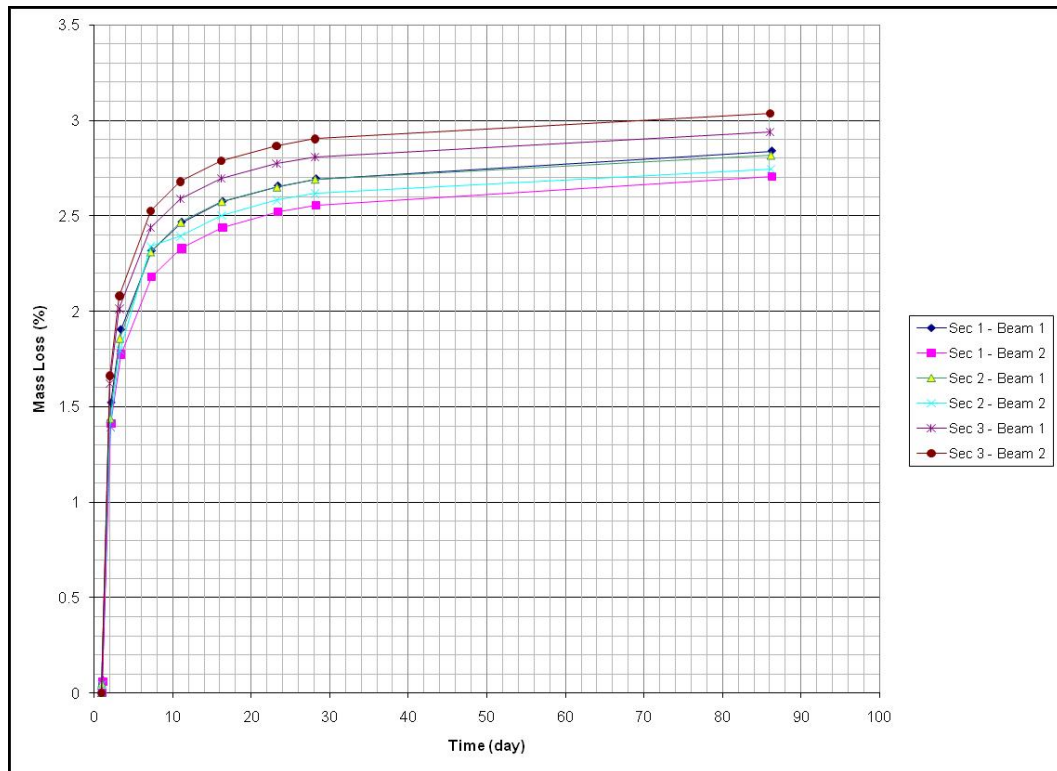


Figure 6. Mass loss data for TCP.

Figure 7 is a plot of free drying shrinkage percentage versus time (ASTM C157). Up until about 11 days the shrinkage percentage is about the same for all of the specimens. At about 90 days the second beam for section 3 had the lowest shrinkage percentage at -0.073%. The highest shrinkage percentage was for section 2 (specimen 2) at -0.066%. The difference between these two beams is 0.007 % which shows that there is little difference in shrinkage percentage between the plain concrete and the FRC mixtures.

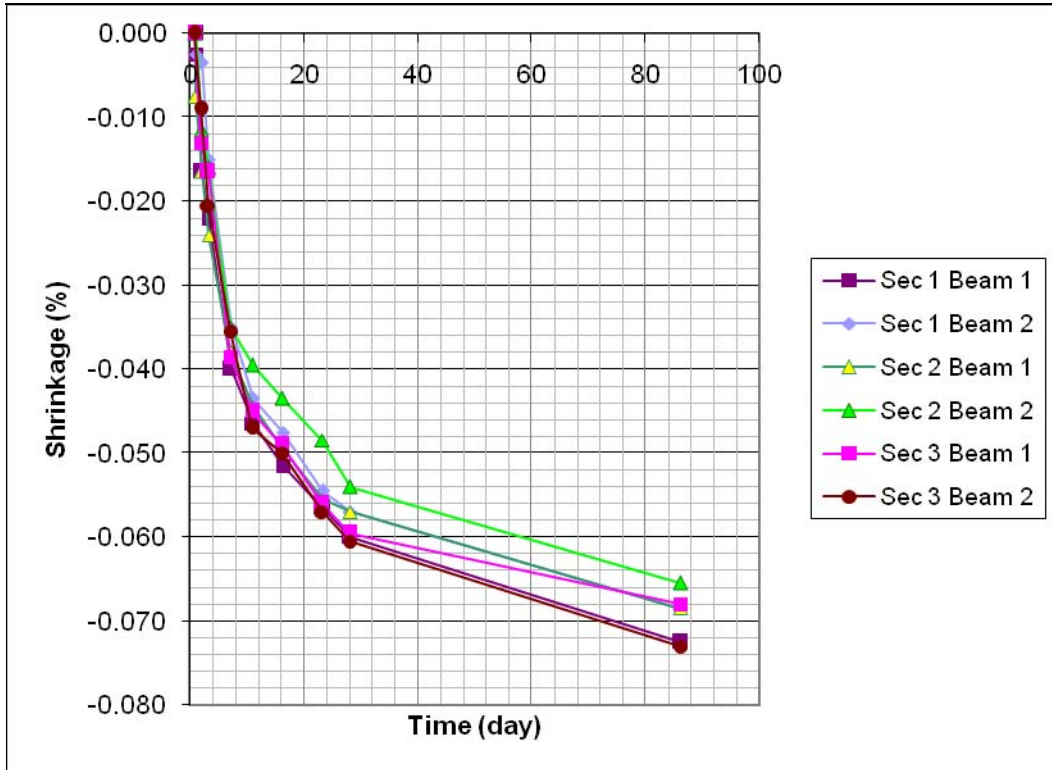


Figure 7. Shrinkage data for TCP.

2.4 GEOTECHNICAL REPORT

A modified proctor test, ASTM D1557, was conducted on the aggregate subbase and subgrade material by Geocon Engineering, Inc. The test showed that the granular base, made up of 50/50 ratio by weight of CA6 and CA11 graded limestone material per IDOT specification, had a maximum dry density of 133.7 lb/ft³ and a optimum moisture content of 4.8%. The subgrade material was determined to be brown silty-clay with trace sand. The maximum dry density for the soil was 122.6 lb/ft³ and the optimum moisture content was 10.7%. The report of moisture-density relationship for both materials can be found in Appendix A.2.

Dynamic Cone Penetration (DCP) test were conducted before and after the subgrade had been trimmed to the correct elevation and placement of the aggregate subbase was complete. The DCP plots can be found in the Appendix A.3 The lower subgrade CBR values after the placement of the subbase was a result of significant rainfall.

2.5 THEORETICAL STRESS ANALYSIS

Prior to construction, ILLISLAB simulations were conducted to determine the location of the maximum top and bottom tensile stress. This information was later used in the placement of the dynamic strain gauges. Simulations were run to determine the load level required to produce a fatigue crack in the slab during the first week of testing. The simulations were conducted for the free edge and repeated for the wheel path loading (12-inch offset). The free edge simulations showed that a maximum bottom tensile stress occurs at the mid-slab along the free edge. The maximum tensile stress on the top of the slab occurred at the mid-slab location in the transverse direction when the wheel was placed at the corner of the slab. For the wheel path simulations, a maximum bottom tensile stress occurred at the transverse joint approximately 20 inches from the free edge. The maximum longitudinal tensile stress for the wheel path loading was still observed at the mid-slab location. Figure 8 is a schematic of the described results. A summary of the complete ILLISLAB results can be found in the Appendix A.4

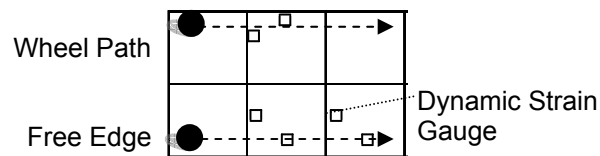


Figure 8. Schematic of dynamic strain gauge placement.

2.6 INSTRUMENTATION AND MONITORING

The instrumentation for the test section included both static and dynamic sensors. The static thermocouple sensors were installed prior to construction to monitor the temperature throughout the early-age and as a back-up temperature reading for the trafficking of the sections. These measurements were taken to primarily assist in quantifying the magnitude of the slab's built-in curling. The sensors needed for monitoring the response testing and trafficking were LVDTs and strain gauges. The LVDTs will be used to measure vertical and horizontal displacement along the edge of the slab. The strain gauges were placed on the bottom-edge of the pavement at the mid-slab location, at the top at mid-slab transverse joint, and 20 inches from the edge along the bottom of the transverse joint. The surface profile of the section was measured periodically during trafficking with a dipstick.

To collect the static temperature and the weather station data two Campbell Scientific units were used. Each unit consists of a data logger, either a Campbell Scientific CR10X or a CR800. The CR10X unit is capable of storing 128 kb of information between information downloads and the CR800 can store 4 Mbytes of information.

Type T thermocouples were used in this project and were connected to the AM25T multiplexer. The thermocouple wire was purchased from Omega Engineering, Inc. (FF-T-24-TWSH). 24 gauge wire allowed for a sensor distance of 100 ft and as such the placement of the Campbell Scientific boxes was optimized to minimize the amount of thermocouple wire. At each thermocouple station, which can be found in the instrumentation section of the appendix, there were either 4 or 5 thermocouples placed vertically in the concrete slab depending on the thickness of the slab.

The strain gauges were purchased from Texas Measurements (PML-60-2L). These strain gauges are specified to be used in concrete and mortar applications, have

a gauge factor of 2 and a 120 Ω resistance. The strain gauges were placed at the locations of maximum strain in accordance to ILLISLAB simulations. They were held at the right vertical and horizontal location using a steel chair and zip ties as shown in Figure 9. During paving, concrete was hand placed around the strain gauge to ensure adequate consolidation and reduce the probability of damaging the gauge. For the free edge testing, a total of 4 strain gauges were placed per sub-section. For the wheel path testing, 2 strain gauges were placed per sub-section totaling 6 gauges per sub-section. To counter the effects of temperature on the gauges resistance, dummy strain gauges were cast in concrete beams and were connected in a half bridge configuration during accelerated pavement testing.



Figure 9. Strain gauge on steel chair prior to paving.

2.7 CONSTRUCTION

The first step in the construction process was to provide the correct grade. The asphalt concrete section was cold milled to the specified height shown in Figure 5. The asphalt concrete surface was then broom cleaned. The top of the subgrade in sections 2 and 3 was trimmed to the proper elevation. The non-woven geotextile was then placed over the subgrade in preparation for the aggregate subbase material as shown in Figure 10 and Figure 11. The granular subbase was compacted using a vibratory roller, Figure 12, and finally the forms were set into place. Once the subbase and forms were finalized, the thermocouples and strain gauges were installed as seen in Figure 13.

To minimize the probability of the construction crew damaging the instruments that had been placed, concrete was hand placed around the instruments and flags were inserted to mark the position of the instruments as shown in Figure 14. Once the concrete had reached initial set, the curing agent was applied. Early entry saw-cutting began after the final set of the concrete as shown in Figure 15. Figure 16 shows a hand-held saw was used to cut the joint at the edge. After the forms had been removed and the pavement had cured for more than 28 days, one steel stake was driven per slab at the mid-slab location (see Figure 17) to prevent lateral movement of the slab during accelerated load testing.



Figure 10. Milled asphalt concrete.



Figure 11. Granular base over geotextile.



Figure 12. Compaction of granular base.



Figure 13. Instrumentation installation.



Figure 14. Casting day.



Figure 15. Saw-cutting.



Figure 16. Manual saw cutting of edges.



Figure 17. Lateral restraint pins.

CHAPTER 3 PRE-TRAFFIC MONITORING

This chapter presents data collected before trafficking began. This includes the results of joint crack development and falling weight deflectometer testing.

3.1 JOINT CRACK DEVELOPMENT

The concrete slabs were periodically inspected for the initiation of the joint cracks. Figure 18 is a graphical representation of the percentage of cracked joints as a function of days after construction of the section. Table 3 presents the percentage of slab joints that were cracked on the day of inspection. After 15 days 28% of the joints had cracked, primarily on the thinner sections. By 31 days the number of cracked joints increased to 52% and after 5 months 83% of the joints had cracked. One observation to note is that on the day after the concrete slabs were cast a hairline transverse crack appeared on the south side of slab 51. By day 28, the transverse crack had propagated across to the north side slab. This was the only random crack observed in the test pavement. The crack was near the location where all of the thermocouple wire exited the pavement that connected to the data logging system. The transverse crack was not noticed at the other data logger location because that pavement section was 15 cm on an asphalt base as opposed to 8cm on a granular base.

Table 3. Percentage of cracked joints.

Days After Casting	1	2	15	22	24	29	31	148
Cracked Joints (%)	3	6	28	43	48	51	52	83

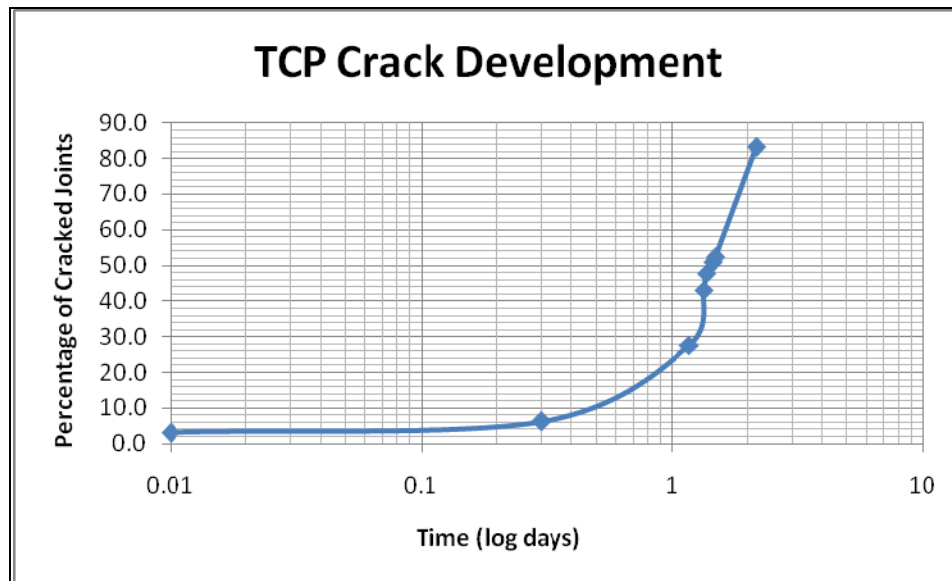


Figure 18. Plot of first observation of crack at a specific joint.

3.2 FALLING WEIGHT DEFLECTOMETER

Falling weight deflectometer (FWD) analysis was conducted on the north row of concrete slabs 29 days after casting. Figure 19 is a photograph of the FWD device that was utilized. The center slab normalized deflections for 9-kip load are plotted versus the slab number in Figure 20. This plot confirms that the deflection is the smallest when the concrete slabs are supported by the asphalt concrete layer (section 1). Section 2a had higher deflections than section 2b as expected due to its thinner slab thickness (15 versus 20 cm). The highest deflection was observed at slab 56 which is the transition slab between the 8cm plain and fiber reinforced concrete section.



Figure 19. FWD used for center slab deflections and joint load transfer efficiency.

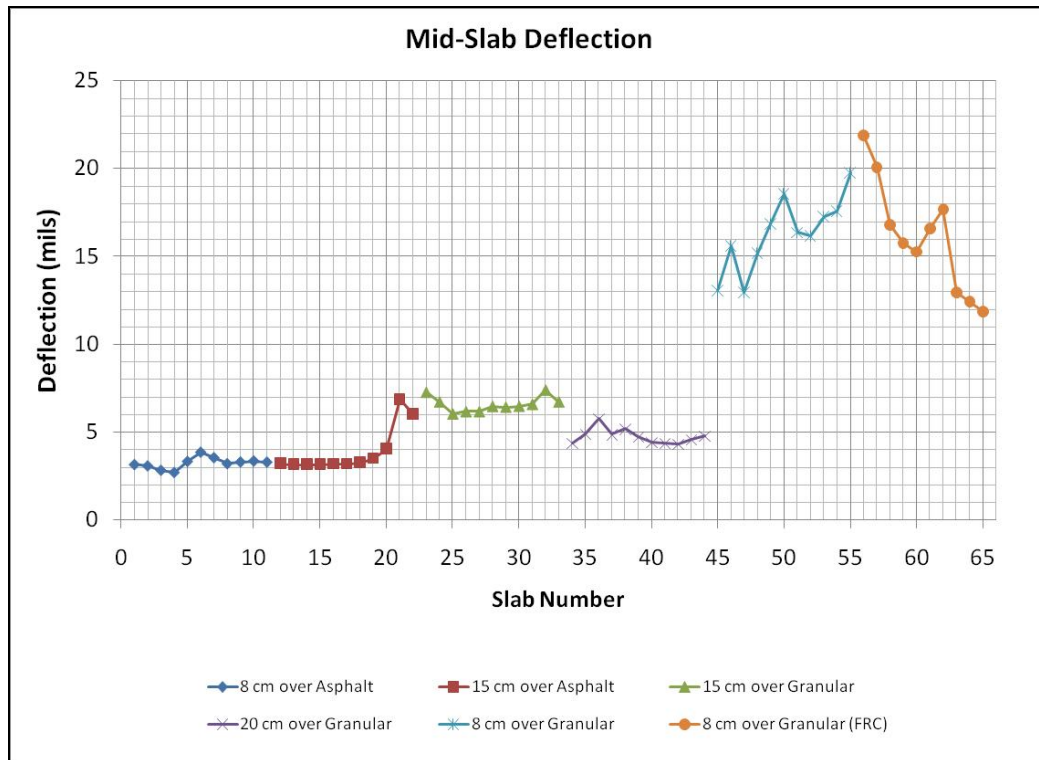


Figure 20. Center slab 9-kips normalized deflections (mils=0.001 inch).

The load transfer efficiency (LTE) across each of the joints was calculated from the FWD data as seen in Figure 21. Joints 20, 23, 32, 35, 45, and 55 had a LTE less than 80%. These joints were some of the first to form full-depth cracks after the pavement had been cast. Figure 22 shows the deflection at a given joint.

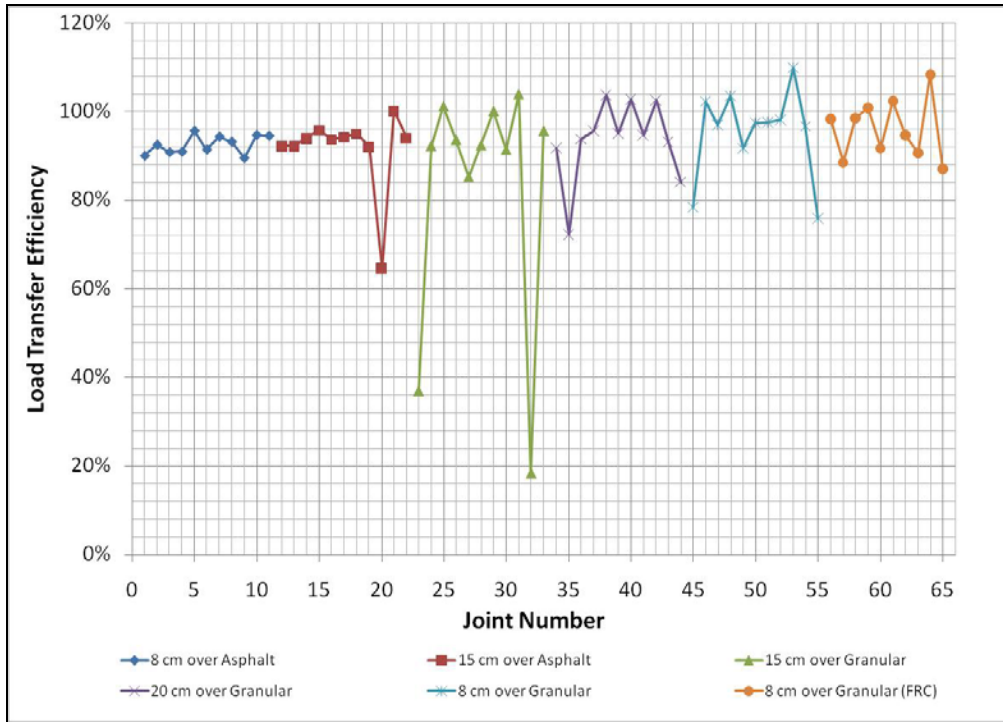


Figure 21. Load transfer efficiency of transverse contraction joints.

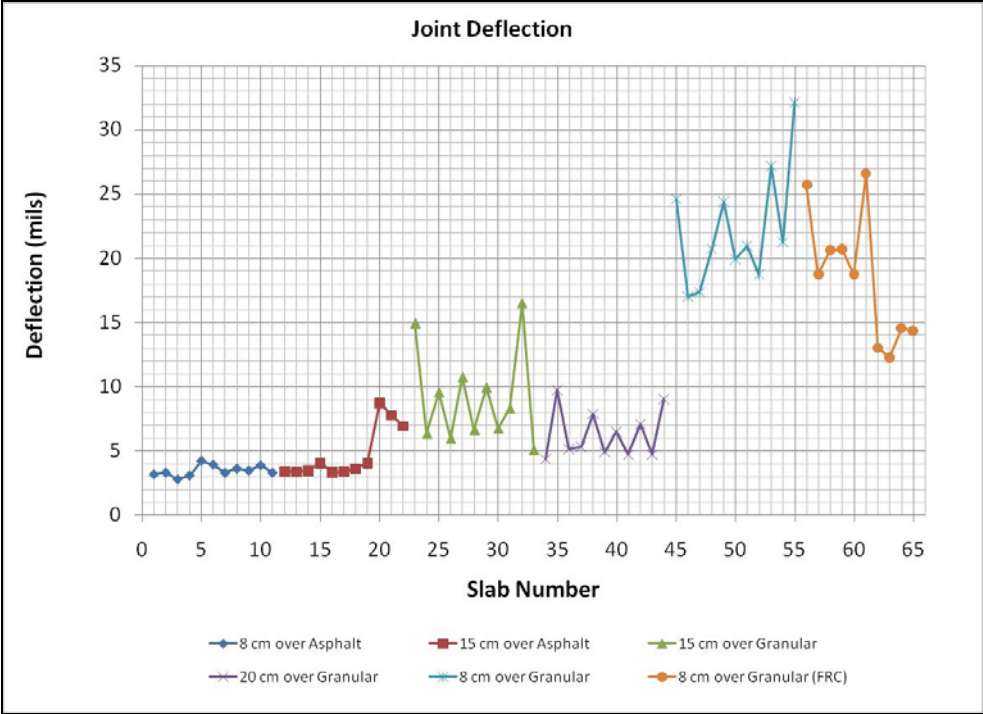


Figure 22. 9-kip deflection at a given joint location.

CHAPTER 4 ACCELERATED PAVEMENT TESTING RESULTS

The results and discussion of the accelerated pavement testing are presented in this chapter. Each test section will be presented independently and will then be subsequently compared to one another. The main parameters used to quantify the accelerated pavement test results are the number of cracked slabs, vertical deflections, horizontal deflections, and strains.

4.1 ACCELERATED TRANSPORTATION LOADING ASSEMBLY (ATLAS)

In order to determine the fatigue and joint performance of concrete pavements with optimized slab geometry, accelerated pavement testing (APT) was conducted. The purpose of APT is not necessarily to traffic the pavement with similar wheel load and repetitions experienced in typical roadways since this could take an indefinite amount of time. The main objective is to overload the test section with the APT device so that slab failure occurs in a shorter amount of time and then the results are equated to standard loading levels and repetitions expected for in-service pavements.

The ATLAS device, seen in Figure 23, was utilized to complete the response and failure testing of the three test sections. The ATLAS is approximately 124 ft long, 12 ft. high, and 12 ft. wide and weighs 180-kips. The loading length of the ATLAS is 85 ft., which can be programmed for either uni- or bi-directional movements. In this testing, only uni-directional testing was employed. The machine transmits a load up to 80,000 pounds to the pavement through a hydraulic ram attached to a wheel carriage. The wheel carriage assembly can accommodate a single tire, dual-wheel tire, or an aircraft tire. For most of the testing, an aircraft tire was used except for some trafficking with a super single tire on section 3. A winch motor pulls the wheel carriage back and forth on the test section. The ATLAS could apply approximately 2,500 repetitions per day in the uni-directional mode. The ATLAS is mounted on two pairs of rotating crawler tracks, which provide translational and rotational maneuverability of the ATLAS around the testing grounds. For most of the test sections, the ATLAS was exposed to the ambient conditions except for section 3 (north) where the temperature panels enclosed the test section.



Figure 23. Accelerated Transportation Loading Assembly (ATLAS) device.

4.2 IDEALIZED ATLAS TESTING PLAN

The testing plan for each test section included monitoring of the environmental behavior of the slabs with and without loading and monitoring deformations under damaging load levels. The initial loading testing was near the free edge of the test

section (south side of sections). A 2nd phase of loading occurred on the same test section in the wheel path (12 inch offset) on the north side of the test section Figure 2. A total of 28 slabs and 28 joints were tested per test section (free edge and wheel path loading). The following testing plan was completed for both the free edge and wheel loading in a single section:

- 1) Monitoring of the slab environmental movements for 24 hours without mechanical loading through collection of slab deflections, strains, and temperature profile.
- 2) Combined 9-kip load plus environmental monitoring for deflections and strains for 24 hours.
- 3) Trafficking of the test sections at damaging load levels so that failure of the test section occurs at a reasonable number of repetitions.

4.3 LOAD AND REPETITION MAGNIFICATION FACTOR

Accelerated pavement testing typically exposes the test section to loading conditions that will cause significant levels of pavement damage (cracking) at a lower number of wheel passes. The overloading and accelerated pavement damage must then be related to more commonly understood loading terms used in pavement design, such as ESALs. In past research efforts with accelerated pavement testing, the use of individual wheel loads, number of load repetitions, and Miner's cumulative damage theory has not provided a better approach relative to ESALs (Rao 2005; Kohler and Roesler 2006). For this study, the equation which was used to correlate number of passes to number of ESALs was:

$$ESAL = \beta * n * \left(\frac{P}{9000} \right)^{4.2}$$

where β is a channelized magnification factor approximately equal to 20 for channelized edge loading on JPCP (Zollinger and Barenberg 1989; PCA 1984), n is the number of passes for a given wheel load, P , and the exponent 4.2 approximately represents the load equivalency factors from the AASHTO Road Test and is also used as a means to calculate ESALs in the California Department of Transportation pavement design manual (Caltrans 2008).

During load testing the magnification factor was initially set to 10 for edge loading on slabs with optimized geometry based on past analysis and accelerated pavement testing experience (Kohler and Roesler 2006). However, one issue with a constant lateral wander magnification factor is the wheel offset was not constant as well as the trafficking was channelized.

In order to establish a lateral wander magnification factors for each section and wheel offset, a finite element analysis using ILLISLAB was required. The first step in this analysis was determination of the modulus of subgrade reaction (k) for each of the test sections. The maximum mid-slab deflection measured for an offset of 4 inches (except for the 3.5 inch section over granular – north) was matched with the maximum deflection obtained from ILLISLAB by changing the soil's k -value. Table 4 summarizes the backcalculated k -values that were obtained from the ILLISLAB analysis along with the magnification factor that was used for each section.

Table 4. Modulus of Subgrade Reaction (k) Values for Each Section Backcalculated from Edge Loading (except for 3.5 in. over granular – north) and Magnification Factor

Section		k (psi/in)	Magnification Factor
4 in. / AC	North/South	250	20
6 in. / AC	North/South	500	20
6 in. / Granular	North	100	18
6 in. / Granular	South	300	19
8 in. / Granular	North	100	15
8 in. / Granular	South	150	16
3.5 in. / Granular	North*	50	20
3.5 in. / Granular	South	150	20

*12 inch offset

The next step in the analysis was to find the tensile stresses at the bottom of the mid-slab edge as the load was moved laterally in one inch increments (0 to 20 inches). The tables of the calculated bottom tensile stresses at each load offset can be found in the Appendix A.5

One significant challenge in determining the channelized magnification factor (β) was what fatigue algorithm to use to translate stresses to allowable number of repetitions. Most of the concrete fatigue algorithms are extremely sensitive to changes in tensile stresses and therefore only wheel loads adjacent to the slab edge contribute to the fatigue damage. The approach utilized by Zollinger and Barenberg (1989) and the PCA (1984) was tried with various published fatigue algorithm for these shorter concrete slab geometries but without success.

A fatigue equation developed by Vesic and Saxena (1969) based on the AASHO Road Test concrete sections was finally selected since it had full-scale traffic with wander and the concrete pavement failed under various modes, i.e., erosion and cracking. The following Vesic and Saxena (1969) fatigue equation was used to calculate the number of allowable repetition (N_a):

$$N_a = 225000 * \left(\frac{\sigma_n}{MOR} \right)^4$$

where σ_n is the stress at a given distance from the edge and the MOR is the modulus of rupture of the concrete. Since all the trafficking was channelized, the magnification factor (M) for each section was calculated using a ratio of the fatigue damage produced at the channelized trafficking offset over the fatigue damage at the edge of the slab produced by a load in the wheel path (18 inch offset). The following equation was used for the calculations:

$$M = \frac{\left(\frac{n_e}{N_{allow(n)}} \right)}{\left(\frac{n_e}{N_{allow(18)}} \right)}$$

where n_e is the expected number of passes at any lateral offset, $N_{allow(n)}$ is the number of allowable passes at a given lateral offset, and $N_{allow(18)}$ the number of allowable passes at 18 inches.

Figure 24 demonstrates the various lateral offset magnification factors for the sections tested. As expected this magnification factor is a function of the slab thickness and base type. In order to use a magnification factor of 10 the channelized wheel

trafficking would have to be approximately 5.5 inches away from the edge for the case of the 8 inch pavement over the granular base. During the trafficking of the sections, the wheel was typically offset from the free edge approximately 4 to 5 inches, thus the magnification factor was calculated based on a 5-inch lateral offset with a maximum value of 20 as shown in always more than the original conservative value of 10. A magnification factor was not used when the load was applied in the wheel path, which was offset 12 inches laterally from the edge.

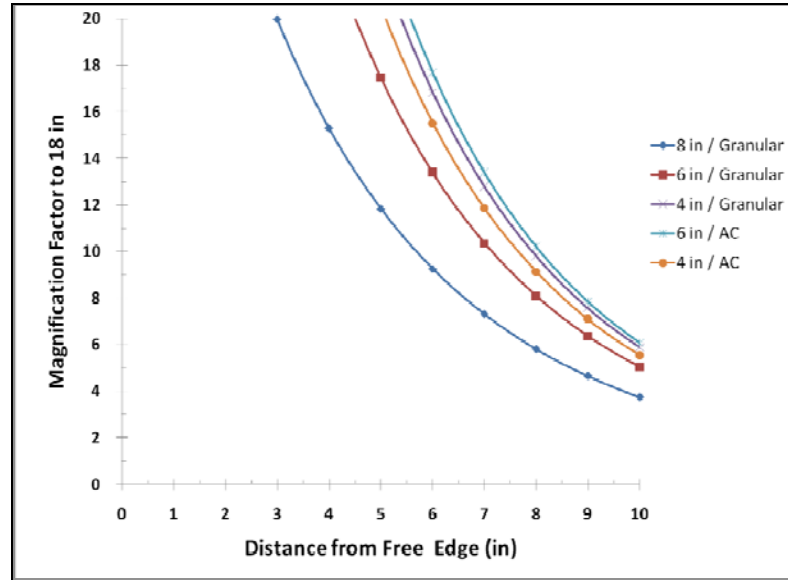


Figure 24. Lateral offset magnification factor for the various concrete test sections.

The following sections will now describe the loading sequence, the approximate number of ESALs applied, the concrete slab failure patterns, and the instrumentation results for each test section.

4.4 SECTION 1 LOADING

4.4.1 CRACK DEVELOPMENT SECTION 1- SOUTH

Detailed cracking pattern records were kept in order to determine the failure modes of the various sections and how they continued to deteriorate after further trafficking. The information is organized by section and by the location of loading. The cracking that occurred when testing on the south section will be shown first followed by the cracking pattern of the north side of the section.

Section 1 (south) consisted of 4 and 6 inches of concrete thickness over asphalt concrete. Slabs 5 through 11 are 4 inches thick and slabs 12 through 18 are 6 inches. The pattern and date in which the slabs cracked can be seen in Figure 25 to Figure 29. Note, the 4 and 6 inch section were tested at the same time. Fatigue cracking began on the 4 inch section at approximately 5.4 million ESALs. At the end of trafficking all seven slabs on the 4 inch section had significantly cracked and only 1 slab out of 7 slabs had exhibited any signs of cracking on the 6 in section. The cracks on section 1 (south) were not as severely deteriorated after the testing, as was the case in some of the other sections including section 1 (north).

The initial cracking was longitudinal as seen on slabs 10 and 11 in Figure 25. Tight longitudinal cracking were then noticed on slabs 5, 6, 8, and 9 after a rain event. Longitudinal cracks are attributed to a combination of heavy load repetitions, loss of support, and slab curling. As the loading continued, corner breaks occurred on slabs 5, 6, 8, 10, and 11. The cracks developing on slab 5 can be partially attributed to repeated static loading at this location since this is where the ATLAS wheel load was initially applied at the beginning of each pass. Table 5 is a summary of load repetitions to cracking. The cracked slab columns in Table 5 refers to the number of slabs that are cracked a given load level and cumulative ESAL count. Section 1 (south) was loaded with approximately 57 million ESALs which completed failed the 4 inch sections and did not produce any significant failure cracks in the 6 inch slabs.

Slab 5	6	7	8	9	10	11
Slab 12	13	14	15	16	17	18

Figure 25. Section 1 south cracking performance after 5/9/09 testing (7.2 Million ESALs).

Slab 5	6	7	8	9	10	11
						

Slab 12	13	14	15	16	17	18

Figure 26. Section 1 south cracking performance after 5/11/09 testing (12.7 Million ESALs).

Slab 5	6	7	8	9	10	11
						

Slab 12	13	14	15	16	17	18
						

Figure 27. Section 1 south cracking performance after 5/12/09 testing (37.1 Million ESALs).

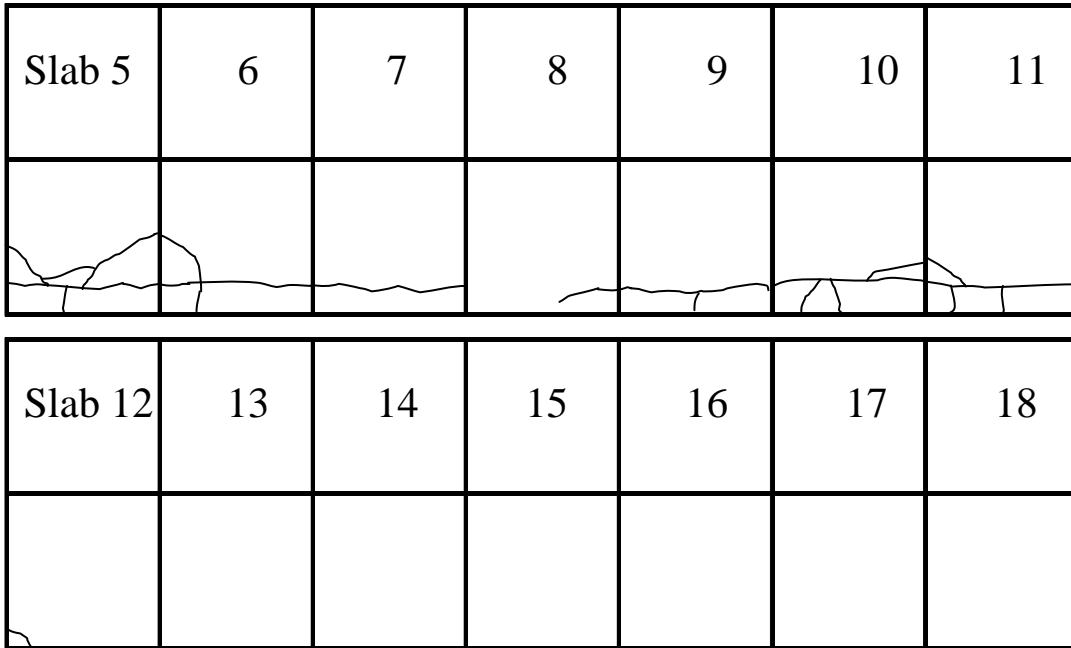


Figure 28. Section 1 south cracking performance after 5/14/09 testing (44 Million ESALs).

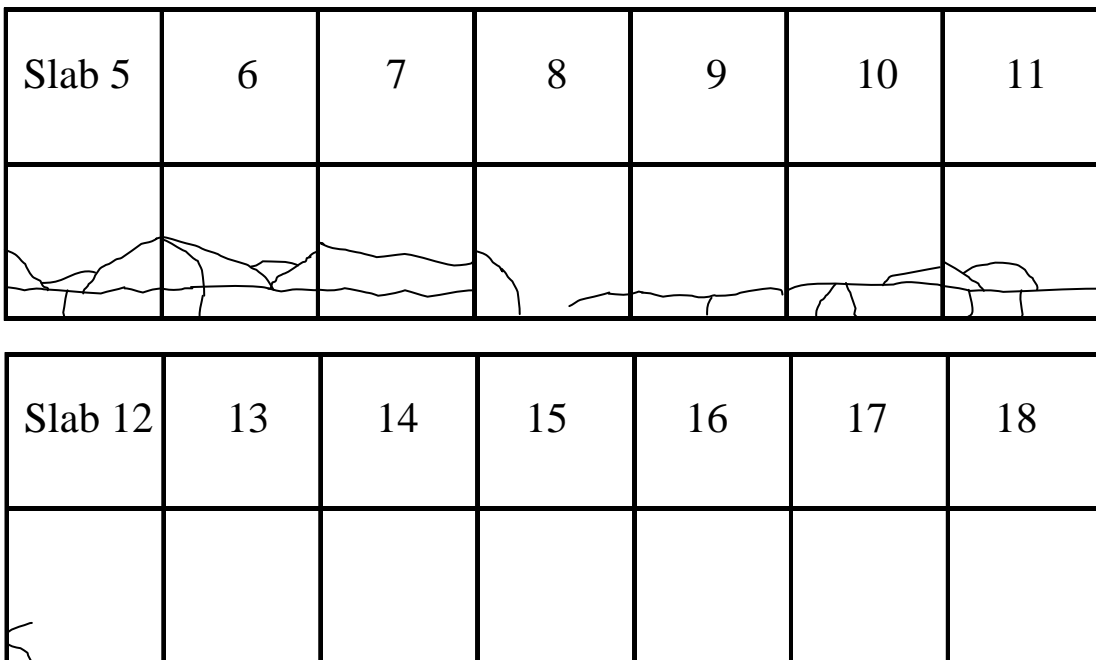


Figure 29. Section 1 south cracking performance after 5/15/09 testing (57.5 Million ESALs).

Table 5. Load repetitions and Cracking Summary for Section 1- South (Edge Loading)

Load (lb)	Passes	Cumulative Passes	ESALs	Cumulative ESALs	Cracks 4 in. / Asphalt	Cracks 6 in. / Asphalt
9,000	2,506	2,506	50,120	50,120	0	0
15,000	2,500	5,006	427,302	477,422	0	0
18,000	2,500	7,506	918,959	1,396,381	0	0
21,000	3,499	11,005	2,457,403	3,853,784	0	0
25,000	1,126	12,131	1,644,742	5,498,526	1	0
25,000	1,211	13,342	1,768,901	7,267,428	2	0
28,000	2,300	15,642	5,407,581	12,675,009	5	0
31,000	2,200	17,842	7,931,462	20,606,471	5	0
34,000	25	17,867	132,850	20,739,321	5	0
35,000	2,730	20,597	16,385,507	37,124,828	6	1
35,000	1,170	21,767	7,022,360	44,147,188	7	1
33,000	1,642	23,409	7,697,384	51,844,572	7	1
33,000	347	23,756	1,626,670	53,471,243	7	1
33,000	274	24,030	1,284,460	54,755,703	7	1
33,000	62	24,092	290,644	55,046,347	7	1
35,000	416	24,508	2,496,839	57,543,186	7	1
Total	24508		5.75E+07		7	1

*ESAL magnification factor = 20

4.4.2 CRACK DEVELOPMENT SECTION 1 - NORTH

Section 1 (north) was first trafficked in the wheel path for two days. The direction of trafficking was from the east to west. The wheel position was then moved near the edge since no cracking was observed and the slab responses were small. Section 1 (north) began exhibiting corner crack failures, which was different than section 1 (south), which began showing longitudinal cracks. Corner breaks are typically attributed to the loss of slab support or erosion during loading. During section 1 (north) trafficking, there were several days of raining which contributed to the loss of support. Testing was not stopped while raining unless there was a thunderstorm.

Figure 30 to Figure 37 demonstrate the development of the structural cracking. Slabs 5 through 11 are 4 inches thick and slabs 12 through 18 are 6 inches. The cracking began first on the 4 inch section at approximately two million ESALs. By the end of the load testing, all 7 slabs had severe cracking. As seen in the figures, longitudinal cracking appeared after significant loading and cracking. Cracking typically occurred at night time as expected due to the combination of wheel loading and upward curling.

The 6 inch section had a better cracking performance and only 4 of the 7 slabs cracked. The fatigue cracking began to appear after 24 million ESALs on slab 12 and

began as corner breaks near the transition joint between the 4 and 6 inch sections (joint 11). After additional loading, the corner breaks continued to progress to adjacent slabs such as slabs 13 and 14. Slab 18 also exhibited a corner break by the end of the testing. The slabs at the end of the sections typically are more likely to crack first since they sustain more slow moving wheels as the ATLAS begins loading or slows down to take off the load. Table 6 summarizes the load level, number of repetitions, cumulative ESAL count, and number of cracked slabs in section 1 (north).

						
Slab 5	6	7	8	9	10	11
Slab 12	13	14	15	16	17	18

Figure 30. Section 1 north cracking performance after 4/20/09 testing (2 Million ESALs).

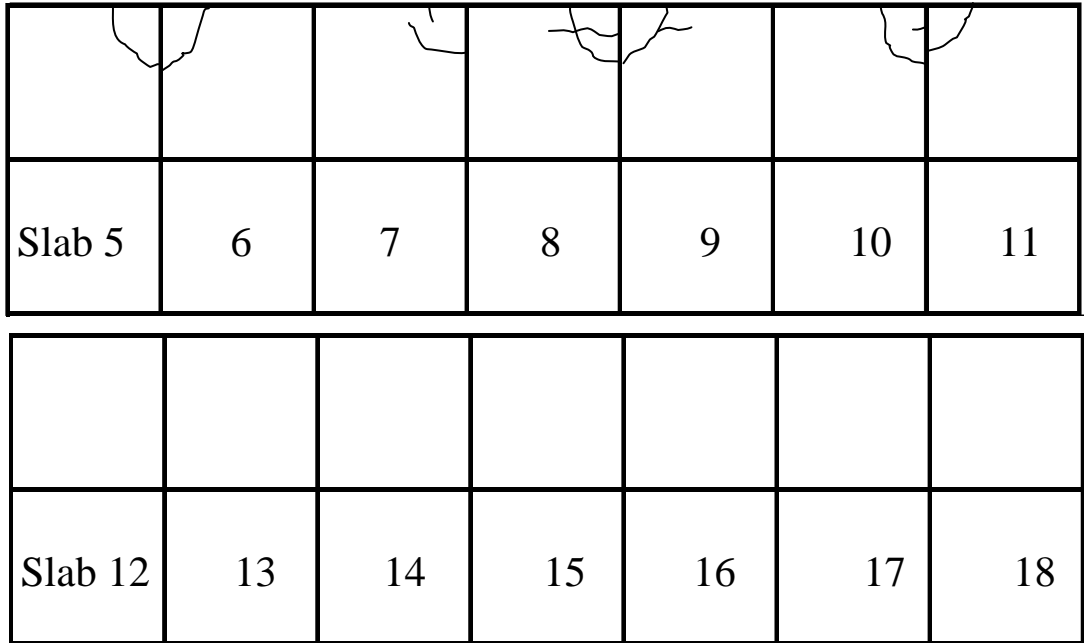


Figure 31. Section 1 north cracking performance after 4/21/09 testing (2.2 Million ESALs).

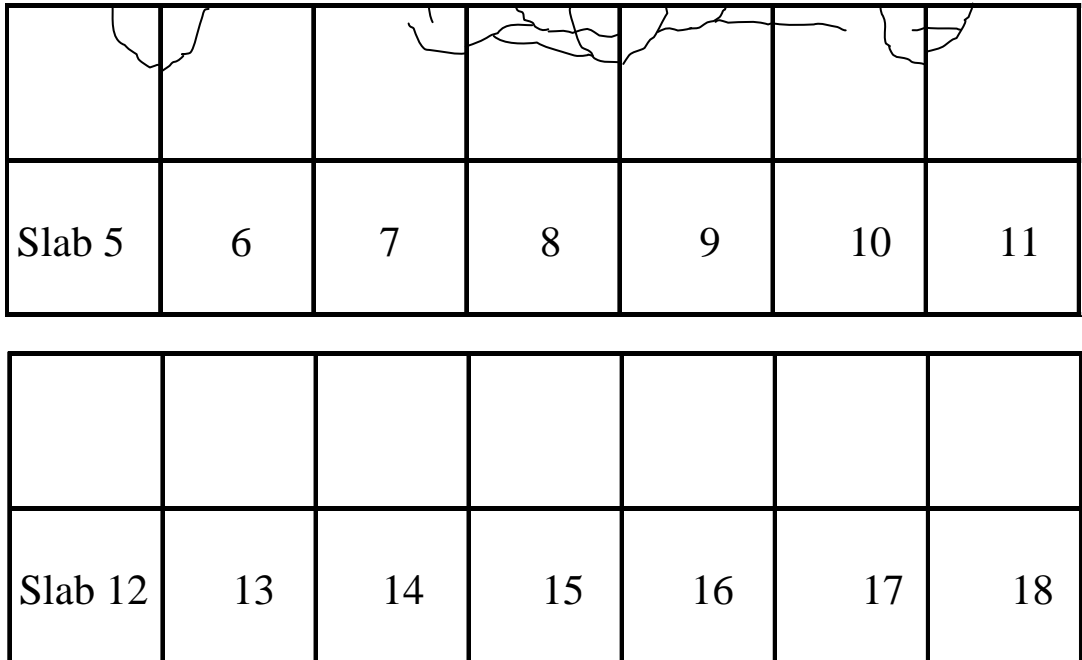


Figure 32. Section 1 north cracking performance after 4/22/09 testing (6.3 Million ESALs).

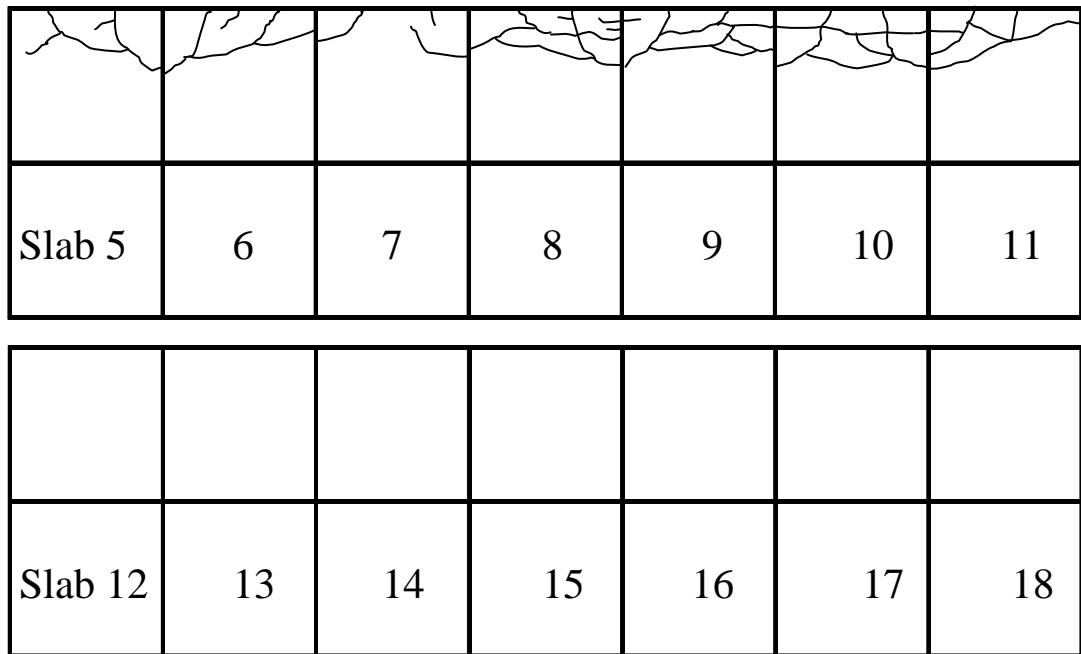


Figure 33. Section 1 north cracking performance after 4/23/09 testing (13.2 Million ESALs).

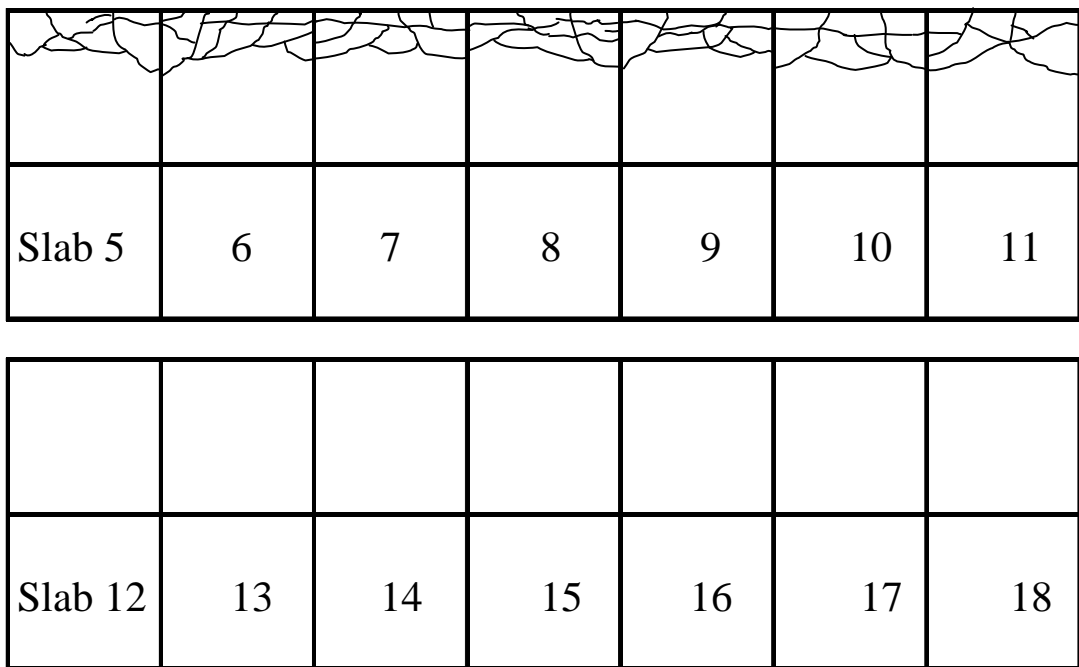


Figure 34. Section 1 north cracking performance after 4/24/09 testing (21.6 Million ESALs).

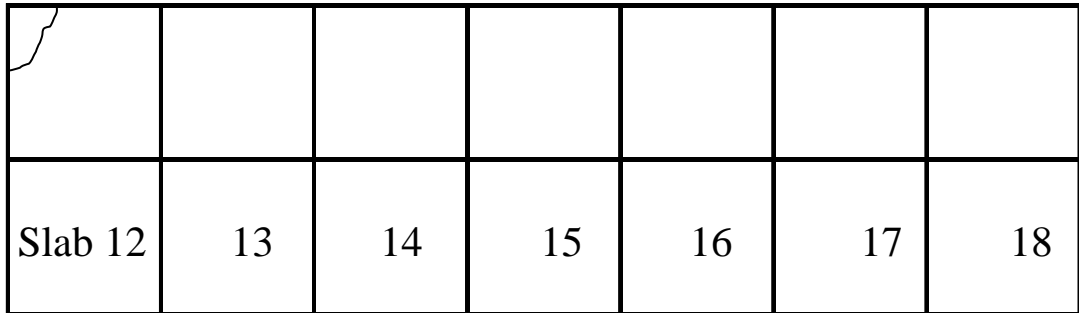
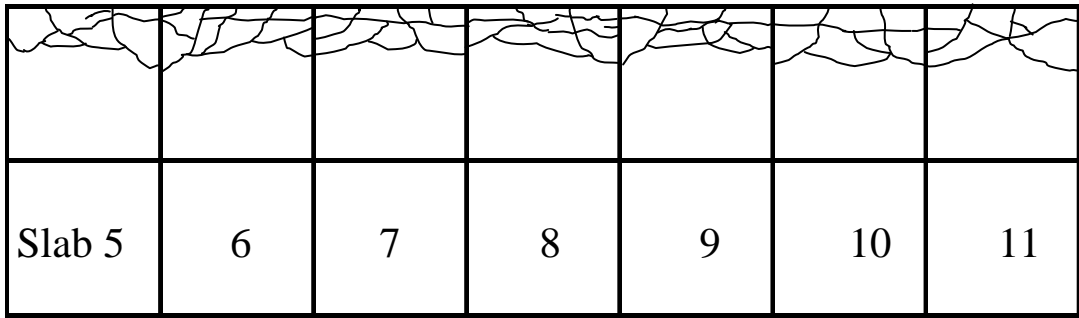


Figure 35. Section 1 north cracking performance after 4/25/09 testing (30.6 Million ESALs).

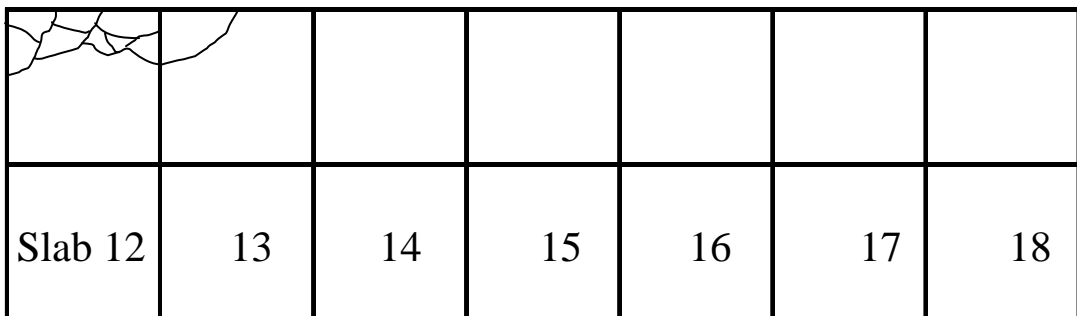
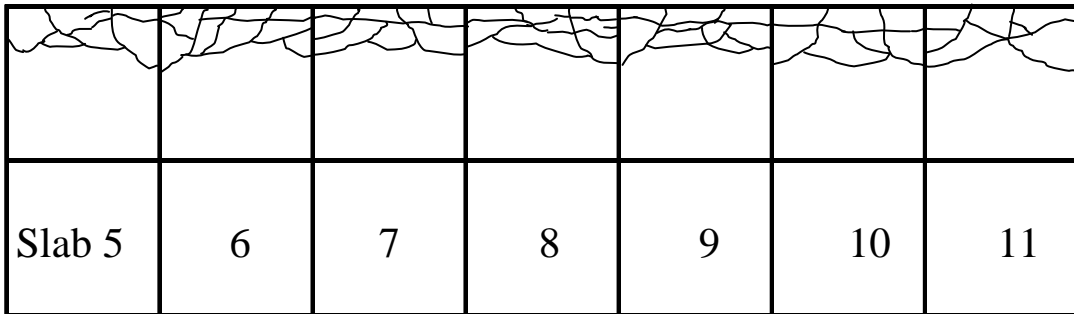


Figure 36. Section 1 north cracking performance after 4/26/09 testing (51.6 Million ESALs).

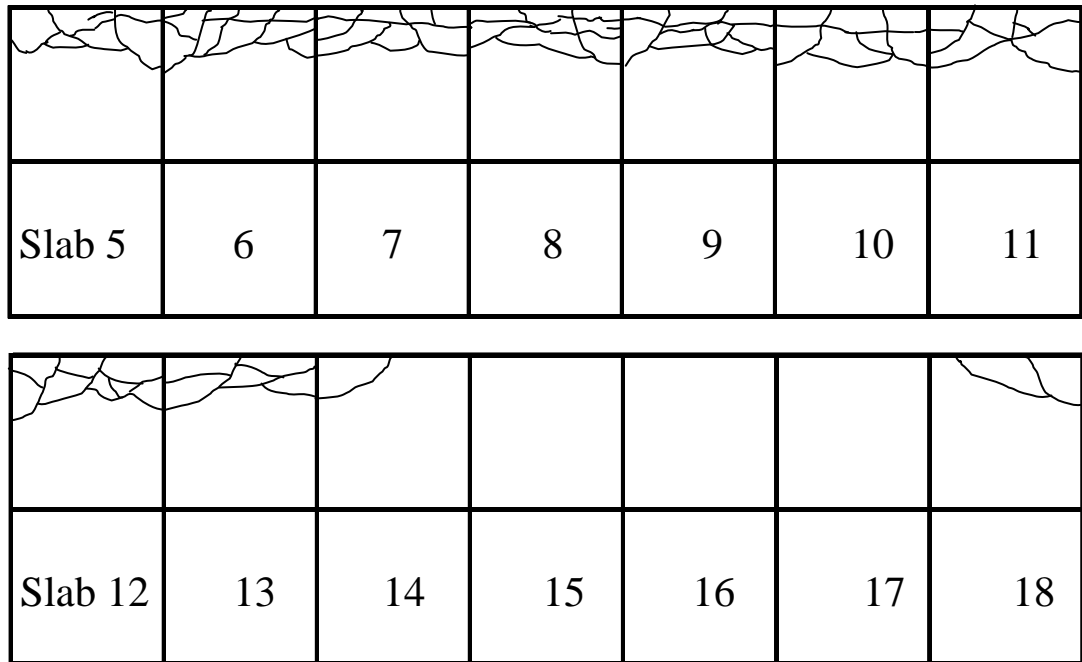


Figure 37. Section 1 north cracking performance after 4/27/09 testing (69.3 Million ESALs).

Table 6. Load Repetitions and Cracking Summary for Section 1 North

Load (lb)	Passes	Cumulative Passes	ESALs	Cumulative ESALs	Cracks 4 in. / Asphalt	Cracks 6 in. / Asphalt
Wheel Path - 12 in. offset						
9,000	2,136	2,136	2,136	2,136	0	0
15,000	2,500	4,636	21,365	23,501	0	0
Total	4636	9272	23501			
Edge Loading - 5 in. offset						
9,000	2,700	2,700	54,000	54,000	0	0
15,000	2,500	5,200	427,302	481,302	0	0
21,000	2,230	7,430	1,566,164	2,047,466	6	0
21,000	270	7,700	189,625	2,237,092	6	0
25,000	136	7,836	198,654	2,435,746	6	0
25,000	2,680	10,516	3,914,662	6,350,408	7	0
30,000	4,870	15,386	15,298,529	21,648,938	7	0
*Trafficking on 6 in. slabs only.						
35,000	500	15,886	3,001,009	24,649,946	7	1
35,000	1,000	16,886	6,002,017	30,651,964	7	1
35,000	3,500	20,386	21,007,061	51,659,024	7	2
35,000	2,954	23,340	17,729,959	69,388,983	7	4
Total	23,340		69,388,983		7	4

*ESAL magnification factor = 20

4.4.3 VERTICAL LVDTs – SECTION 1 SOUTH

Rebound deflection values were chosen to report the vertical deflection responses of the pavement. Rebound deflection is defined as the maximum downward deflection in any given pass minus the unloaded deflection of the slab for the same pass. The maximum rebound deflection almost always occurs when the wheel load is adjacent to the LVDT. Since there is no cumulative deformation included in the rebound deflection, it can be used for matching theoretical calculations. In the following figures, the legend numbers refer to the slab number and the letter is the location of the LVDT with respect to the cardinal points. For example 8 W refers to the LVDTs placed on the west side of slab 8 at the joint. M and E designate middle and east part of the slab, respectively. Figure 38 is an example of the LVDT nomenclature.

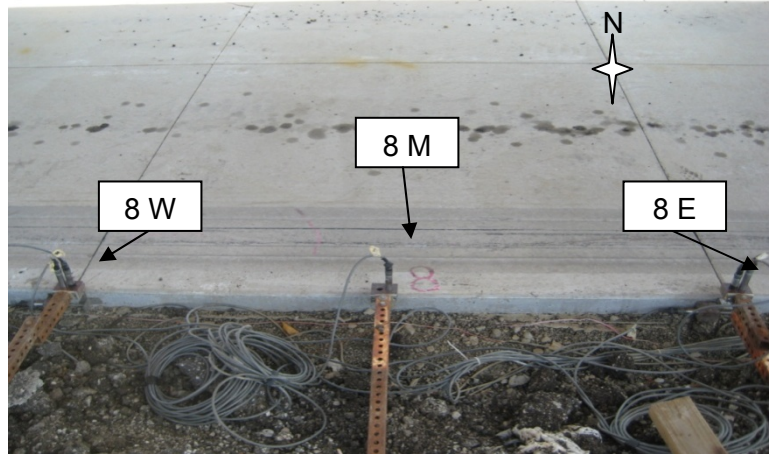


Figure 38. Description of LVDT nomenclature.

The rebound deflections presented in Figure 39 and Figure 40 represent the concrete pavement deflections during edge trafficking for various load levels. The rebound deflections for both slab thicknesses were less than 0.015 inch at a 9-kip load level. As expected, increasing the load level increased the rebound deflections. Figure 39 and Figure 40 also clearly demonstrate that there is a dominate joint, i.e., one joint deflects significantly more than an adjacent joint. The rebound deflections also increased during the same load level as a result of larger deformations occurring in the support layers (base and subgrade) and eventually fatigue cracks present on the concrete slabs. Repeated loading of the concrete slab on an asphalt base will also deteriorate the interface condition if some bond existed.

The rebound deflections on both the 4 inch and 6 inch part of section 1 (south) were similar as seen in Figure 39 and Figure 40. This behavior was due to the slabs being supported by a relatively thick asphalt base layer. However, in terms of cracking, all the 4 inch slabs cracked before any of the 6 inch slabs cracked.

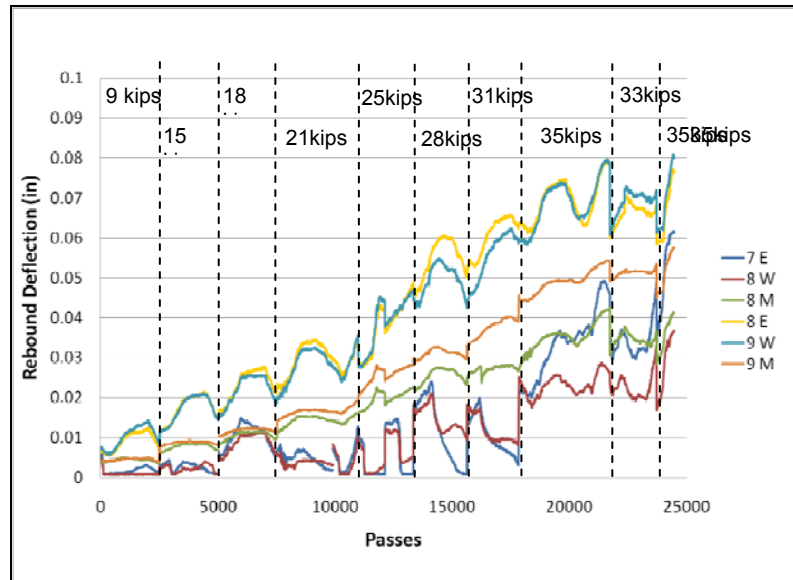


Figure 39. Rebound deflections of 4 in. concrete slab over 6.5 in. asphalt concrete (Section 1-south).

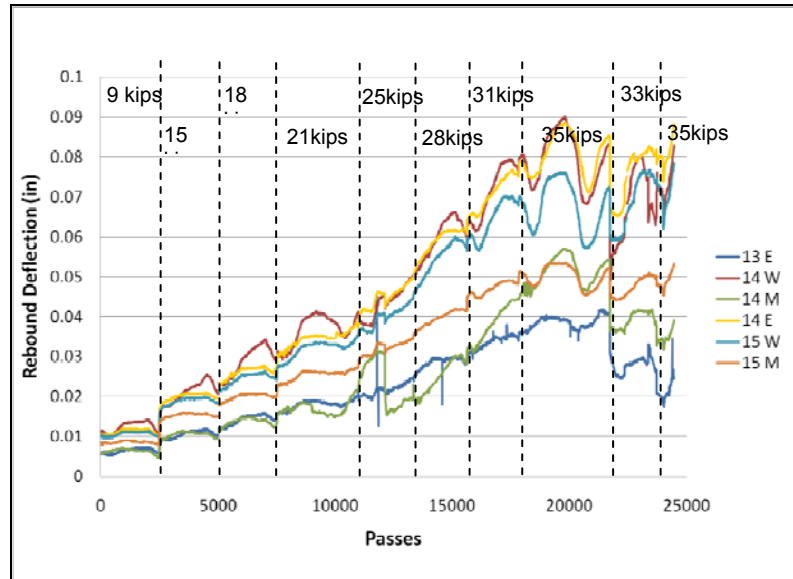


Figure 40. Rebound deflections of 6 in. concrete slab over 4.5 in. asphalt concrete (Section 1-south).

4.4.4 VERTICAL LVDTs – SECTION 1 NORTH

On section 1 (north), testing began in the wheel path (12 inch offset from the edge) for the first 2 days, followed by the trafficking near the edge. Figure 41 and Figure 42 show the rebound deflections for loading in the wheel path. The deflections on the 4 inch section were higher than the deflections on the 6 inch section. The deflections in the wheel path for section 1 (north) was greater than section 1 (south) deflections for near edge loading suggesting the support conditions were not as good (e.g., moisture content was higher in soil or interface condition was different). After approximately 4600 passes in the wheel path, there was no observed cracking and the loading was then moved to the edge position.

When the section was tested near the free edge cracking first appeared on the 4 inch section. These distresses became so great that at about 15,000 passes of the wheel, only the 6 inch section was further trafficked. Figure 43 shows the rebound deflection for the 4 inch section through the 15,000 passes, while Figure 44 describes the rebound deflection for the 6 inch section. Similar to section 1 (south), the deflections in section 1 (north) increased with load repetitions and load level. In Figure 44, there was a decrease in LVDT 13M deflection towards the end of testing, which was attributed to the surface cracking that occurred. Overall, the deflections for section 1 (north) were consistently higher than section 1 (south), which can be attributed to the larger amount of time moisture was present on the test section during trafficking.

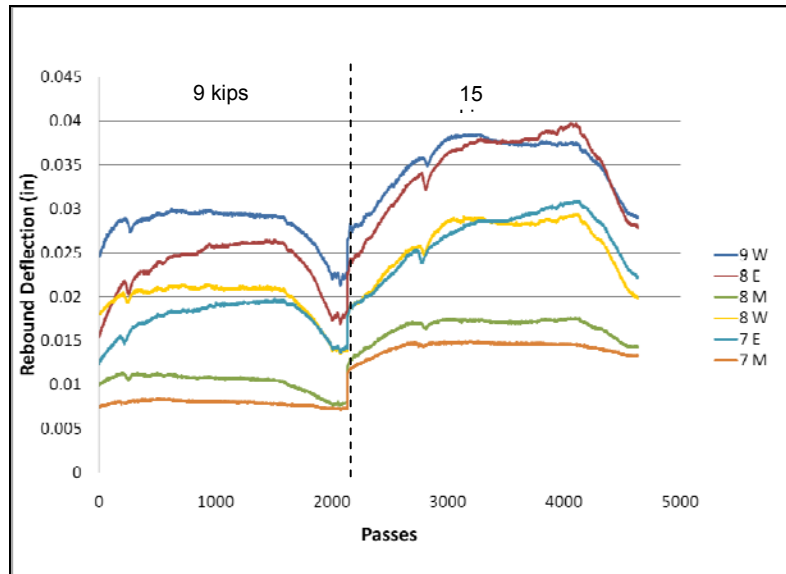


Figure 41. Wheel path rebound deflection of 4 in. concrete slab over 6.5 in. asphalt concrete (Section 1-north).

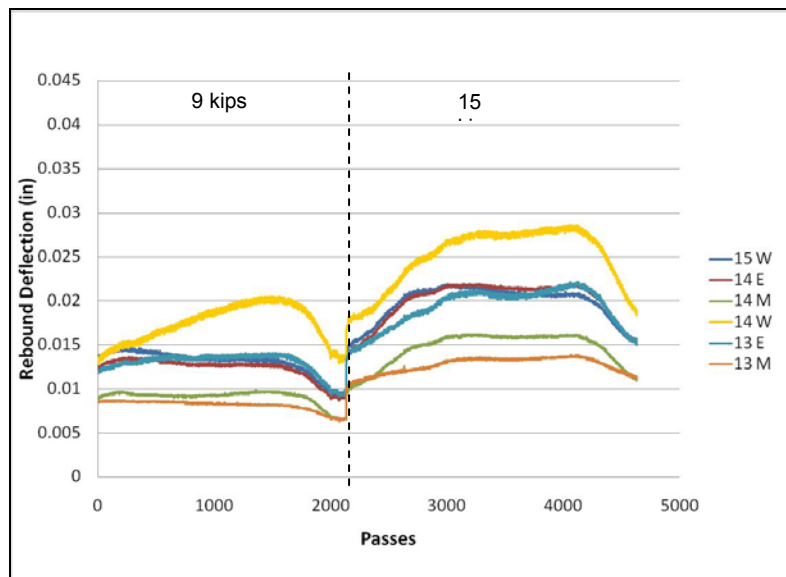


Figure 42. Wheel path rebound deflection of 6 in. concrete slab over 4.5 in. asphalt concrete (Section 1-north).

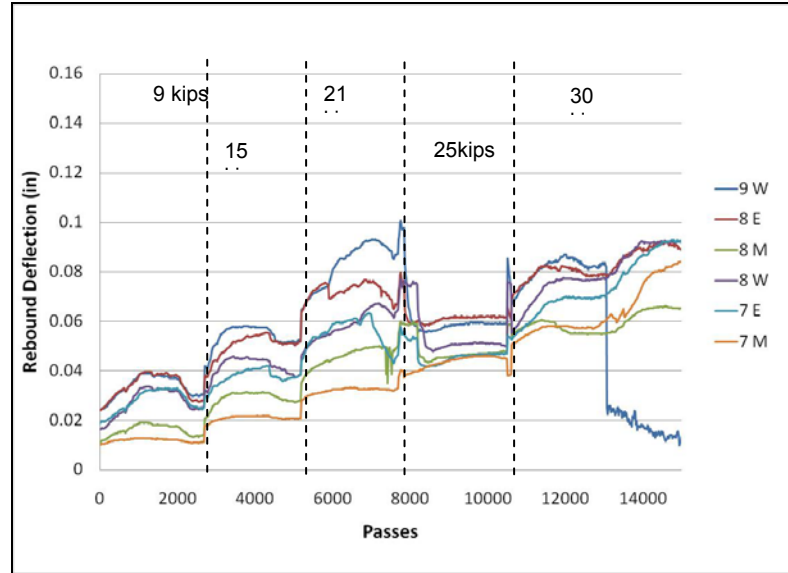


Figure 43. Rebound deflections of 4 in. concrete slab over 6.5 in. asphalt concrete (Section 1-north).

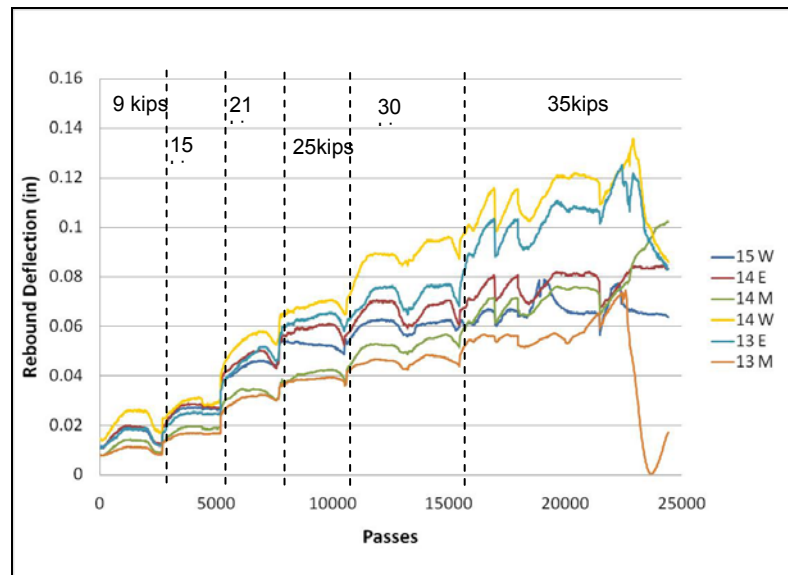


Figure 44. Rebound deflections of 6 in. concrete slab over 4.5 in. asphalt concrete (Section 1-north).

4.4.5 STRAINS – SECTION 1 SOUTH

A review of the strain gauge placement can be found in Appendix A.1. Figure 45 is a plot of the maximum tensile strain response for each gage location on section 1 (south) versus repetitions of various load magnitudes. The legend nomenclature, e.g., 8 J, refers to the slab number, the J is for the joint strain gauge at the top of the slab (0.25 in. from the top) while E is for the strain gauge place at the bottom of the slab (0.25 in. from the bottom) at the edge. In general, the strains increased as the load and the number of repetitions increased. However, the magnitude of the strain level was for the most part less than 100 microstrain. The only strain gauge that reported a high strain

level was included at the edge of slab 9. The results of the strain measurements suggested there was excellent contact friction or bond between the concrete slab and asphalt base layer.

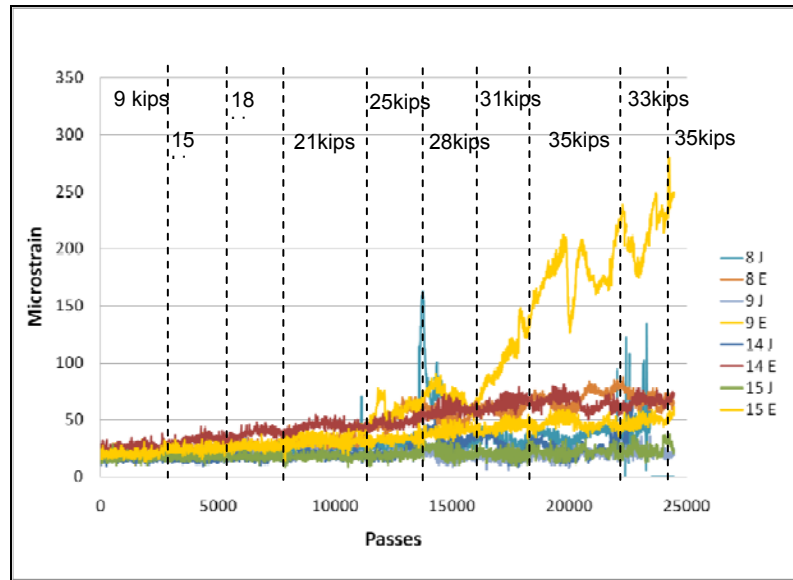


Figure 45. Tensile strain responses for 4 in. and 6 in. concrete over asphalt concrete (Section 1-north).

4.4.6 STRAINS – SECTION 1 NORTH

The strain gauges on the north side were placed differently than on the south side since wheel path loading was planned for these set of slabs. The strain gauges on the longitudinal edge were placed 0.25 inch from the bottom of the mid-slab location. The joint strain gauge was placed transversely near the joint at the bottom (0.25 inch from the bottom) about 20 inches laterally from the edge. Slabs 8 and 14 are on the 4 inch and 6 inch concrete sections, respectively.

Figure 46 is the plot of the strain data that was collected when section 1 (north) was trafficked along the wheel path. The tensile strain levels were below 50 microstrain even with a 15-kip single wheel load. When the loading location was moved to the edge, the strain magnitudes for the 4 inch section increased past 100 microstrain as shown on Figure 47. Surface cracking was seen after 5,000 repetitions on the 4 inch which can be seen in Figure 47 as the region where the strains increase more dramatically. Note, strain measurements will either increase or decrease depending on the location of the crack relative to the strain gauge.

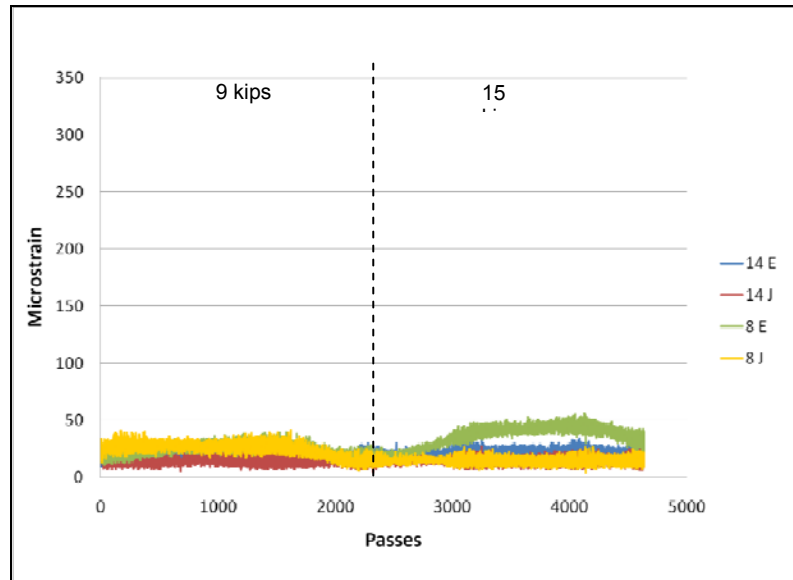


Figure 46. Wheel path tensile strains responses for 4 in. and 6 in. concrete slabs over asphalt concrete (Section 1-north).

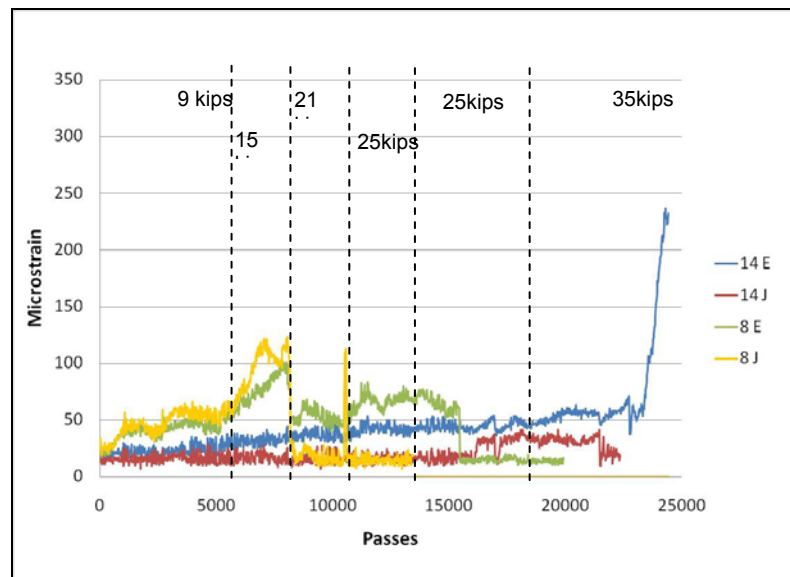


Figure 47. Edge loading responses for 4 in. and 6 in. concrete slabs over asphalt concrete (Section 1-north).

Considering the fatigue crack development, deflections, and strains, the 6 inch section performed better than the 4 inch section as expected. The accelerated pavement testing supports using both thickness of concrete for different levels of traffic. The 6 inch section on asphalt concrete base was generally able to consume 10 times more traffic than the 4 inch concrete section. Another key observation was the stabilized asphalt base layer below the concrete slowed the deterioration of the fatigue cracks, which was not the case for the 4 inch slab on granular base in section 3.

4.5 SECTION 2 LOADING

4.5.1 CRACK DEVELOPMENT SECTION 2 – SOUTH

Section 2 (south) consisted of 6 and 8 inches of concrete thickness over aggregate base. Slabs 27 through 33 are 6 inches thick and slabs 34 through 40 are 8 inches. Trafficking of the wheel carriage occurred near the free edge of the slab. The pattern and date in which the slabs cracked can be seen in Figure 48 to Figure 51. Only 4 out of the 7 slabs that were 6 inches thick on section 2 (south) had cracked after 22.9 million ESALs (See Figure 51). All four cracked slabs (3 corner breaks and one transverse crack) occurred on the 6 inch section (slabs 27 to 33) while no fatigue cracking was observed on the 8 inch (slabs 34 to 40) after 19.5 million ESALs. The fourth crack only appeared on slab 31 after it had been loaded with a 35,000 lb wheel load for 75 passes. Table 7 and Table 8 summarize the load level, number of repetitions, cumulative ESAL count, and number of cracked slabs in section 2 (south). Section 2 south did experience some joint spalling at the very edge of the slab as a result of inadequate sawcutting of the joint during the original construction.

Slab 27	28	29	30	31	32	33
						
Slab 34	35	36	37	38	39	40

Figure 48. Section 2 south cracking performance after 5/5/08 testing (6 inch=16.4 Million ESALs; 8 inch=14 Million ESALs).

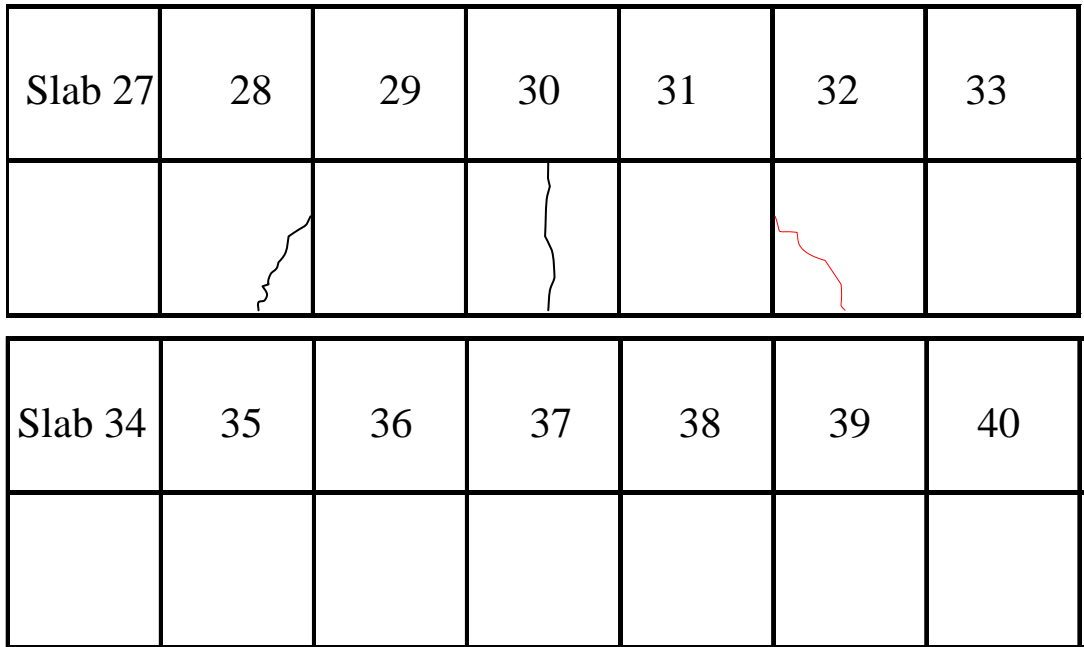


Figure 49. Section 2 south cracking performance after 5/9/08 testing (6 inch=20.2 Million ESALs; 8 inch=17.2 Million ESALs).

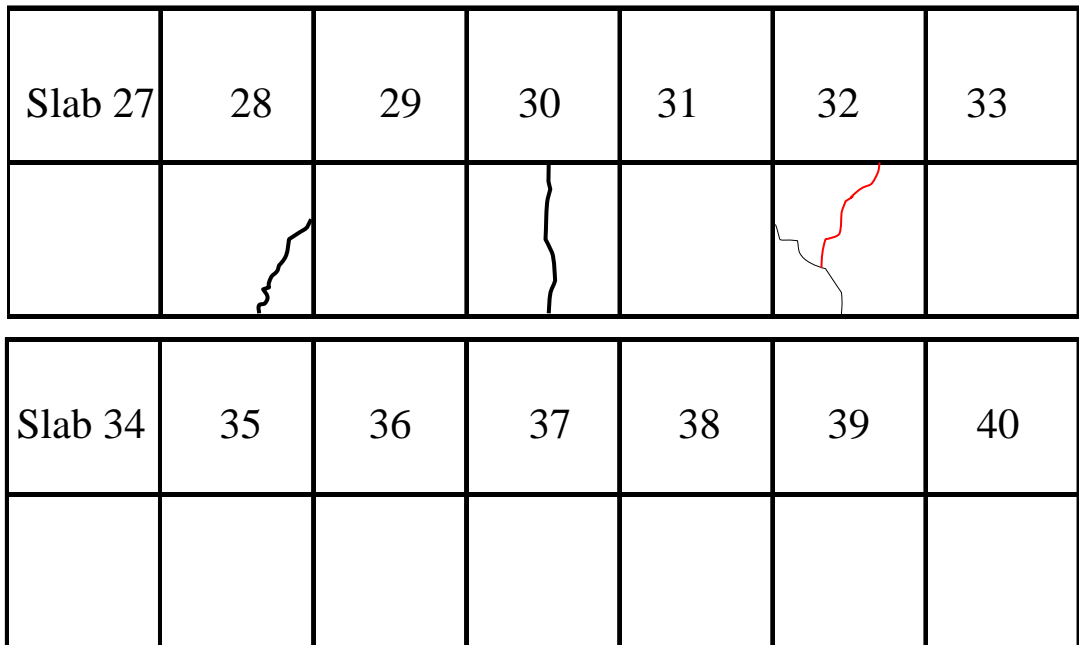


Figure 50. Section 2 south cracking performance after 5/10/08 testing (6 inch=22.5 Million ESALs; 8 inch=19.2 Million ESALs).

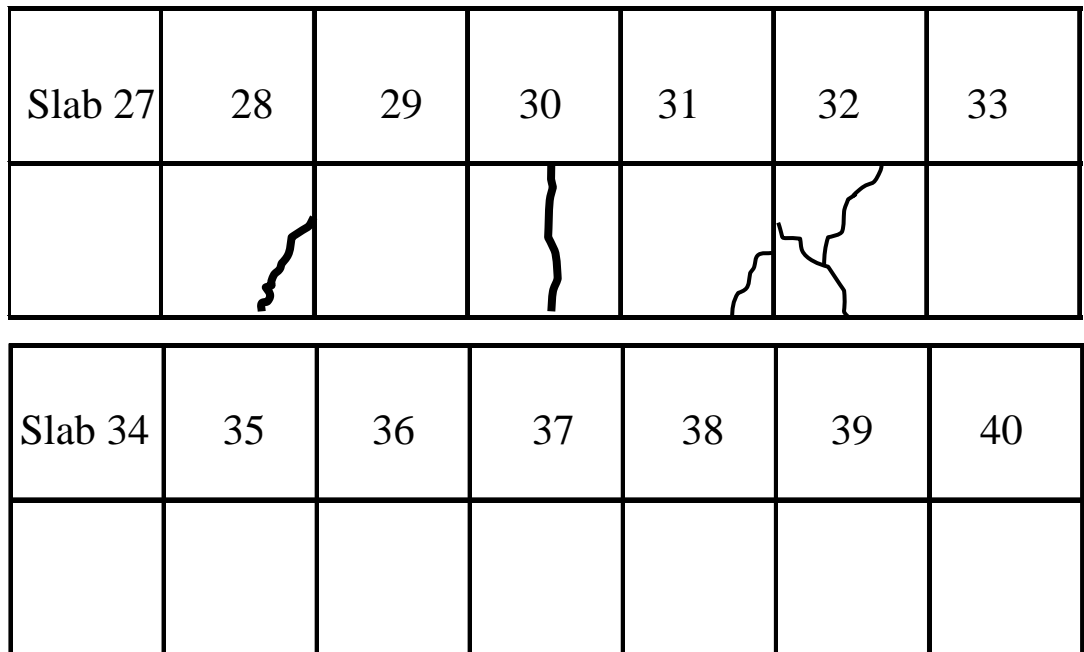


Figure 51. Section 2 south cracking performance after 5/12/08 testing (6 inch=22.9 Million ESALs; 8 inch=19.5 Million ESALs)

Table 7. Load repetitions and cracking summary for Section 2 south (6 in.)

Load (lb)	Passes	Cumulative Passes	ESALs	Cumulative ESALs	Cracks 6 in. / Granular
9,000	5,375	5,375	102,663	102,663	0
9,000	1,912	7,287	36,519	139,182	0
15,000	6,000	13,287	979,376	1,118,557	0
15,000	150	13,437	24,484	1,143,042	0
20,000	2,850	16,287	1,557,348	2,700,390	0
20,000	2,265	18,552	1,237,682	3,938,072	0
20,000	5,112	23,664	2,793,391	6,731,462	0
25,000	6,995	30,659	9,757,770	16,489,232	2
25,000	2,651	33,310	3,698,048	20,187,281	3
25,000	1,655	34,965	2,308,665	22,495,945	3
35,000	75	35,040	429,894	22,925,840	4
Total	35,040		2.29E+07		4

*ESAL magnification factor = 19

Table 8. Load repetitions and cracking summary for Section 2 south (8 in.)

Load (lb)	Passes	Cumulative Passes	ESALs	Cumulative ESALs	Cracks 8 in. / Granular
9,000	5,375	5,375	87,613	87,613	0
9,000	1,912	7,287	31,166	118,778	0
15,000	6,000	13,287	835,802	954,580	0
15,000	150	13,437	20,895	975,476	0
20,000	2,850	16,287	1,329,046	2,304,521	0
20,000	2,265	18,552	1,056,242	3,360,763	0
20,000	5,112	23,664	2,383,888	5,744,651	0
25,000	6,995	30,659	8,327,312	14,071,963	0
25,000	2,651	33,310	3,155,926	17,227,889	0
25,000	1,655	34,965	1,970,222	19,198,111	0
35,000	75	35,040	366,873	19,564,984	0
Total	35,040		1.96E+07		0

*ESAL magnification factor = 16

4.5.2 CRACK DEVELOPMENT SECTION 2 – NORTH

Section 2 (north) was first trafficked in the wheel path for two days. The direction of trafficking was from the east to west. The wheel position was then moved near the edge since no cracking was observed and the slab responses were small. After less trafficking than Section 2 (south), the section began exhibiting large corner cracks or transverse cracks that turned more toward the transverse joint. The progression of cracks can be seen in Figure 52 to Figure 54. The 6 inch section had 6 out of 7 cracked slabs after 16.9 million ESALs, which was earlier and more frequent than the cracks that appeared on Section 2 (south). The main reason for the performance difference is attributed to the large amount of rain storms and the freeze-thaw conditions experienced by the pavement section during trafficking.

At the 14.8 million ESALs level only the 8 inch section was tested. The 8 inch section did not show any fatigue cracking up to 51 million ESALs which was consistent with the trafficking results of section 2 (south). Table 9 and Table 10 are a summary of the load levels, number of repetitions, cumulative ESAL count, and number of cracked slabs in section 2 (north).

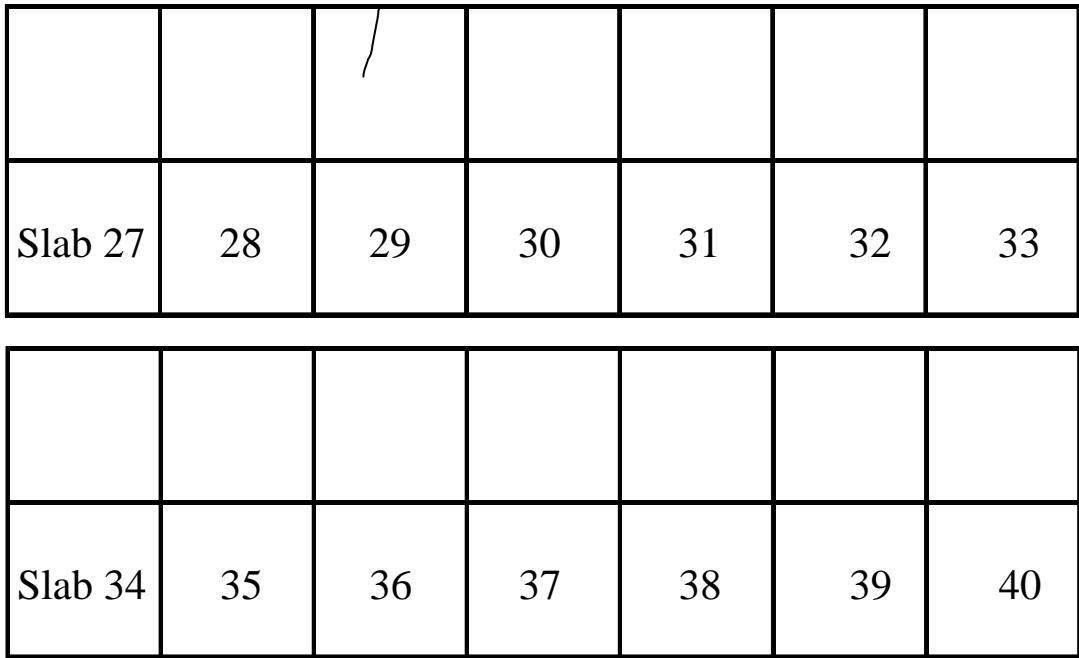


Figure 52. Section 2 north cracking performance after 3/30/09 testing (6 inch = 834,000 ESALs; 8 inch=730,000 ESALs).

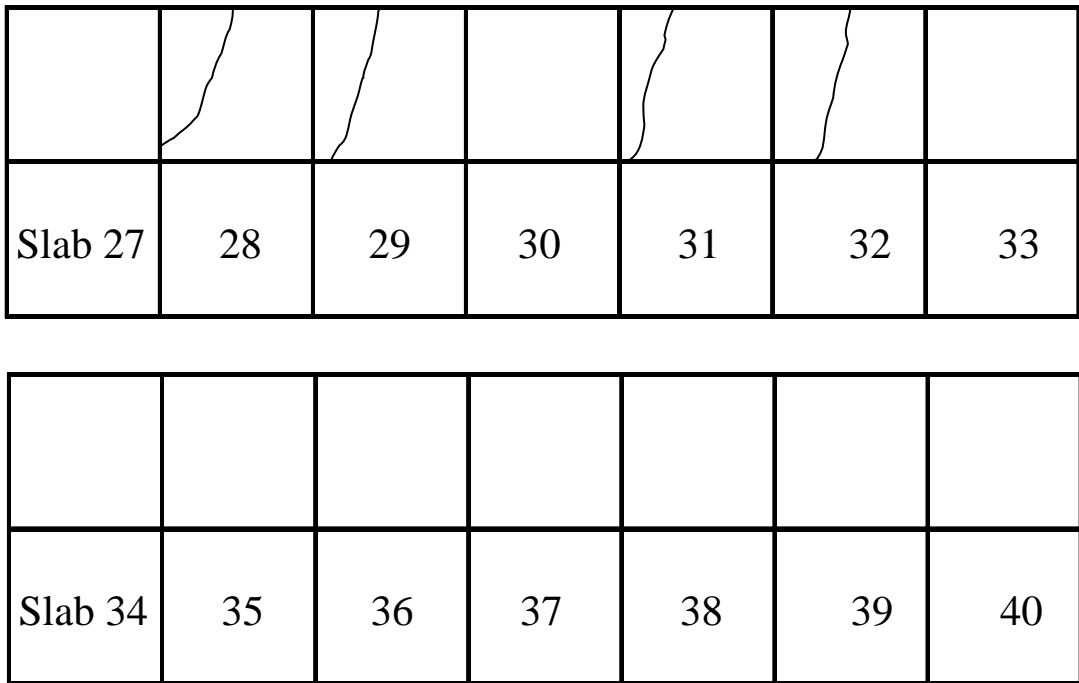


Figure 53. Section 2 north cracking performance after 4/6/09 testing (6 inch = 9.7 Million ESALs; 8 inch=8.5 Million ESALs).

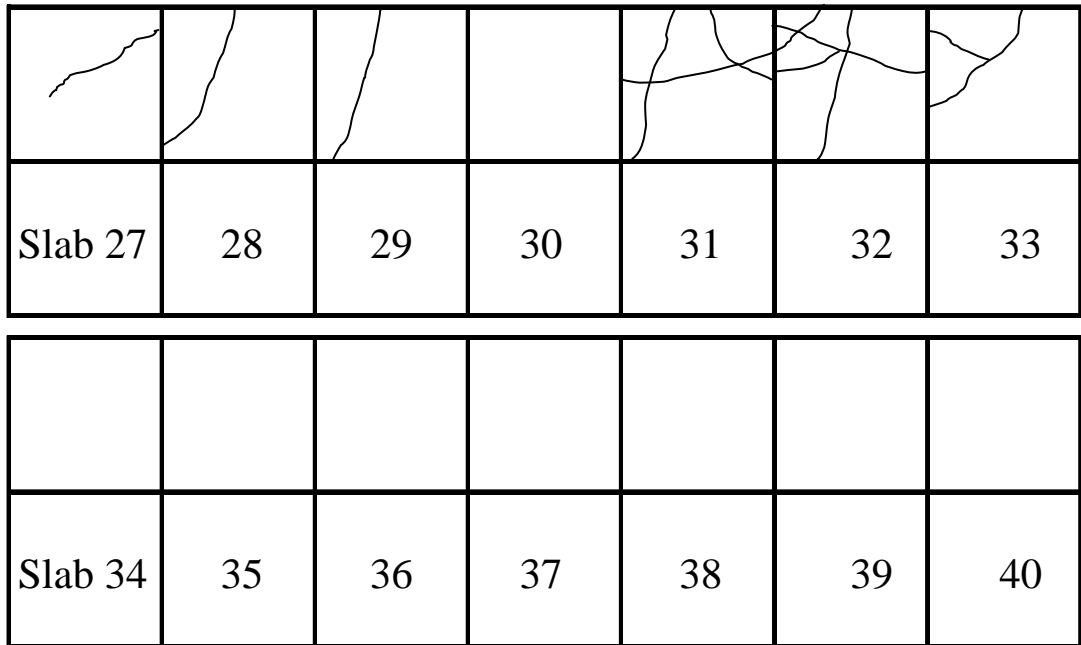


Figure 54. Section 2 north cracking performance after 4/10/09 testing (6 inch = 16.4 Million ESALs; 8 inch=14.3 Million ESALs).

Table 9. Load repetitions and cracking summary for Section 2 north (6 in.)

Load (lb)	Passes	Cumulative Passes	ESALs	Cumulative ESALs	Cracks 6 in. / Granular
Wheel Path - 12 in. offset					
9,000	2,057	2,057	2,057	2,057	0
15,000	3,010	5,067	25,724	27,781	0
Total	5,067	10,134	27,781		0
Edge Loading - 5 in. offset					
9,000	2,850	2,850	50,160	50,160	0
9,000	150	3,000	2,640	52,800	0
15,000	3,187	6,187	479,357	532,157	1
15,000	1,913	8,100	287,735	819,892	1
15,000	100	8,200	15,041	834,933	1
18,000	5,000	13,200	1,617,367	2,452,301	1
21,000	5,000	18,200	3,090,190	5,542,490	1
25,000	816	19,016	1,048,896	6,591,386	1
25,000	1,801	20,817	2,315,026	8,906,412	4
25,000	640	21,457	822,663	9,729,076	4
27,000	2,405	23,862	4,271,073	14,000,149	4
30,000	200	24,062	552,883	14,553,032	4
35,000	200	24,262	1,056,355	15,609,387	5
35,000	150	24,412	792,266	16,401,653	5
35,000	32	24,444	169,017	16,570,670	6
25,000	292	24,736	375,340	16,946,010	6
Total	24,736		16,946,010		6

*ESAL magnification factor = 18

Table 10. Load repetitions and cracking summary for Section 2 north (8 in.)

Load (lb)	Passes	Cumulative Passes	ESALs	Cumulative ESALs	Cracks 8 in. / Granular
Wheel Path - 12 in. offset					
9,000	2,057	2,057	2,057	2,057	0
15,000	3,010	5,067	25,724	27,781	0
Total	5,067	10,134	27,781		
Edge Loading - 5 in. offset					
9,000.00	2,850	2,850.00	43,890.00	43,890	0
9,000.00	150	3,000.00	2,310.00	46,200	0
15,000.00	3,187	6,187.00	419,437.77	465,638	0
15,000.00	1,913	8,100.00	251,767.95	717,406	0
15,000.00	100	8,200.00	13,160.90	730,567	0
18,000.00	5,000	13,200.00	1,415,196.37	2,145,763	0
21,000.00	5,000	18,200.00	2,703,916.17	4,849,679	0
25,000.00	816	19,016.00	917,783.78	5,767,463	0
25,000.00	1,801	20,817.00	2,025,647.77	7,793,111	0
25,000.00	640	21,457.00	719,830.41	8,512,941	0
27,000.00	2,405	23,862.00	3,737,189.08	12,250,130	0
30,000.00	200	24,062.00	483,772.80	12,733,903	0
35,000.00	200	24,262.00	924,310.66	13,658,214	0
35,000.00	150	24,412.00	693,233.00	14,351,447	0
35,000.00	32	24,444.00	147,889.71	14,499,336	0
25,000.00	292	24,736.00	328,422.63	14,827,759	0
25,000.00	152	24,888.00	170,959.72	14,998,719	0
35,000.00	300	25,188.00	1,386,465.99	16,385,185	0
35,000.00	7,070	32,258.00	32,674,381.93	49,059,567	0
25,000.00	2,000	34,258.00	2,249,470.04	51,309,037	0
Total	34,258		51,309,036.68		0

*ESAL magnification factor = 15

4.5.3 VERTICAL DEFLECTIONS – SECTION 2 SOUTH

The subbase in Section 2 had 6 inches of granular material with approximately 6% passing the #200 sieve. The measured rebound deflections in section 2, presented in Figure 55 and Figure 56, were much greater than the deflections in section 1 which was supported by an asphalt concrete base. The deflections along the edge of the slab for both 6 and 8 inch section increased with load repetition and load level as seen in Figure 55 and Figure 56. The deflection difference between the 6 and 8 inch section was not as significant with both slab thickness varying between 1 and 2 mm deflection under

9-kip loading. The deflection of the slabs under 25-kip single wheel was high (3.5 to 5 mm) but due to the optimized slab geometry, cracking did not occur on the 8 inch slabs. The deflections of these slabs (6 and 8 inch) were more dependent on the stiffness of the support condition, i.e., the effective modulus of subgrade reaction. Therefore, higher CBR soils can be expected to produce significantly less deflections and thus should have a longer fatigue life. This is somewhat demonstrated by the section 1 results with the asphalt concrete base layer and section 3 tests completed in the winter with a frozen subgrade.

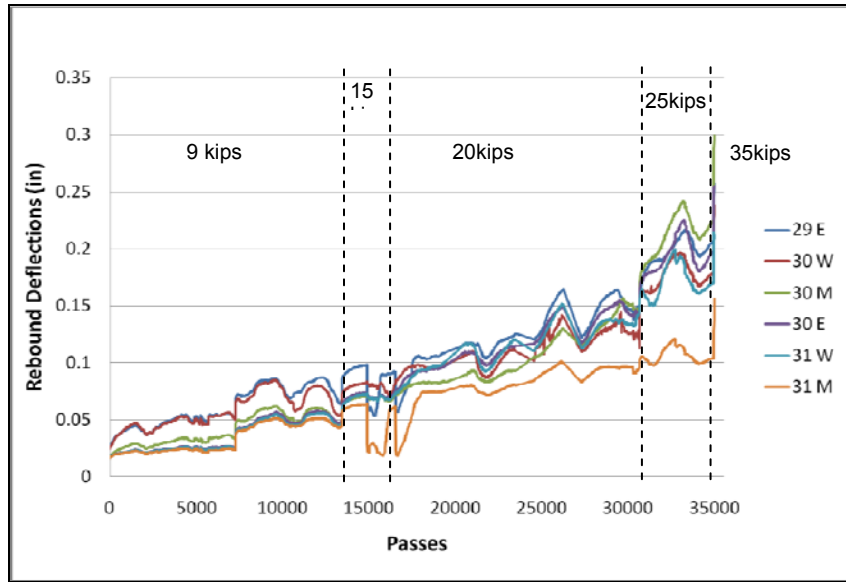


Figure 55. Rebound deflections of 6 in. concrete slab over granular base (Section 2-south).

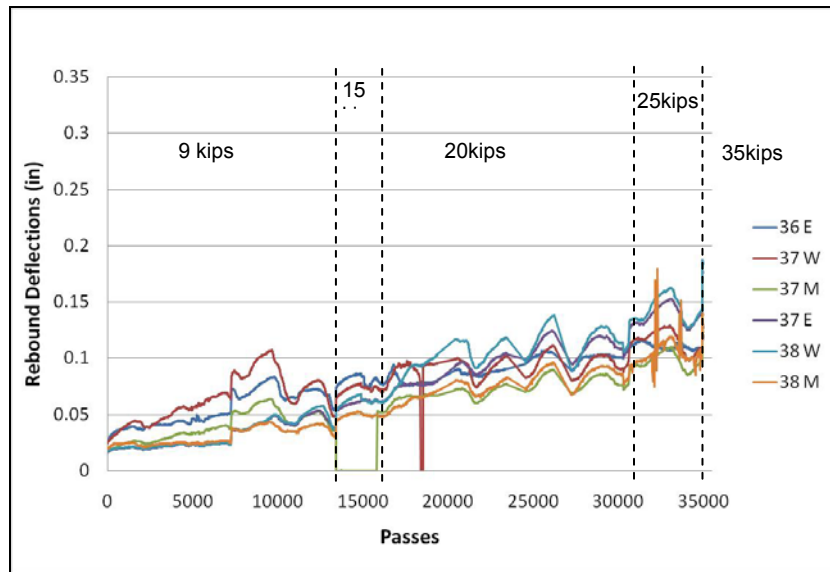


Figure 56. Rebound deflections of 8 in. concrete slab over granular base (Section 2-south).

4.5.4 VERTICAL DEFLECTIONS – SECTION 2 NORTH

Figure 58 and Figure 59 show the rebound deflection along the edge of the slab for two days of wheel path trafficking. As expected the deflections of the 6 in section were higher than the deflections of the 8 in section throughout the wheel path testing. The rebound deflections increased significantly when the wheel carriage was trafficking near the edge of the slab as seen in Figure 60 and Figure 61. The deflections continued to increase as the load level and number of repetitions increase but at a much slower rate for the 8 inch slabs. The rebound deflections were significantly less for the 8 inch slabs compared to the 6 inch slab.

The deflections on the 6 inch slabs for the north and south sections were approximately the same. However, the north section 6 inch slabs contained more cracked slabs and greater severity than the south section. Recall during the section 2 (north) testing, the moisture conditions in the pavement system required placement of a water pump at the edge of the section to facilitate drainage as seen in Figure 57. The deflections of the 8 inch slabs on the north and south parts of section 2 were similar as seen in Figure 56 and Figure 61.



Figure 57. Water pump used to drain Section 2 North.

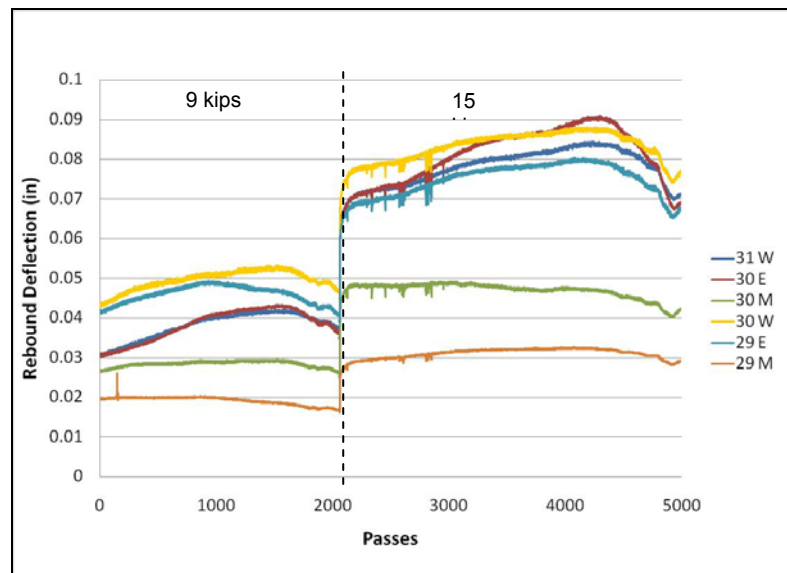


Figure 58. Wheel path rebound deflection of 6 in. concrete slab over granular base (Section 2-north).

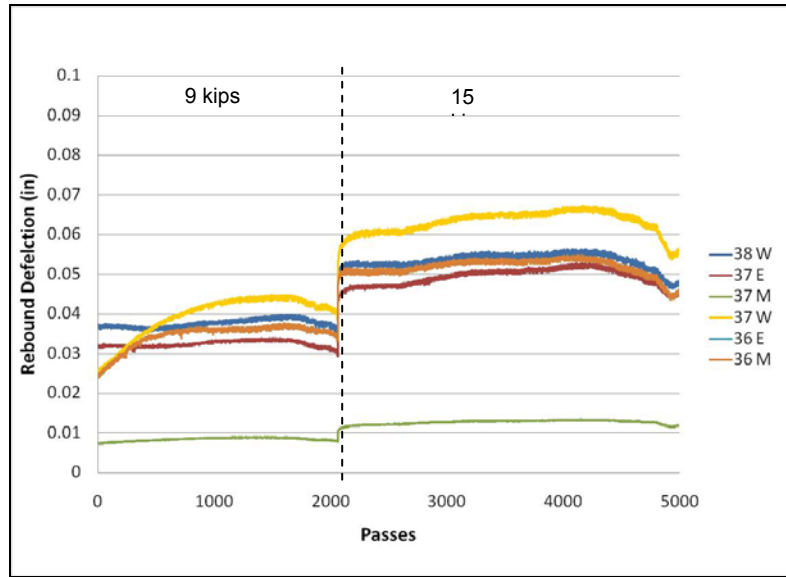


Figure 59. Wheel path rebound deflection of 8 in. concrete slab over granular base (Section 2-north).

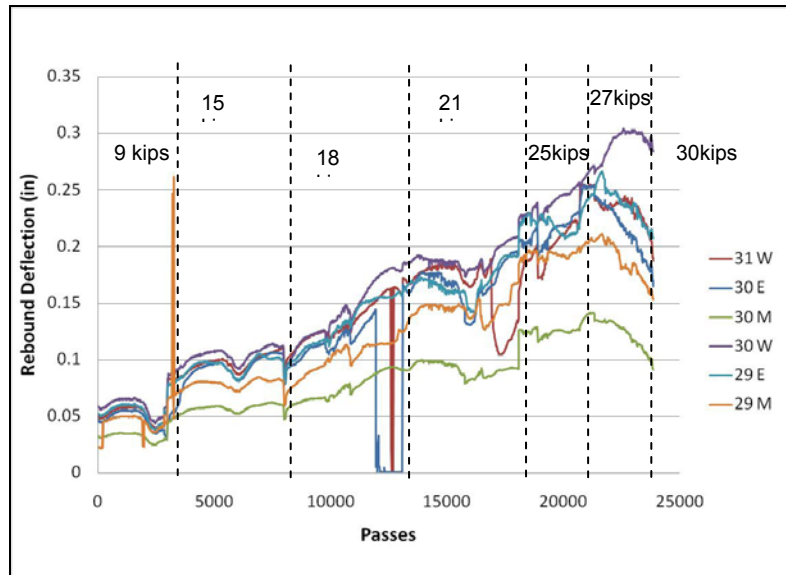


Figure 60. Rebound deflections of 6 in. concrete slab over granular base (Section 2-north).

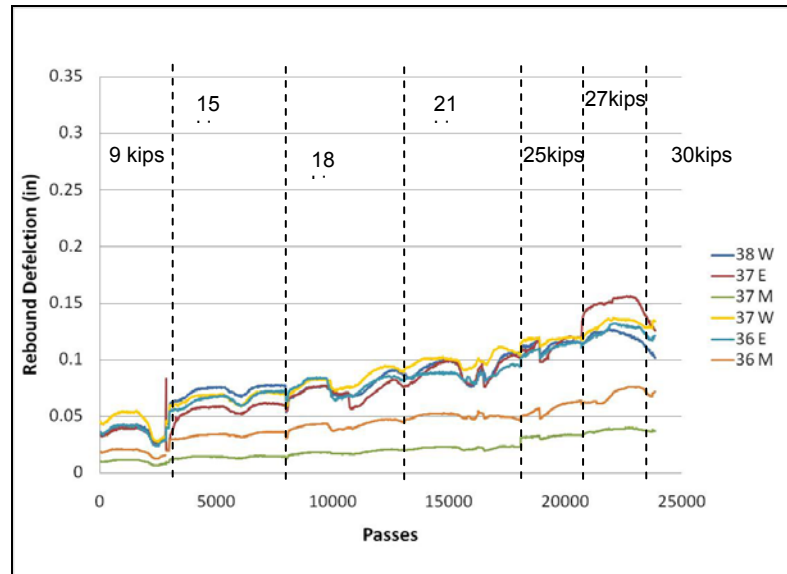


Figure 61. Rebound deflections of 8 in. concrete slab over granular base (Section 2-north).

4.5.5 TENSILE STRAINS – SECTION 2 SOUTH

Figure 62 shows the tensile strains in the 6 and 8 inch slabs while the wheel carriage was trafficking near the slab edge. The strains at the bottom edge of the slab were greater than the top of the slab at the transverse joint. Assuming uniform support beneath the slab, transverse cracking would be expected. Cracking appeared on the surface of the slabs after 30,000 passes of the wheel, which represented more than 16.4 million ESALs. There was one transverse crack and two corner breaks on the 6 inch section suggesting that a greater degree of deformation occurred in the support layers. The measured tensile strains in the 8 inch section were less than 100 microstrain for almost the entire loading period. After 19.6 million ESALs, there was no fatigue cracking observed on the 8 inch section, which was consistent with the magnitude of measured strain.

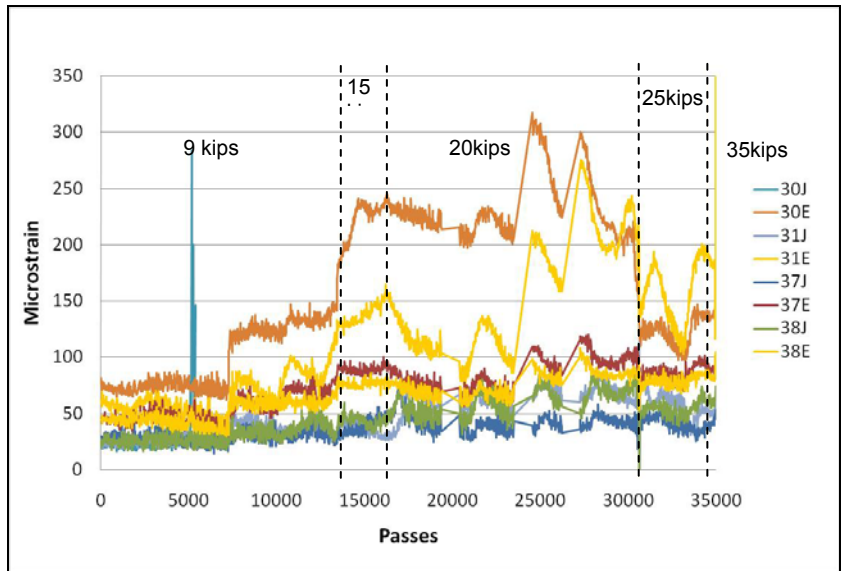


Figure 62. Maximum tensile strain responses for 6 and 8 in over granular base– (Section 2 – south)

4.5.6 TENSILE STRAINS – SECTION 2 NORTH

For section 2 (north), slab 30 was instrumented with strain gauges for the 6 inch section and slab 37 for the 8 inch section. Figure 63 shows the strains at 9 and 15-kips were very small for the wheel path loading. When the concrete slabs were tested near the free edge the tensile strain stayed below 100 microstrain as shown Figure 64, for both the 6 and 8 inch.

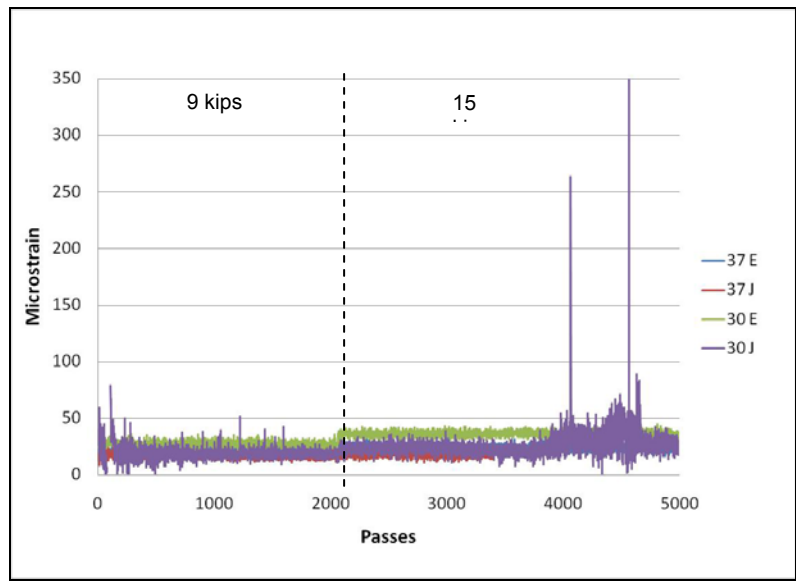


Figure 63. Tensile strains in 6 and 8 inch concrete slab over granular base for wheel path loading.

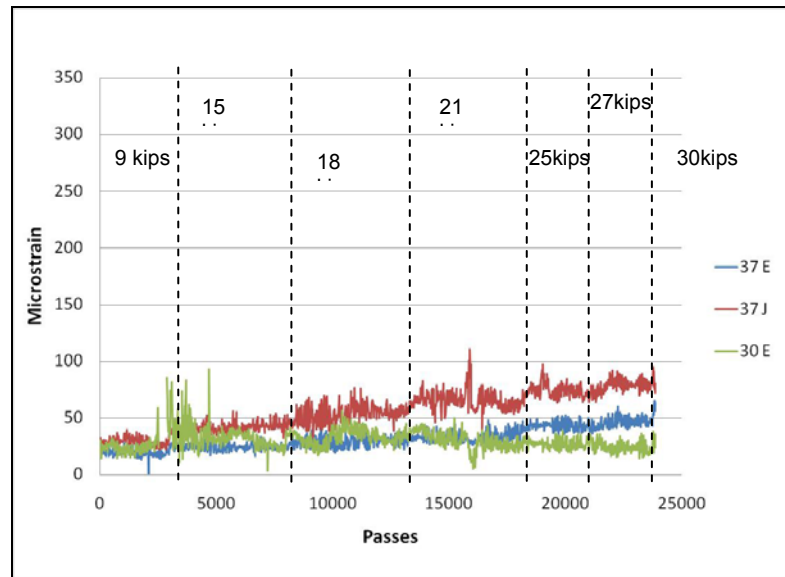


Figure 64. Tensile strains in 6 and 8 inch concrete slab over granular base for edge loading.

The 6 inch slabs over the asphalt concrete in section 1 performed significantly better than the 6 inch slabs over a granular base in section 2. However, both designs can sustain a large amount of ESALs before structural and functional failure. The 8 inch slabs in section 2 performed excellent despite large deformations. The smaller slab size allowed for the reduction in the slab's tensile stresses. Assuming the underlying support and joint conditions could be maintained, this thickness of slab could provide a perpetual concrete pavement. It could also be advantageous to apply to locations where overloads of unknown magnitudes are expected.

4.6 SECTION 3 LOADING

4.6.1 CRACK DEVELOPMENT SECTION 3 – SOUTH

Section 3 consists of 3.5 inch slab thickness over a six inch granular base. The test variable in this section is half of the slabs are plain concrete (slabs 49 to 55) while the other half of the slabs (slabs 56 to 62) are fiber reinforced concrete. The initial crack on slab 51 appeared prior to any load testing and was likely a result of instrumentation wires bundled under the slab going to the datalogger located adjacent to the section.

Section 3(south) was first load tested in January 2008 during frozen conditions. As seen in Table 11, no cracks occurred on the section after more than 229,000 ESALs had been applied. The frozen subgrade condition provided an extremely high CBR support value that did not allow for any fatigue cracking to develop in the slab.

Section 3 (south) was loaded a second time in April 2008 when the soil had thawed. The initial wheel load of 5-kips did not produce any fatigue cracking. The load level was increased to 9-kips for the trafficking and the first slab cracks began to appear 75,000 ESALs. The soil was saturated during the time of testing due to the intermittent rain. The initial fatigue crack began on slab 55 and spread to the adjacent slabs as shown in

Figure 65 to Figure 67. By the end of the trafficking, all of the plain concrete slabs had cracked, while only 3 out of 7 slabs on the fiber reinforced section were cracked. The severity of the plain concrete distresses were much higher than the fiber reinforced concrete slabs. The plain concrete slabs were broken into smaller pieces compared to the fiber reinforced concrete slabs. The structural fibers added to the plain concrete demonstrated two benefits: the FRC slabs were able to resist fatigue cracking for a larger number of ESALs and maintain the continuity across fatigue cracks better than the plain concrete slabs.

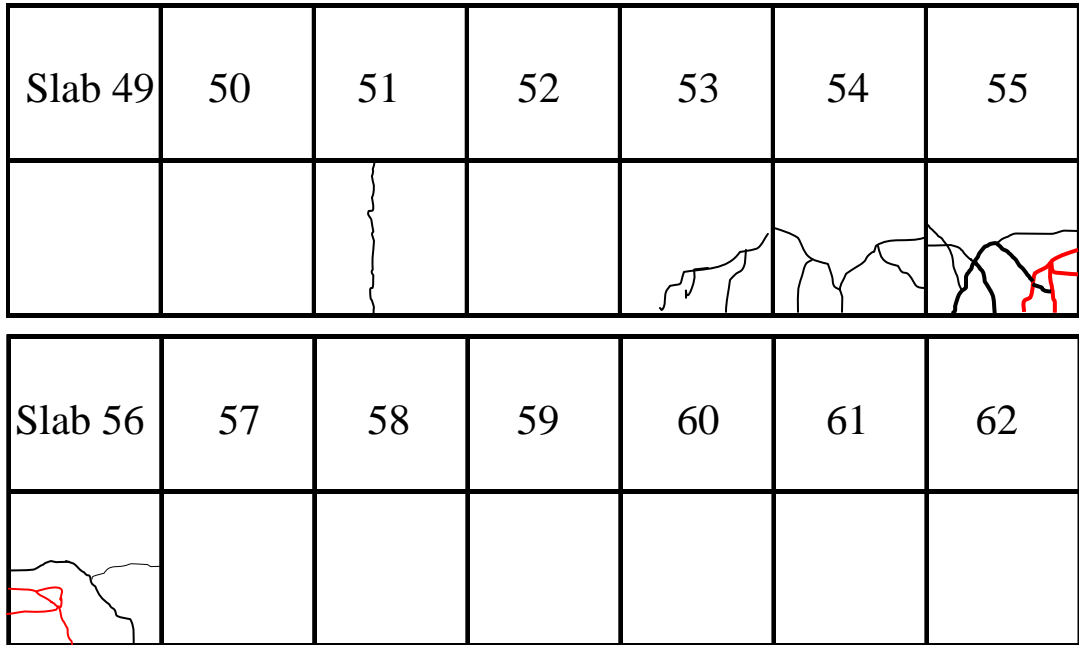


Figure 65. Section 3 south cracking performance after 4/19/08 testing (192,000 ESALs).

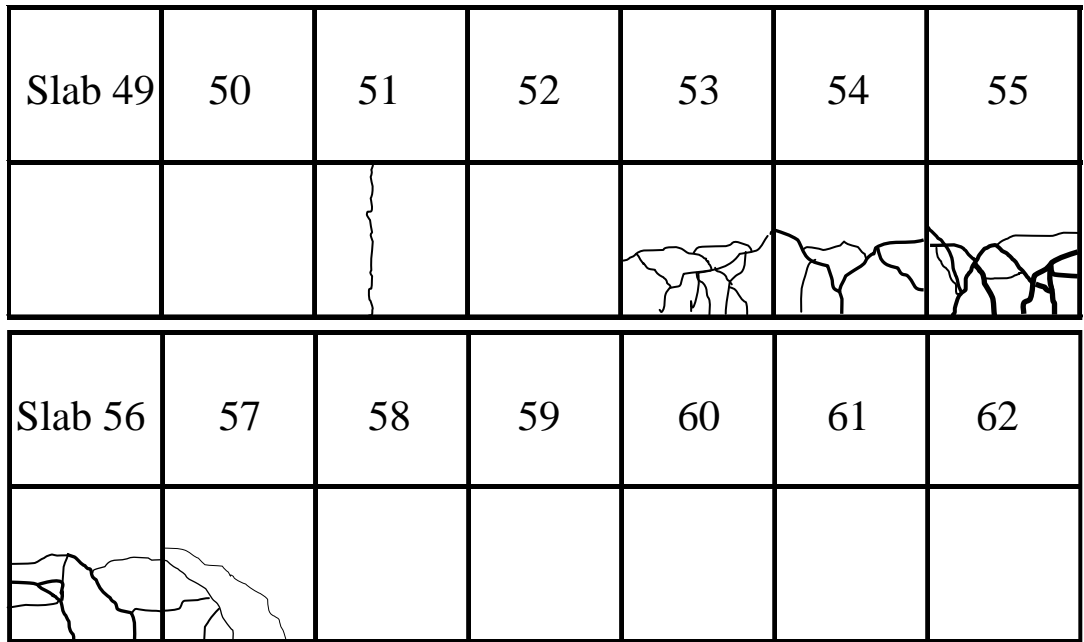


Figure 66. Section 3 south cracking performance after 4/21/08 testing (233,000 ESALs).

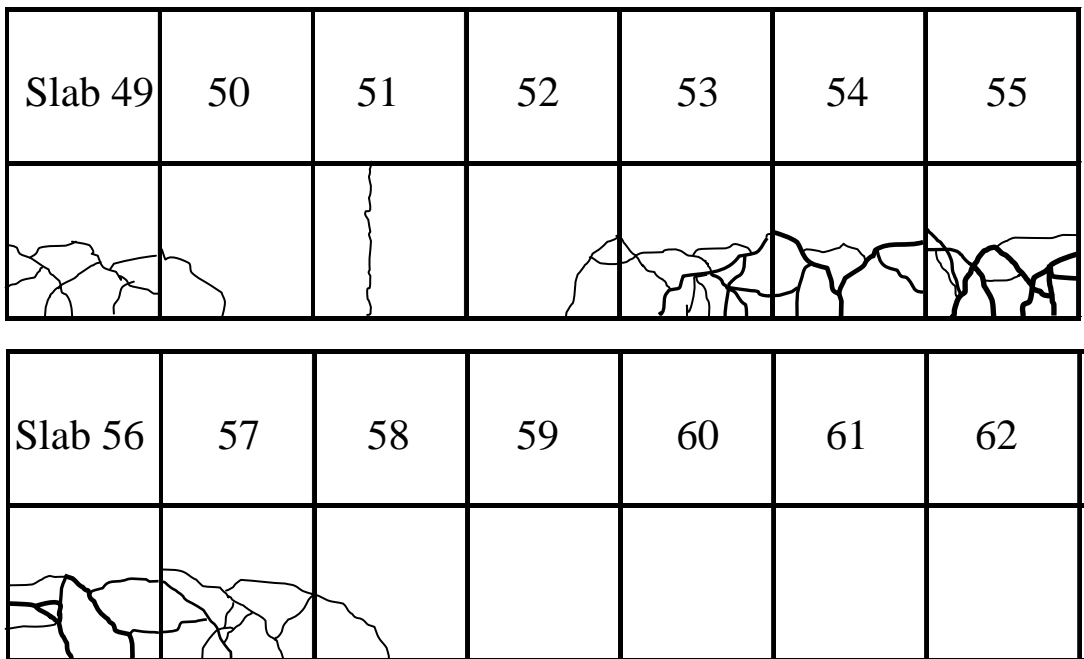


Figure 67. Section 3 south final cracking performance after 234,000 ESALs.

Table 11. Load repetitions and cracking summary for Section 3 south (January 2008)

Load (lb)	Passes	Cumulative Passes	ESALs	Cumulative ESALs	Cracks 3.5 in. Plain / Granular	Cracks 3.5 in. FRC / Granular
5,000	2,640	2,640	4,472	4,472	0	0
9,000	2,825	5,465	56,500	60,972	0	0
9,000	8,414	13,879	168,280	229,252	0	0
Total	13,879		229,252		0	0

Table 12. Load repetitions and cracking summary for Section 3 south (April 2008).

Load (lb)	Passes	Cumulative Passes	ESALs	Cumulative ESALs	Cracks 3.5 in. Plain / Granular	Cracks 3.5 in. FRC / Granular
5,000	2,643	2,643	4,477	4,477	0	0
5,000	2,778	5,421	4,706	9,183	0	0
9,000	3,000	8,421	60,000	69,183	0	0
9,000	309	8,730	6,180	75,363	0	0
9,000	5,875	14,605	117,500	192,863	4	1
9,000	2,053	16,658	41,060	233,923	4	2
12,000	10	16,668	670	234,592	7	3
Total	16,668		234,592		7	3

4.6.2 CRACK DEVELOPMENT SECTION 3 – NORTH

Section 3 (north) was first trafficked in the wheel path for two days. The direction of trafficking was from the east to west. Fatigue cracking began suddenly appeared on the plain section right before 3,000 ESALs. The premature development of cracks changed the test plan wheel path loading to trafficking adjacent to the longitudinal contraction joint. At the time the when the wheel path was tested the soil was in the process of thawing and thus the support strength was extremely low. It is highly likely that the thawing occurred non-uniformly such that the support near the edge of the slab thawed more rapidly than the interior of the slab. These conditions lead to the premature longitudinal cracking of the slabs as seen in Figure 68. After the fatigue cracking was observed on the plain concrete section, the trafficking was only on the fiber reinforced section, i.e., wheel loading only from 55 to 62. The additional loading on the FRC section lead to more cracking as shown in Figure 69 and Figure 70. As in trafficking in Section 3 (south), the fiber reinforced concrete was more resistant to fatigue cracking having only 2 cracked slabs at 4,500 ESALs.

In order to learn more about the fatigue life of thin concrete slabs especially the resistance of this pavement system trafficked along a contraction joint (e.g., concrete shoulder or curb/gutter condition), testing commenced along the longitudinal contraction joint. As expected, the plain concrete section cracked before the fiber reinforced concrete section as seen in Figure 71 to Figure 74. After testing the longitudinal joint for 4,500 ESALs, only the fiber reinforced concrete was loaded. A wander magnification factor was not used in the ESAL calculation for the longitudinal joint trafficking. At the end of the test, all plain concrete slabs were cracked and 4 out of 7 fiber reinforced concrete slabs were cracked along the longitudinal joint. The final trafficking load for the FRC slabs was 24-kips. The total ESALs applied to the longitudinal joint was 64,000. Unequivocally, the trafficking on the 3.5 inch section demonstrated the structural benefit of macrofibers in enhancing the fatigue life of plain concrete slabs. Table 13 and Table 14 are summaries of the load levels, number of repetitions, cumulative ESAL count, and number of cracked slabs in section 3 (north).

Slab 49	50	51	52	53	54	55
Slab 56	57	58	59	60	61	62

Figure 68. Wheel path testing of Section 3 north (2,960 ESALs).

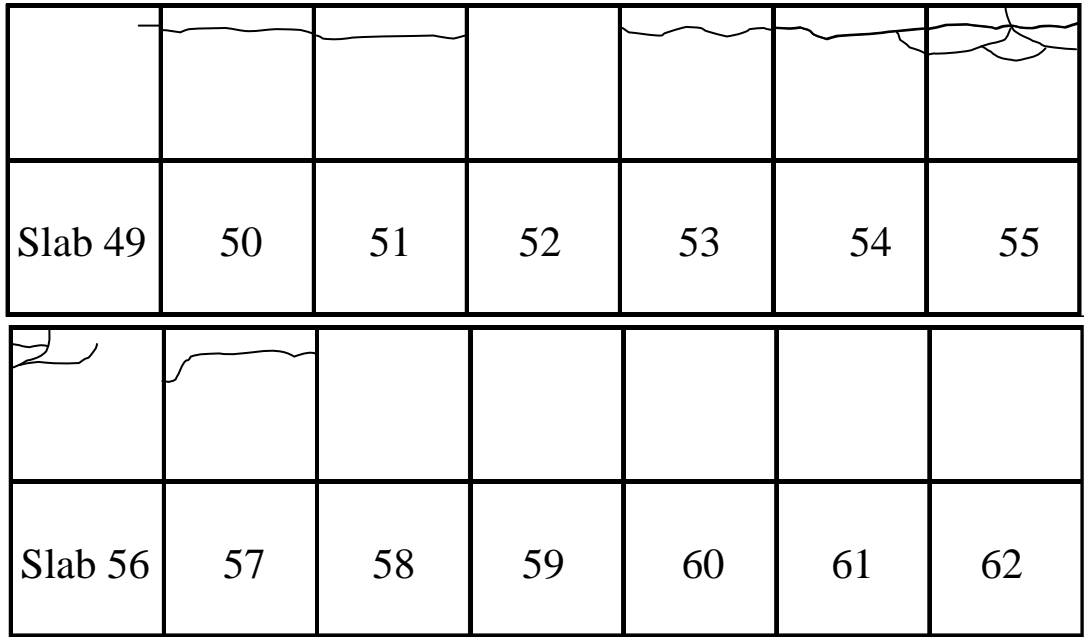


Figure 69. Wheel path testing Section 3 north FRC 3/9/09 (3,103 ESALs).

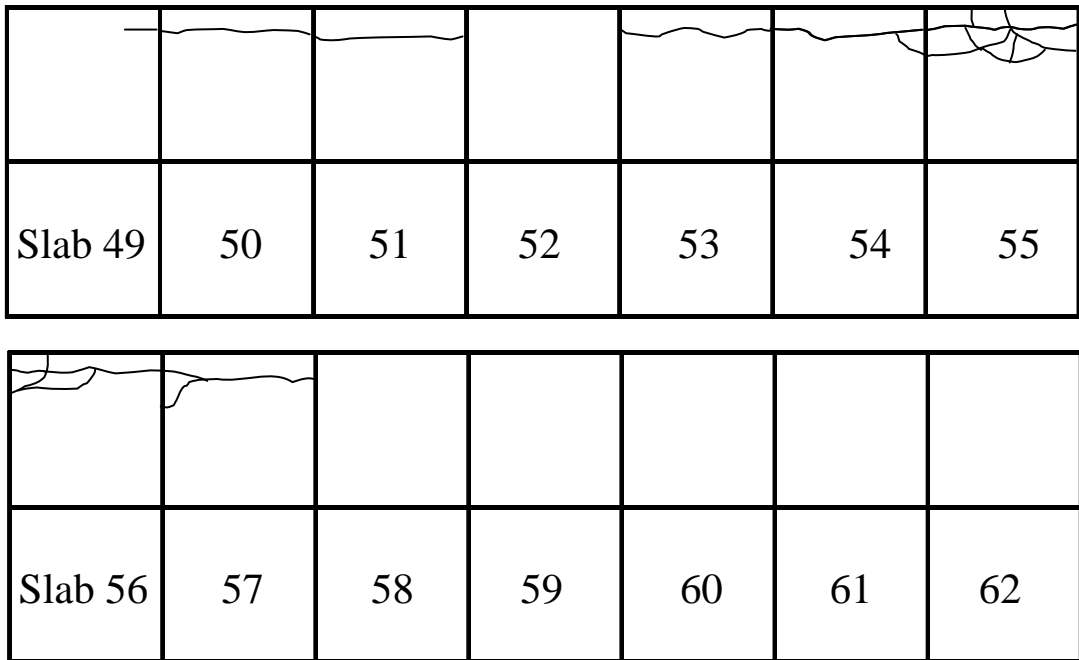


Figure 70. Wheel path testing Section 3 north 3/10/09 (4,545 ESALs).

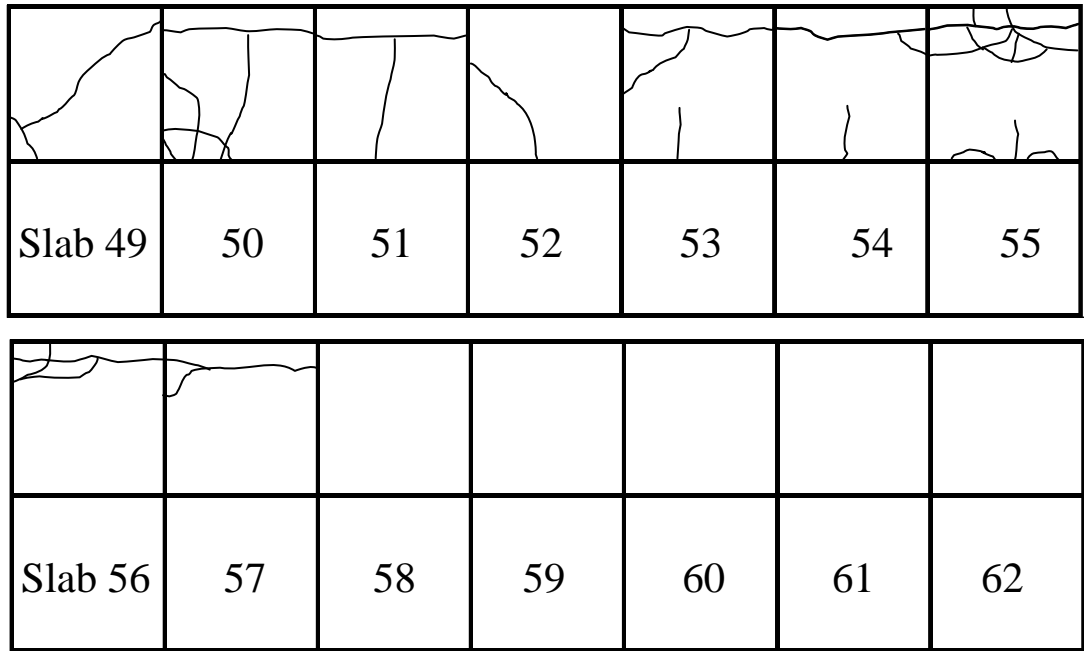


Figure 71. Longitudinal joint loading cracking pattern 3/14/09 (4,700 ESALs).

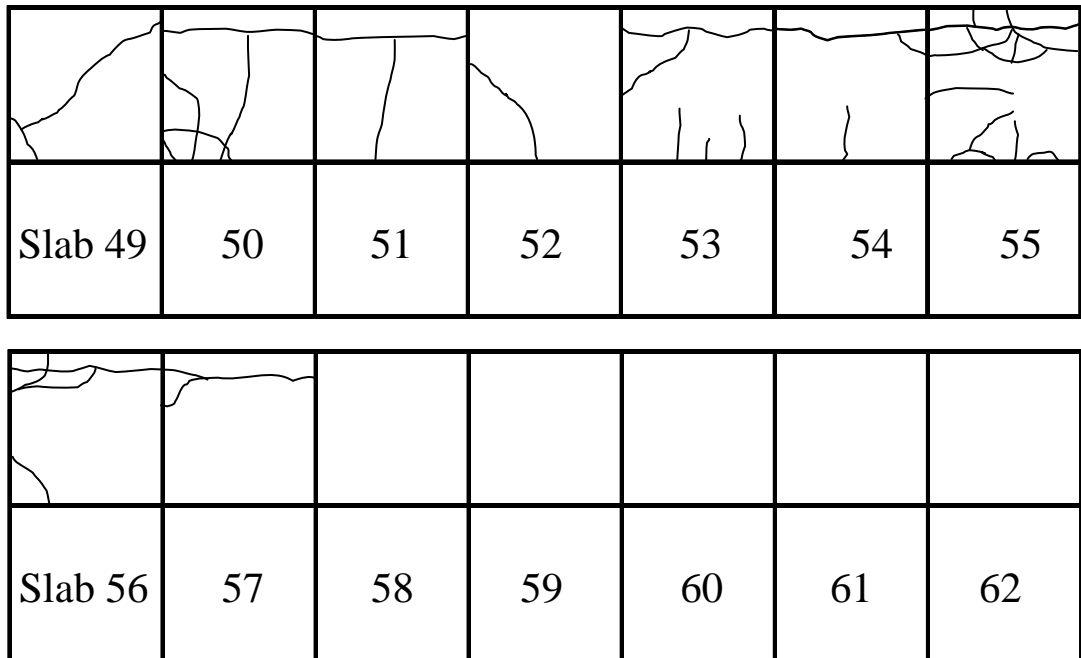


Figure 72. Cracking pattern for longitudinal joint trafficking on 3/15/09 (48,000 ESALs).

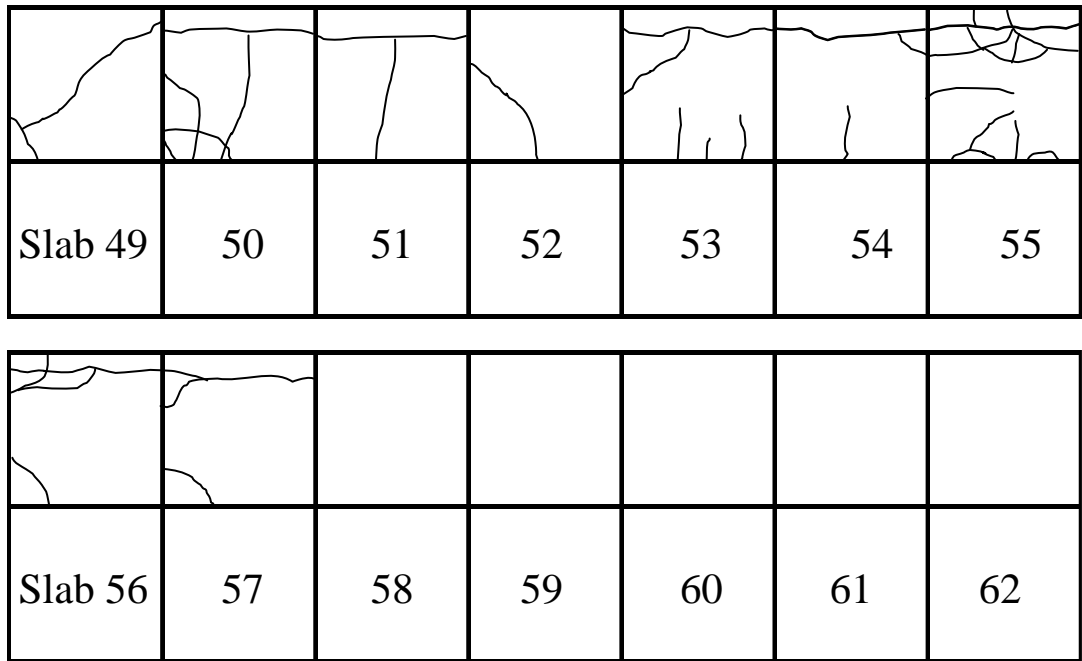


Figure 73. Cracking pattern for longitudinal joint trafficking on 3/16/09 (58,000 ESALs).

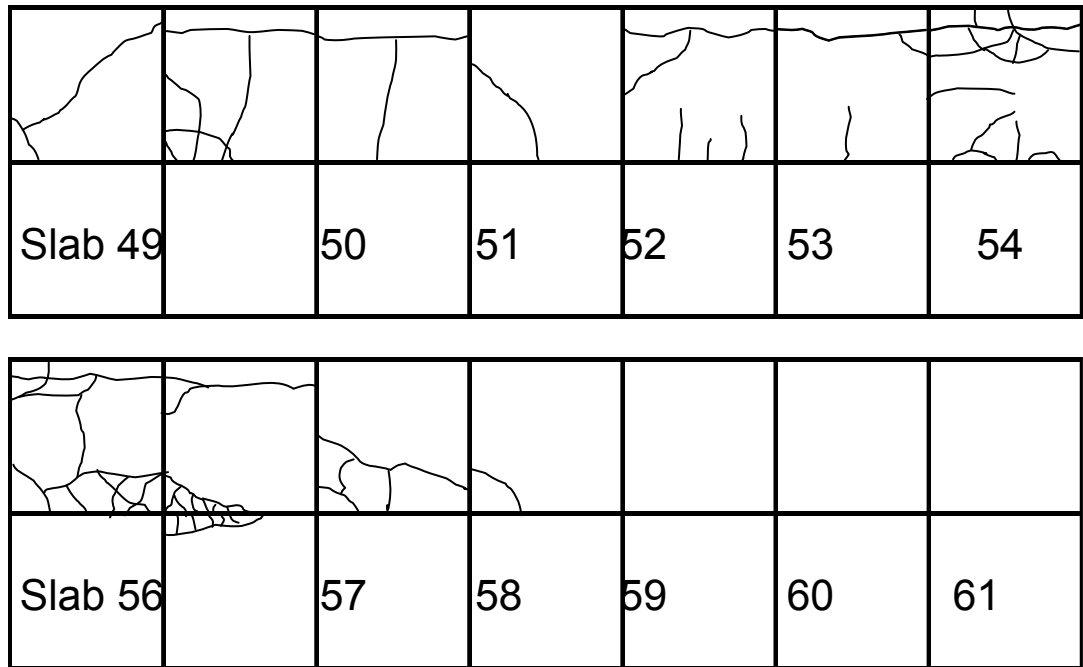


Figure 74. Cracking pattern for longitudinal joint trafficking on 3/19/09 (64,000 ESALs).

Table 13. Wheel Path Loading and Cracking for Section 3 North

Load (lb)	Passes	Cumulative Passes	ESALs	Cumulative ESALs	Cracks 3.5 in. Plain / Granular	Cracks 3.5 in. FRC / Granular
9,000	2,509	2,509	2,509	2,509	0	0
9,000	451	2,960	451	2,960	6	1
Total	2,960		2,960		6	1
*Testing only on FRC						
9,000	1,585	4,545	1,585	4,545	6	2

Table 14. Longitudinal Joint Loading and Cracking for Section 3 North

Load (lb)	Passes	Cumulative Passes	ESALs	Cumulative ESALs	Cracks 3.5 in. Plain / Granular	Cracks 3.5 in. FRC / Granular
9,000	280	280	280	280	6	2
9,000	1,720	2,000	1,720	2,000	6	2
9,000	150	2,150	150	2,150	6	2
9,000	2,560	4,710	2,560	4,710	7	2
9,000	2,800	7,510	2,800	7,510	7	2
12,000	2,710	10,220	9,072	16,582	7	2
12,000	2,660	12,880	8,905	25,487	7	2
12,000	2,710	15,590	9,072	34,559	7	2
12,000	2,620	18,210	8,771	43,330	7	2
12,000	680	18,890	2,276	45,606	7	2
Total	18,890		45,606		7	2
*Testing only on FRC						
15,000	300	19,190	2,564	48,170	-	2
18,000	250	19,440	4,595	52,765	-	2
21,000	150	19,590	5,267	58,032	-	2
24,000	100	19,690	6,153	64,185	-	4
FRC Total	19690		64,185		7	4

4.6.3 VERTICAL DEFLECTIONS – SECTION 3 SOUTH

Section 3 south was first trafficked during in the January of 2008 (winter) and then in the spring of 2008. Figure 75 and Figure 76 are the deflection data of the winter time testing which show very small deflections especially for the FRC section. The rebound deflections at the corner and mid-slab for the spring 2008 testing varied largely under 5-kip loading (0.025 to 0.1 inch) as seen in Figure 77. As the load increased to 9-kips, the rebound deflections continued to increase and likewise significant deflection variability existed between joints. By about 15000 passes (approximately 192,000 ESALs) the pavement was reaching deflections close to 0.25 inch at one joint as seen in Figure 77.

The main differences between the FRC slabs and plain slabs were the deflection magnitudes on average were smaller, the variability between different joint and mid-slab measurements were small, and finally the rate of increase in deflection under increasing load repetitions were smaller than the plain concrete section. The deflection behavior of the FRC section can be seen in Figure 78 and contrasted with the deflection of the plain concrete slabs in Figure 77. The peak deflection measured in Figure 78 coincides with the observation of cracks on the slab 57. Overall, the slab deflections were less than 0.1 inch after a significant number of repetitions of the 9-kip wheel load.

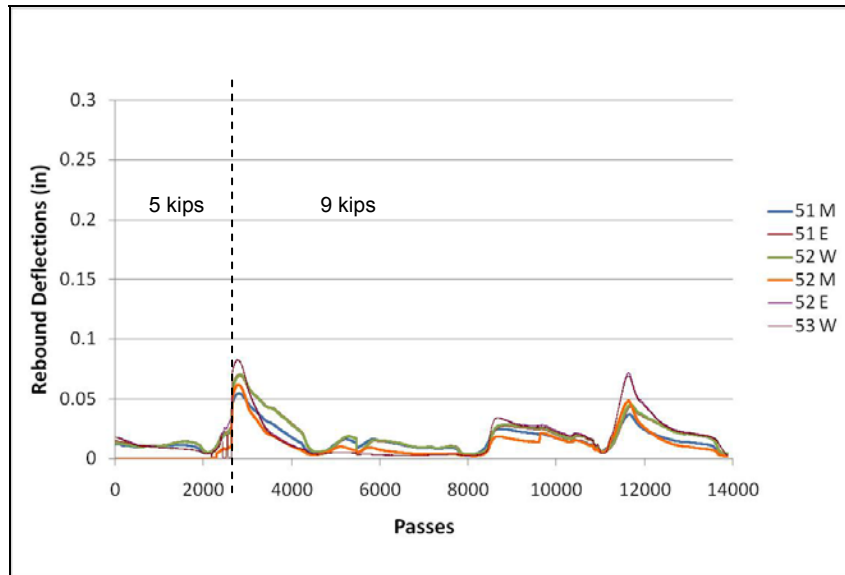


Figure 75. Rebound deflection of 3.5 in. plain concrete slab over a granular base during January 2008 (Section 3-south).

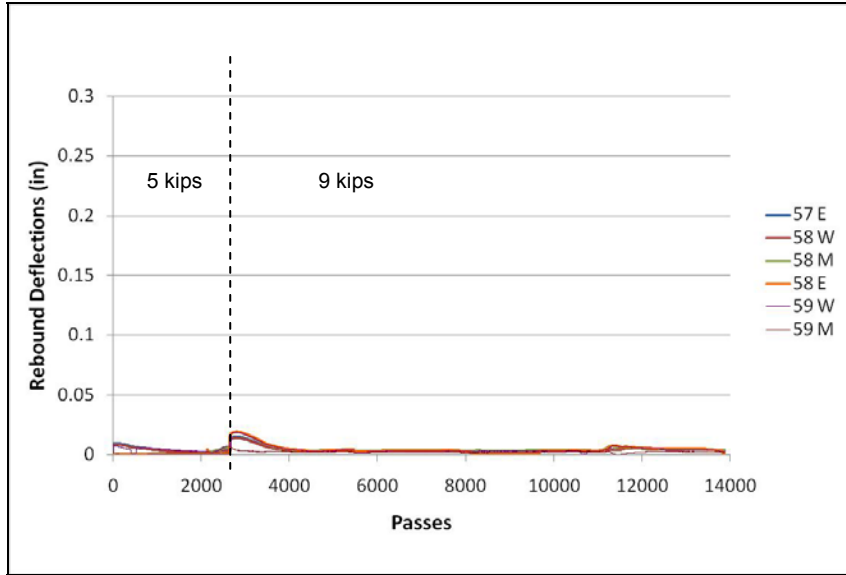


Figure 76. Rebound deflection of 3.5 in. FRC slab over a granular base during January 2008 (Section 3-south).

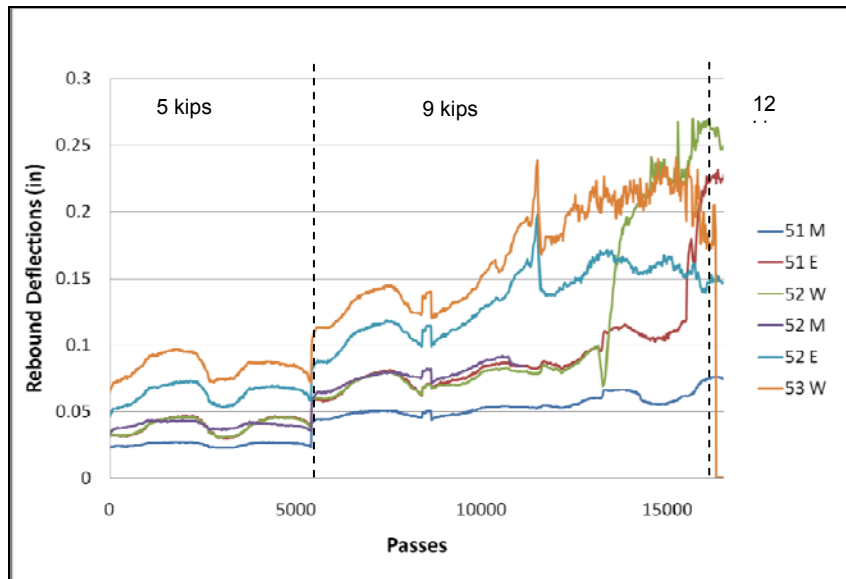


Figure 77. Rebound deflection of 3.5 in. plain concrete slab over a granular base (Section 3-south).

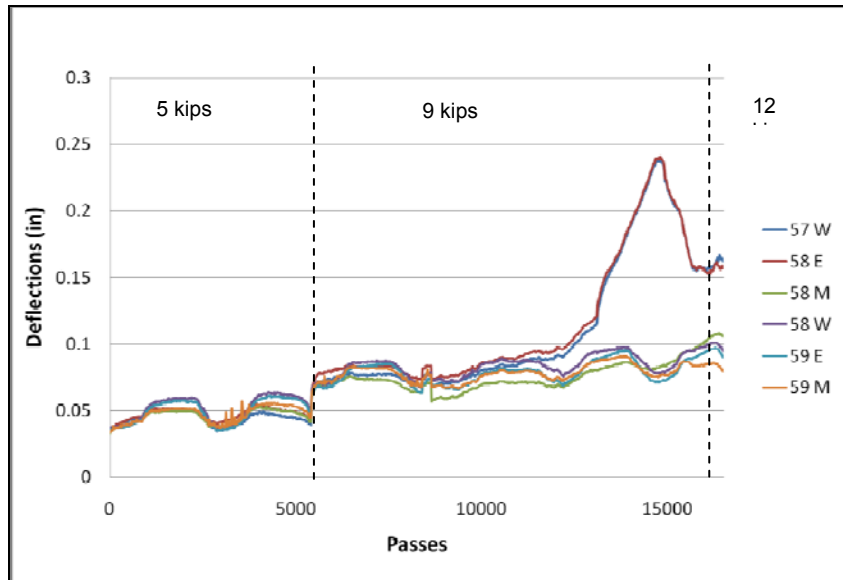


Figure 78. Rebound deflection of 3.5 in. FRC slab over a granular base (Section 3-south).

4.6.4 VERTICAL DEFLECTIONS – SECTION 3 NORTH

Section 3 (north) was trafficked in the wheel path, 12 inch offset from the edge of the slab. Figure 79 and Figure 80 show that the 9-kip deflections on the plain and fiber reinforced concrete slabs. The deflection on the plain slabs were slightly lower and could have been a results of cracking beginning before 1000 wheel passes as seen in Figure 79. Longitudinal cracks fully-developed in the plain concrete sections just under 3,000 ESALs. The deflections on the fiber reinforced slabs continued to increase with load repetitions in the wheel path with only one cracked slab.

After the longitudinal cracks appeared on the plain concrete slabs, trafficking was moved to the longitudinal contraction joint and cracking data recorded, as seen in

Table 14. Deflection data was collected for the longitudinal joint loading, but the location of the sensors along the free edge recorded the slab lifting (as expected) and thus is not presented here.

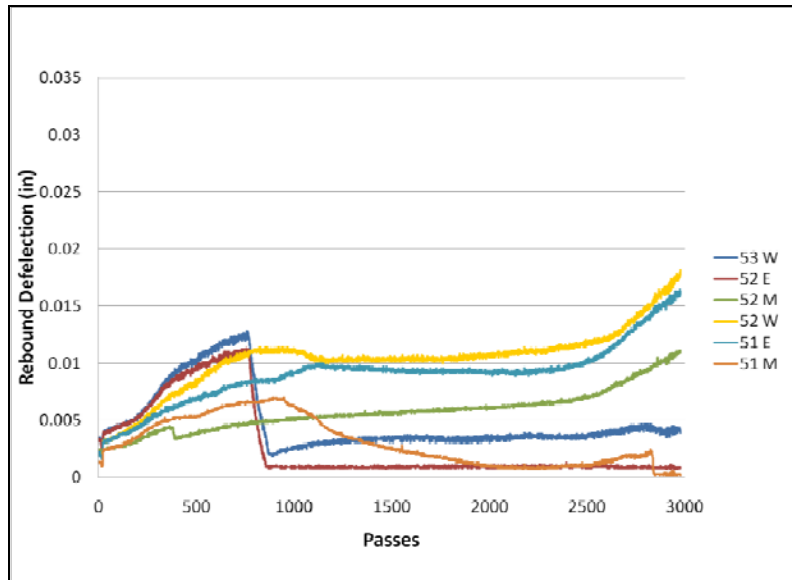


Figure 79. Wheel path rebound deflection of 3.5 in. plain concrete slab over a granular base (Section 3-south).

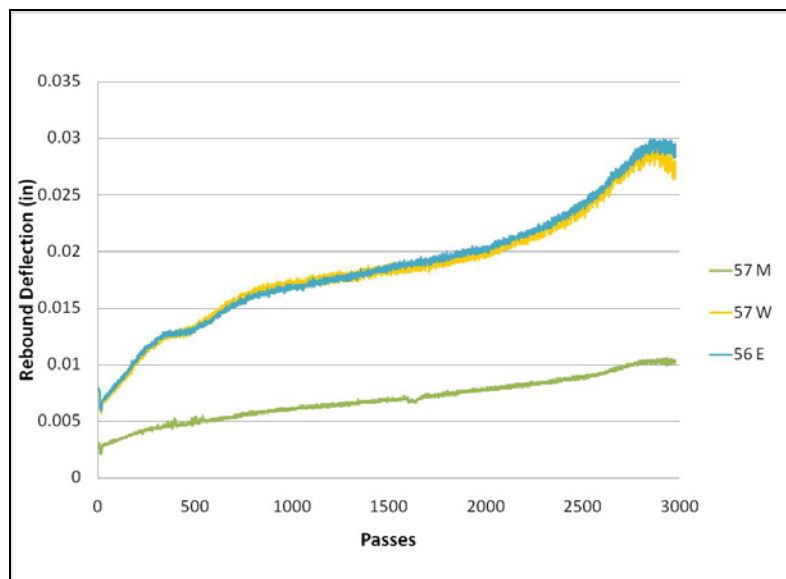


Figure 80. Wheel path rebound deflection of 3.5 in. FRC slab over a granular base (Section 3-south).

4.6.5 TENSILE STRAINS – SECTION 3 SOUTH

The strain responses from section 3 (south) in the winter time are seen in Figure 81 and Figure 82. The strain responses for section 3 (south) in the spring 2008 are seen in Figure 83. Testing at the 5-kip load level did not result in any cracks and the tensile strains were less than 100 microstrain. Figure 83 shows a rapid increase in tensile strain in the 3.5-inch plain concrete section when the load was increased to 9-kip. Strain gauge 53E, reached about 850 microstrain between 5000 and 10000 passes, which coincided with the first observed fatigue crack on the pavement surface. The strains for slab 52 stayed below 200 microstrain and did not crack until 12-kips were applied to the pavement. The plot also shows that for slabs 58 and 59 the maximum tensile strain was measured along the edge between 150 and 200 microstrain. Slab 58 eventually cracked during the trafficking of the wheel at 12-kips.

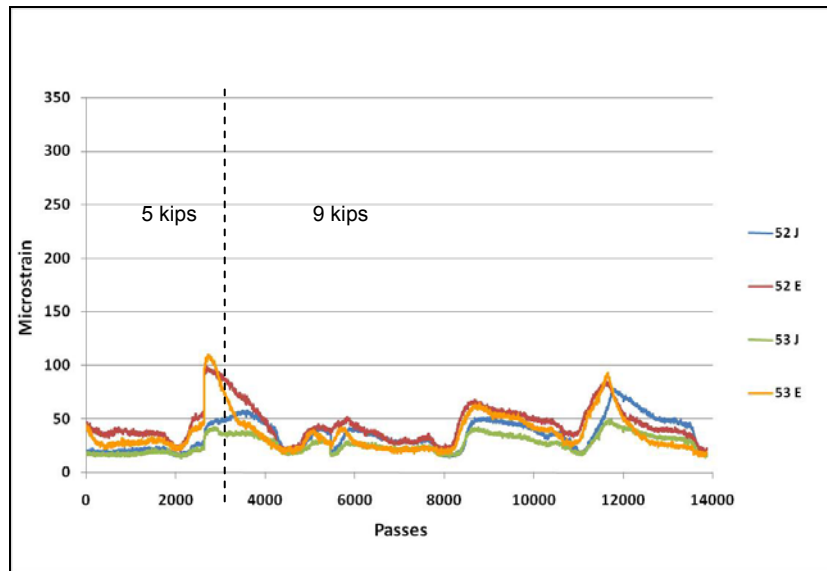


Figure 81. Maximum tensile strain responses for 3.5 in. plain over a granular base during Winter 2008 (Section 3 – south).

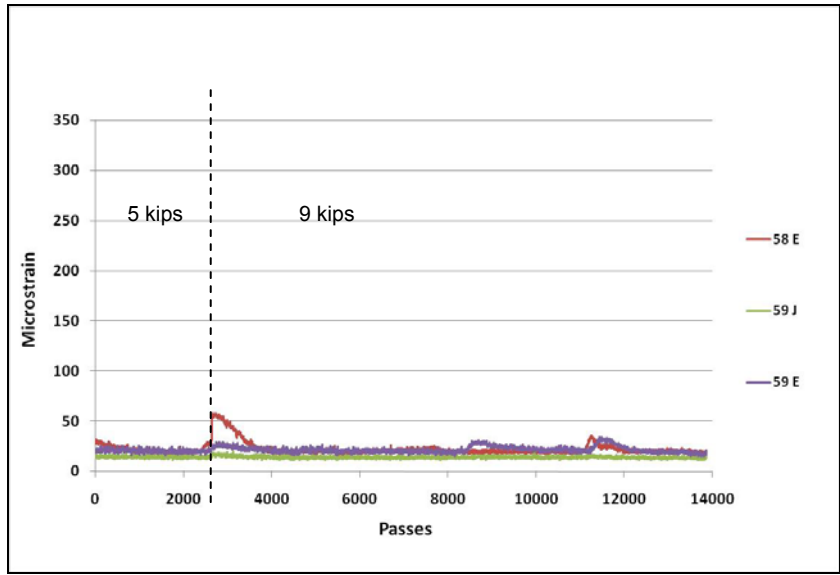


Figure 82. Maximum tensile strain responses for 3.5 in. FRC over a granular base during Winter 2008 (Section 3 – south).

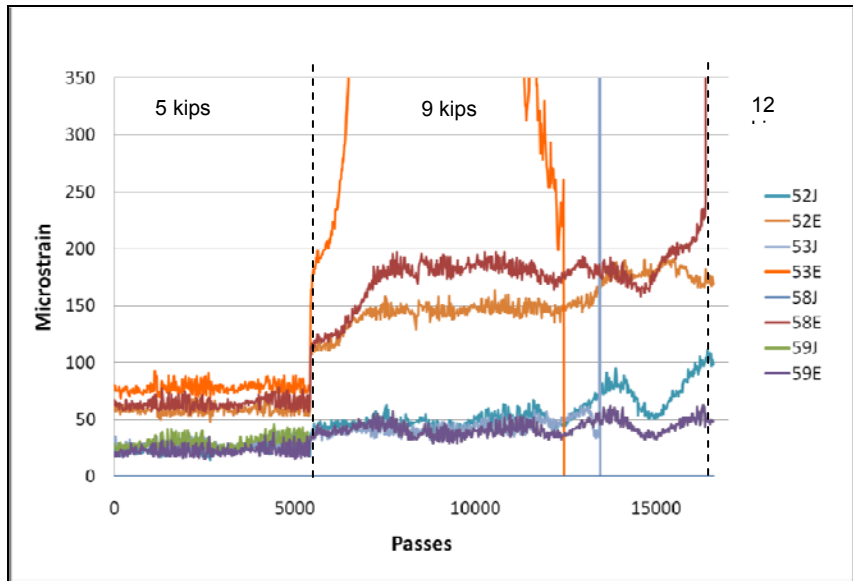


Figure 83. Maximum tensile strain responses for 3.5 in. plain and FRC over a granular base (Section 3 – south).

4.6.6 TENSILE STRAINS – SECTION 3 NORTH

The tensile strains on the wheel path did not increase beyond 50 microstrain even though the plain concrete slabs cracked from the bottom-up after approximately 3000 passes of 9-kips. The likely reason for this behavior was the strain gages were located at 20 inch offset from the edge on the bottom and did not significantly increase from the cracking occurring in the wheel path at 12 inches from the slab edge. After the

longitudinal cracks appeared from the wheel path loading, it was decided to traffic the section along the longitudinal joint but no strain data was collected.

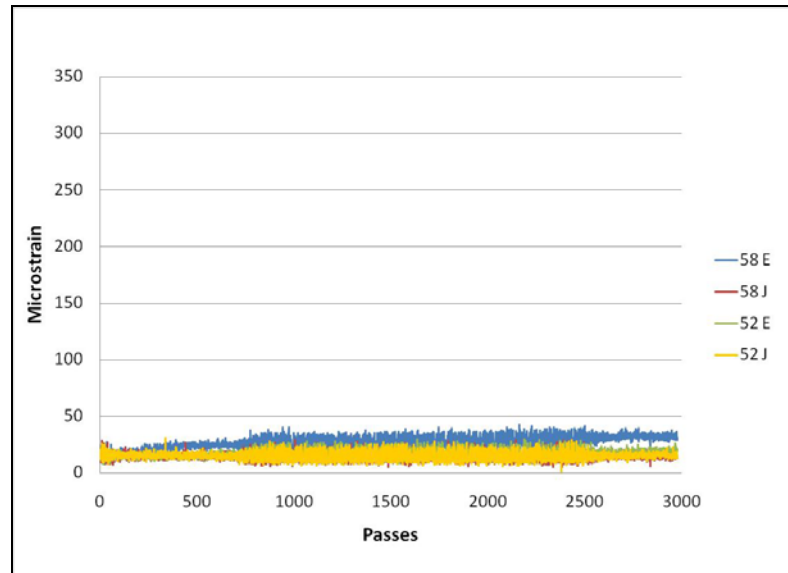


Figure 84. Wheel path maximum tensile strain responses for 3.5 in. plain and FRC over a granular base (Section 3 – north).

Climatic conditions played an important factor in the varying performance between the south and north testing of section 3. The saturated conditions during the testing of the south side led to edge pumping and loss of foundation support that resulted in corner break failures. During the north side trafficking, the pavement was undergoing thawing conditions during the trafficking. It is highly likely that the subgrade was thawing non-uniformly from the edge to the interior of the slab allowing for the pavement to crack prematurely in the longitudinal direction. Table 4 shows the backcalculated k-values for section 3 were extremely low especially for the north side. The only other discrepancy between the south and north side trafficking was that a super single wheel loaded the south side slabs while an aircraft tire was used on the north side. It is unlikely that this loading geometry had any effect on the results.

Overall, the structural design of section 3 (3.5 inch slab thickness) has to be considered for very low volume traffic facilities. The performance of these thin slabs is directly related to the support condition stiffness, i.e., no cracking occurred on frozen subgrade while rapid cracking appeared on thawing slab support. Note, the 4 inch concrete slab on the asphalt concrete base lasted at least 35 times longer. Plain concrete did not perform as well as the concrete that contained structural fibers. The fibers prolong the life of the concrete slabs before the appearance of the fatigue cracks and furthermore, extend the service life of the pavement system (lower rate of crack deterioration) relative to plain concrete slabs. The rebound deflections for FRC slabs also demonstrated less deflections at the joints and mid-slab and less variability in deflection between various joints compared with the plain concrete section.

4.7 JOINT PERFORMANCE AND LOAD TRANSFER EFFICIENCY

One proposed advantage of concrete slabs with optimized geometry is the potential for limiting the placement of man-made load transfer devices. In order to justify elimination of dowels across the transverse contraction joints, the LTE across the joints

must be maintained at a certain level throughout the testing. Load transfer efficiency values were calculated versus load repetitions for the same joints that were instrumented with the deflection sensors. Figure 85 shows the deflection load transfer efficiency for section 1 (south). Joint 8 is on the 4-inch concrete section and Joint 14 is on the 6 inch section. This test section had a high load transfer efficiency above 80% for both sections after 57.5 million ESALs. Figure 86 is a plot of the deflection LTE values measured at the free edge while the pavement was trafficked in the wheel path. Joint 13, which is on the 6-inch section, has a lot of noise and is the only joint to fall below the 60%. The deflection LTE for the wheel path and edge loading is not expected to be the same due to the location of the load relative to the deflection sensors. Figure 87 is the LTE of section 1 north near the edge.

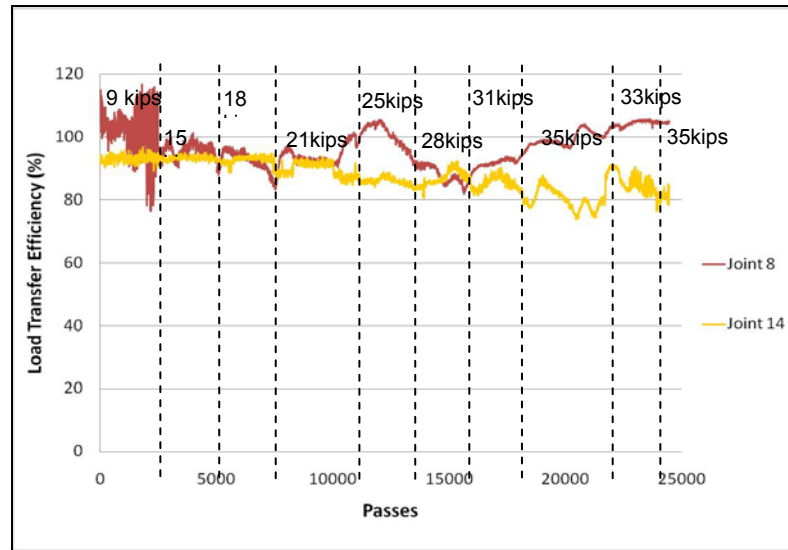


Figure 85. Deflection load transfer efficiency for edge loading (Section 1 – south).

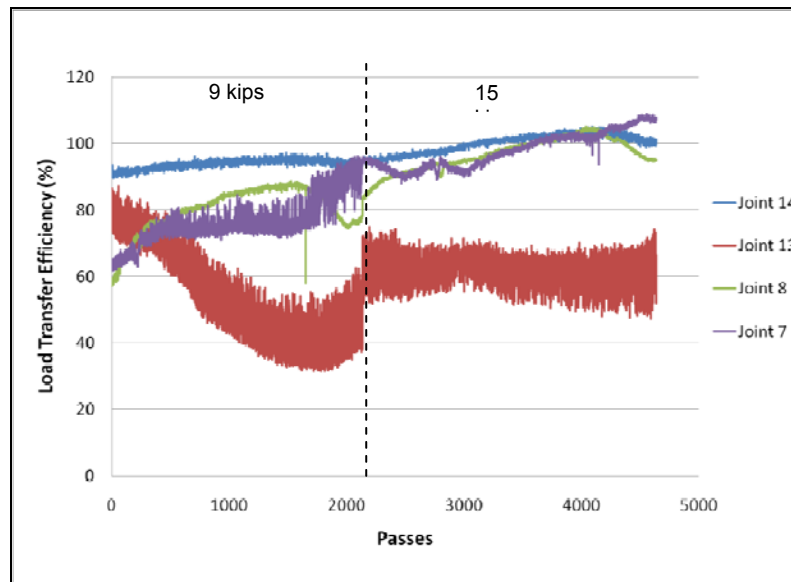


Figure 86. Deflection load transfer efficiency measured at free edge for wheel path loading (Section 1 – North).

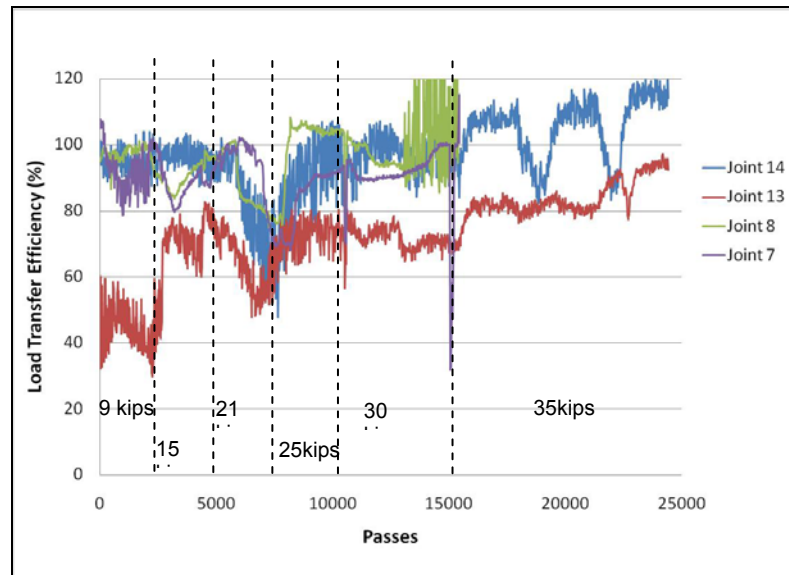


Figure 87. Deflection load transfer efficiency at free edge (Section 1 – North).

For section 2 (south), the range of LTE at the start of the testing was between 100% and 80% as seen in Figure 88 for the 6 and 8 inch concrete slabs. This is a result of the dominant joint effect, i.e., joints that crack early tend to have a greater crack width than joints that propagate later. The LTE for joints 30 and 37 fell below 40% at about 7000 passes but ended at about 75% at the end of testing. The interesting behavior of the joints in section 2 was that the LTE converged to approximately 75% suggesting that the slabs eventually distributed the joint movement between the slabs. Figure 89 shows the deflection LTE of section 2 (north) trafficked in the wheel path. The LTE for all but one joint was above 75% at 9-kips and increased closer to 100% when loaded at 15-kips. Joint 36 was on the 8-inch concrete section and had a lower LTE which can be attributed to the dominant joint effect. Figure 90 is a replicate of the LTE being tested on near the edge of the pavement.

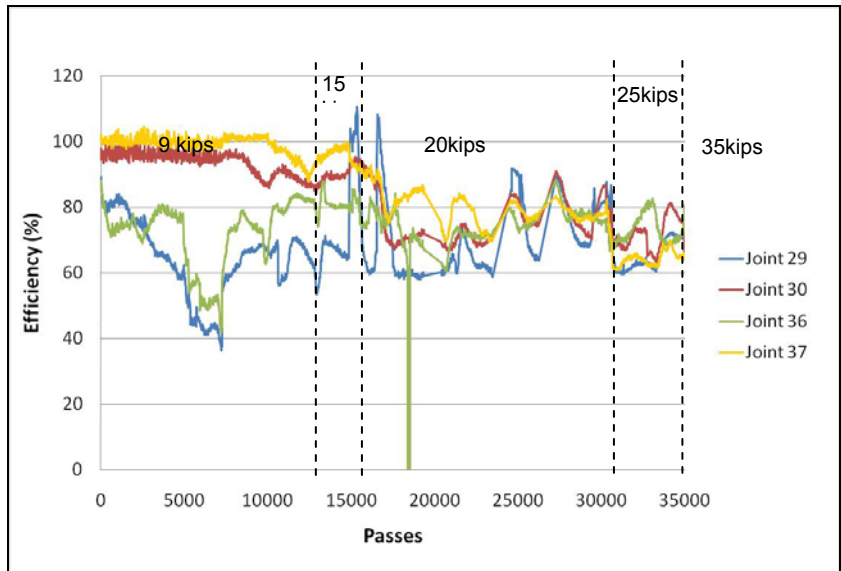


Figure 88. Deflection load transfer efficiency for edge loading (Section 2 – south).

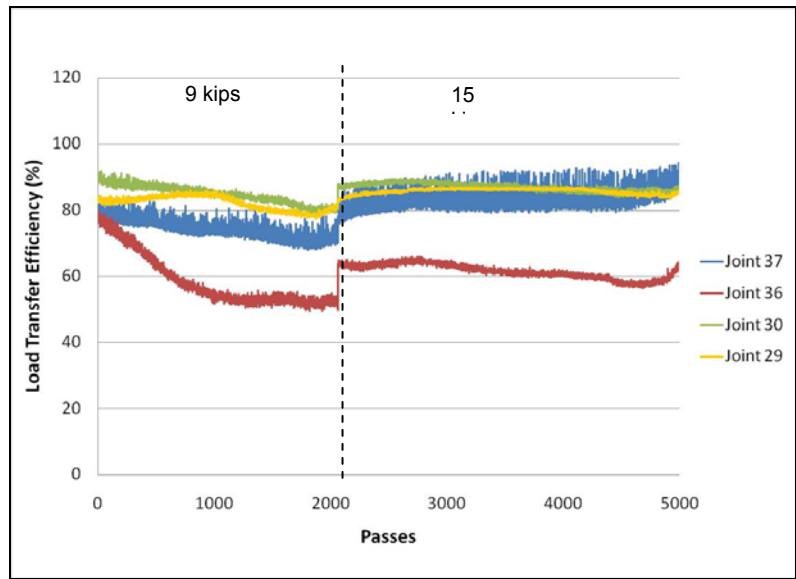


Figure 89. Deflection load transfer efficiency measured at free edge for wheel path loading (Section 2 – north).

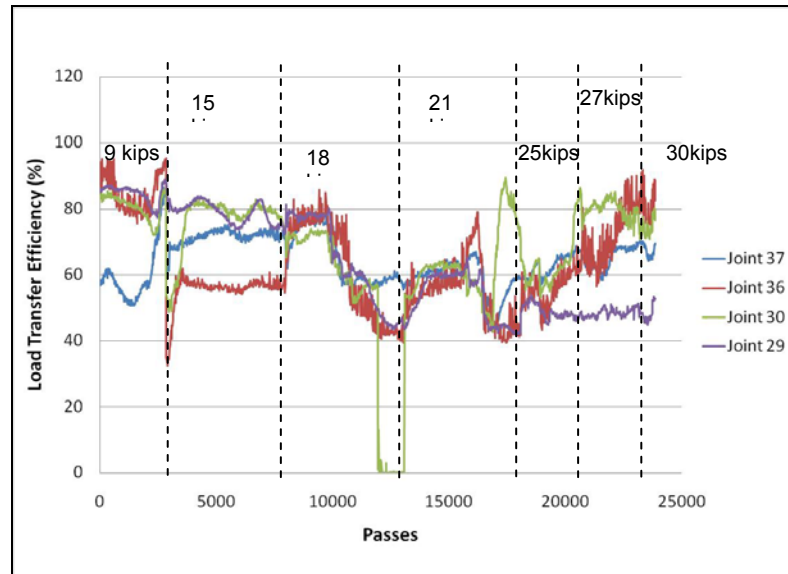


Figure 90. Deflection load transfer efficiency at free edge loading (Section 2 – north).

The LTE calculated for section 3 (south) is seen in Figure 91. Joint 51 was on the plain concrete section and joint 58 was of the FRC section. The LTE was high throughout the testing with a slight decrease towards the end. The drastic decrease in LTE in slab 51 correlates to when the slabs became distressed. Figure 92 is the deflection LTE data collected on section 3 (north) when trafficked in the wheel path. The joint on the FRC section stayed close to 100 % which is consistent with the cracking performance data. The joint on the plain section showed more variance shifting between 75% and 95% despite the appearance of longitudinal cracks at approximately 2900 passes.

Overall, the transverse contraction joints in the various test sections relied on aggregate interlock as the primary load transfer mechanism except the FRC section. There was no measurable faulting on any transverse contraction joints. The fibers greatly enhanced the load transfer capabilities of plain concrete slabs as demonstrated by the high LTE values versus traffic repetitions and the exceptional performance of the longitudinal contraction joint testing on section 3 (north). The LTE levels for the 6 inch and 8 inch slabs were also at acceptable magnitudes despite the large overloads employed to achieve the ESALs. The accelerated pavement test data suggest that the slabs with optimized geometry (6ftx6ft) can have adequate joint performance without load transfer devices for low to medium volume facilities. Whether the joints will continue to function at a high level over a 20-year period for high ESAL facilities is still uncertain but several sections did have adequately performing joints with over 50 million ESALs. One potential solution for extending joint performance for high ESAL facilities may be structural fibers but this has not been tested under accelerated pavement loading.

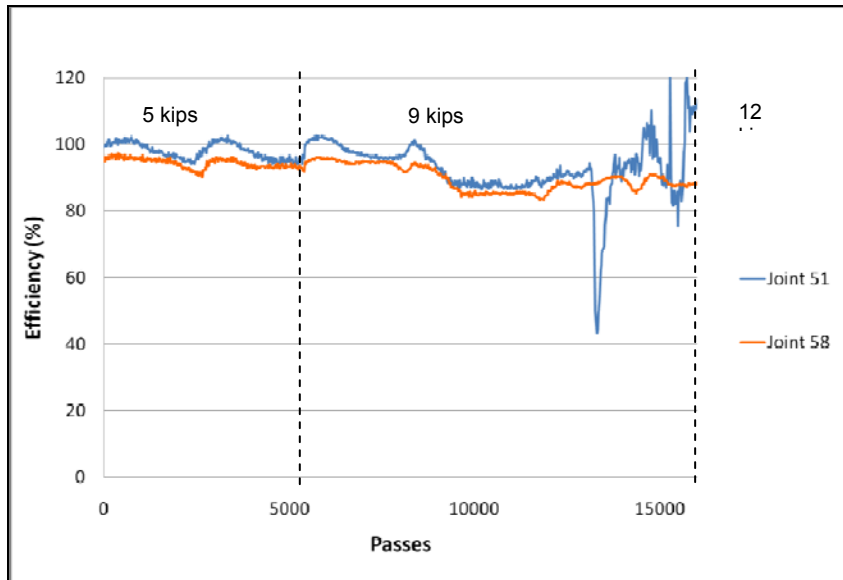


Figure 91. Deflection load transfer efficiency for edge loading (Section 3 – south).

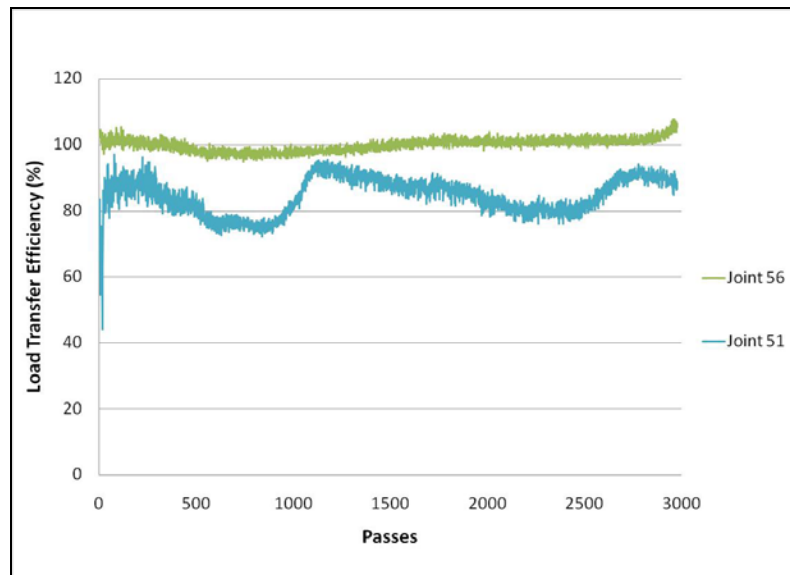


Figure 92. Deflection load transfer efficiency measured at free edge for wheel path loading (Section 3 – north).

CHAPTER 5 SIGNIFICANCE OF THE CONCRETE SLAB TESTING RESULTS

With the immense amount of data generated from the accelerated pavement testing of the concrete slab system with optimized geometry, there is a possibility of numerous discussions following the various factors addressed in the testing. In this chapter, a key set of issues will be briefly discussed in order to summarize the main points taken from the accelerated pavement testing.

5.1 APPLICATION TO PAVEMENTS WITH SIGNIFICANT OVERLOADING

One of the main objectives of the concrete slabs with optimized geometry system (TCPavements) is to only have one wheel on each slab at a time. This would mean that the slabs should be loaded at about 9,000 lbs. at any given time. The ATLAS device can only apply one wheel a time and for concrete pavements an aircraft tire is typically used to simulate overloading conditions. For this testing, the pavement was loaded to 35,000 lb at times, which is equivalent to 17.5 ton wheel load. In practical terms, a monitored roadway does not experience this type of loading conditions. Single axle loads in the United States are typically between 13,000 and 20,000 lb. The repeated trafficking with overloaded axles can eventually result in fatigue failure of the slabs, which has been reported by numerous researchers in other countries. The performance of the concrete slabs with optimized geometry under overloading conditions suggest that this pavement system may be ideal for locations where the magnitude of overloading and number of overloads is not known nor enforced. For example, an 8-inch concrete slab on granular base was able to withstand 51.3 million ESALs and thousands of repetitions of 35-kip wheel load or 70-kip axle load.

5.2 EFFECTS OF SUPPORT LAYER STIFFNESS

The base and subgrade stiffness is an extremely important parameter in designing the thickness of concrete slabs with optimized slab geometry. Since the slab thickness values are thinner than conventional concrete pavements with 15 ft joint spacing, then the deformations accumulating in the underlying layers are more critical. The trafficking of the sections at different times of the year relayed some insight into how the support conditions extended or decrease the fatigue life of the section. When the trafficking was done in the winter (January 2008) with a frozen base and subgrade layer, section 3 (south) was able to sustain more than 229,000 ESALs without showing any signs of distresses. When section 3 (south) was tested in the spring time (April 2008), it began showing corner fatigue cracks at about 75,000 ESALs. Wheel path testing on section 3 (north) during a thaw cycle (March 2009) result in significant cracking after 3,000 ESALs. The backcalculated k-value for section 3 (south) testing in the spring was found to be 150 psi/in, whereas for section 3 (north) the backcalculated k value was approximately 50 psi/in. The lower soil k-value was directly correlated to the adverse performance of section 3 (north). The structural fibers significantly prolonged the initial cracking and serviceability performance of the 3.5-inch section under poor soil conditions.

In the thicker slab sections, the k-value had less of an influence on the performance of the slab since the stresses in the underlying foundation layers were smaller. The 8-inch concrete slabs in section 2 south and north had a k-values of 150 psi/in and 100 psi/in, respectively, and resisted the largest number of ESALs without failure, 19.6 and 51.3 million ESALs, respectively. The 6-inch slabs in section 2 were somewhat influenced by the soil support layer. The south section had an initial k-value of

300 psi/in and eventually had 4 cracked slabs at 22.9 million ESALs. On section 2 (north), the 6-inch slabs had experienced 6 out of 7 slabs cracked at 16.5 million ESALs with a k-value of 100.

Section 1 included an asphalt concrete support layer over the natural subgrade. The backcalculated k-value for both the north and south 6-inch slabs was 500 psi/in. In terms of cracking performance, the south section had one slab with some minor cracks at 29 million ESALs while the north section had 4 cracked slabs at 34 million ESALs. The 4-inch slabs over asphalt concrete base on section 1 (north) were much more distressed than the same section on the south side. The backcalculated k-value for both sides (4 inch slab) was approximately 250 psi/in. Figure 93 shows distressed slab 6 of section 1 (north) at 20 million ESALs and Figure 94 is slab 6 of section 1 (south) at 56 million. The loss of support due to trafficking during rainy days and lack of an adequate drainage system is evident in Figure 93 as the surface concrete slabs have settled into the asphalt layer.



Figure 93. Fatigue cracking of 4 in. concrete slab over asphalt base on section 1 north at 20 million ESALs.



Figure 94. Fatigue cracking of 4 in. concrete slab over asphalt base on section 1 south at 56 million ESALs.

5.3 EFFECTS OF STRUCTURAL FIBERS ON FATIGUE CRACKING AND SERVICEABILITY

Full-scale testing of FRC slabs in the early 1970's by the U.S. Army Corps of Engineers demonstrated enhanced fatigue life of FRC over plain concrete slabs (Parker 1974; Rollings 1981). More recent research with application to slab on ground design has shown significant enhancement in concrete slab cracking performance by the addition of structural fibers (Beckett 1990; Falkner and Teutsch 1995; Roesler et al. 2004). Finally, theoretical analysis of the flexural capacity of FRC slabs using fracture mechanics and cohesive zone modeling in the finite element framework has clearly demonstrated the increased load capacity fibrous slabs have over plain concrete slabs (Gaedicke 2009).

The accelerated pavement testing of 3.5 inch slabs with and without structural fibers clearly confirmed their benefit to extending the fatigue and service life of plain concrete slabs. The increase in load carrying capacity afforded by addition of fibers came without the need to increase the concrete's flexural strength. The fibers also helped extend the service life of the FRC slabs by maintaining vertical and horizontal slab alignment. Structural fibers also aided in maintaining high load transfer efficiency or aggregate interlock throughout the concrete pavement's life. The load transfer efficiency measured on section 3 was quite high throughout the testing and may be an advantageous addition to increase the performance and service life of concrete slabs with optimized geometry with larger required slab thicknesses. One other benefit of fibers could be to prevent adjacent slab movement due to hard braking, e.g., intersections, superelevations, etc. This phenomenon has occurred on ultra-thin whitetoppings where slabs move longitudinally if significant truck braking on the slab happens (Roesler et. al 2008).

5.4 THICKNESS AND SIZE EFFECT ON CONCRETE SLAB FATIGUE LIFE

Researchers over the years have recognized that the specimen size (e.g., thickness) affects the concrete's nominal strength (Bazant and Planas 1998). This translates into thinner specimens have a greater nominal strength than thicker concrete specimens with the same geometric ratios and boundary conditions. Rao (2005) developed curves based on Bazant's size effect method (Bazant and Kazemi 1990) to account for the decrease in apparent strength as concrete slab thickness increased to explain full-scale test results of varying slab thickness. Roesler (2006) also summarized the results of beam and slab tests which clearly demonstrated that the beam flexural strength test underestimated the slab concrete flexural strength by a factor of 1.3 to 3.5. This ratio was related to the concrete material itself (plain vs. fiber reinforced concrete), the thickness of the slab, and the non-dimensional slab size. The ATLAS tests results support the previous findings on thickness and size effect. The thinner slabs (3.5-inch) were able to be loaded past their apparent flexural strength and still not crack. Since the slabs were not geometric similar as the thickness increase it is difficult to conclude if there was a strong thickness size effect. However, a correction factor to account for the scaling of beam flexural to slab flexural strength based on the thickness of the slab can be supported in order to explain the cracking performance of the thinner slabs.

5.5 TEMPERATURE CURLING EFFECTS

Another contributing factor to the performance of smaller slab size rigid pavement systems is the reduction in slab curling. Figure 95 shows a plot of the deflection at the two consecutive joint corners. As expected, the corner deflections increase as the temperature difference through the slab thickness becomes more negative. The 6 ft x 6 ft x 8 inch slab had a relative deflection range of about 0.02 in. (0.5mm) and a temperature difference range of +15°F to -5°F. The magnitude of the slab curling was compared with published data by Rao (2005). Concrete slabs with dimensions of 12 ft x 12 ft and a thickness of 8 inches had a deflection range of about 0.08 in. (2 mm) during a 24 hour period (temperature differential of +23°F to -9°F).

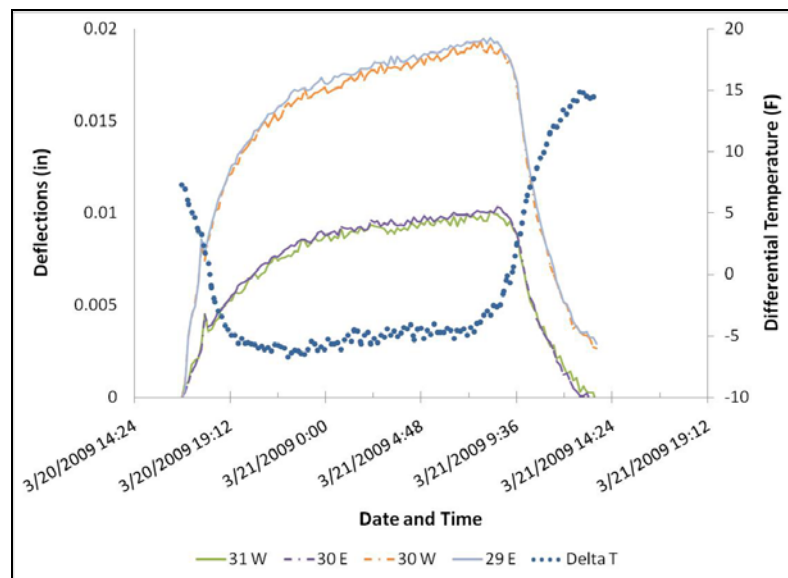


Figure 95. Slab temperature curling for 8 in. over granular base without loading.

Temperature data were simultaneously collected with strain and deflection data. Figure 96 is a plot of the maximum rebound deflection on section 2 south for sensors 29E, 30R, and 30M along with the surface temperature, mean temperature, and temperature differential of the pavement (top temperature minus bottom temperature) for a 24 hour period of loading. The maximum rebound deflection increased as the temperature decreased. This same relationship between temperature and deflections was also noticed on the horizontal deflection sensors located at the joints. The overall rebound deflection is not as sensitive to temperature curling as conventional jointed plain concrete slabs (Rao 2005).

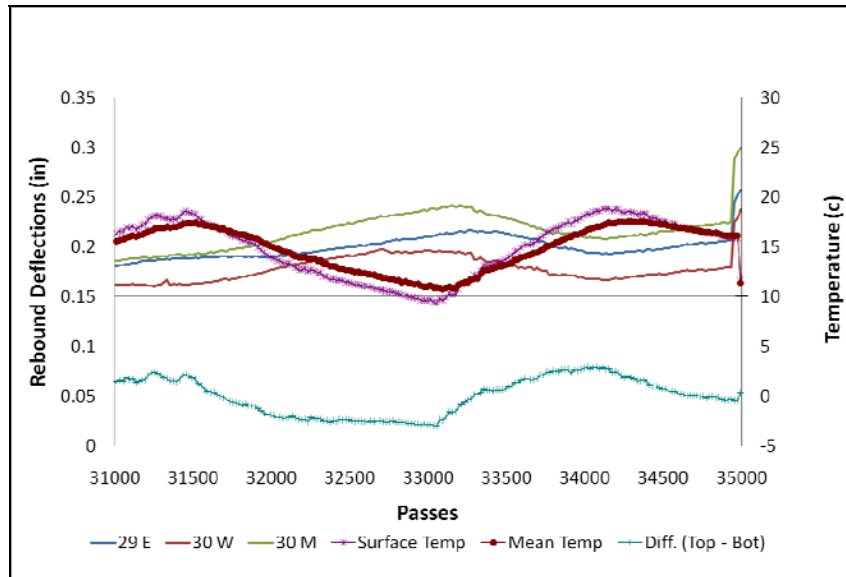


Figure 96. Effect of temperature change on vertical deflections (Section 2 – south).

5.6 LATERAL RESTRAINT PINS

Due to the large deflections, relatively light slabs, and lower level of slab-base friction, it is important to have some sort of lateral restraint to avoid the longitudinal contraction joint from opening excessively. Currently, these concrete slab systems employ steel pins driven next to the pavement edge to offer resistance to lateral slab spreading. These pins can be replaced by a curb and gutter system on urban streets or by a concrete shoulder. The ATLAS testing did not seem to offer support for the effectiveness of these steel pins since the loading didn't really produce lateral thrusts in the slab. As shown in Figure 97 the longitudinal joint opening up during loading due to the slab settling at the edge and the slab rotating. The longitudinal joint trafficking on the 3.5 inch concrete slab, Figure 98, demonstrate that adding structural fibers appear to be a better choice to promote load transfer across the transverse joints, increase the load capacity of the slab, and lastly to hold the longitudinal joint together.



Figure 97. Longitudinal joint opening on 3.5 inch plain concrete section.



Figure 98. Longitudinal joint on 3.5 inch FRC section.

CHAPTER 6 CONCLUSIONS

A new concrete pavement thickness design concept based on optimizing the slab dimensions was assessed through full-scale test section construction and accelerated pavement testing (APT). Three concrete pavement test sections 132 ft each were designed for APT with the *ATLAS* device to determine the concrete slab fatigue cracking and joint performance. The main factors addressed in the tests sections were slab thickness (nominally 4, 6, and 8 inches), base stiffness (aggregate versus asphalt concrete base), concrete material type (plain versus fiber reinforced concrete), and wheel trafficking position relative to the free edge. All slabs had 6 ft by 6 ft panel sizes.

APT was completed on all sections until significant cracking distresses were present and showing signs of crack deterioration. In most cases, significant overloads were required to fail the concrete sections. The approximate ESALs applied to each section were calculated based on lateral wander magnification factor calculated based on a fatigue damage ratio. For each section, vertical rebound deflection and tensile bending strains were measured for each load repetition.

The results of the APT showed that the 8 inch concrete section over a granular base sustained the greatest number of ESALs (average of 35 million) without showing any distress. In fact, this section sustained almost 7400 passes of a 35-kip wheel load without a single slab failure. The 6-inch section over an asphalt base sustained an average of 30 million ESALs before significant cracking. The 6-inch concrete slab over the granular base resisted 12 million ESALs on average before exhibiting primarily corner cracking. The 4-inch concrete sections over asphalt concrete withstood over 4 million ESALs on average before fatigue cracking began developing on the section. Finally, the 3.5-inch concrete slabs on aggregate base began developing cracks after 75,000 ESALs when the soil was in poor condition. The repeated load testing on the 3.5-inch slabs clearly demonstrated that fiber reinforced concrete extended the fatigue cracking life of plain concrete, reduced the rate of fatigue crack deterioration, and were effective in maintaining load transfer across the transverse and longitudinal contraction joints.

The support conditions affected the cracking performance of the sections especially for the thinner sections. The 3.5-inch concrete slab on 6-inch aggregate base was tested for over 229,000 ESALs without any cracking when the base/subgrade was frozen. In the spring time testing, this same section began showing signs of fatigue cracking starting at 75,000 ESALs. The effect of support conditions on the allowable repetitions to fatigue cracking could be further seen as the 4 and 6 inch concrete slab on an asphalt concrete base could take approximately 50 and 5 times more ESALs compared to the sections 4 or 6 inch concrete slabs on granular base, respectively. This confirms that the support condition stiffness is much more important to the thinner slab performances.

One of the current design features of the slabs with optimized geometry is the exclusion of man-made load transfer devices. The accelerated pavement testing demonstrated that the aggregate interlock joints can still provide medium to high deflection load transfer efficiency after a significant amount of ESALs. The addition of fibers can further improve the load transfer efficiency across the joints based on the limited joints tested. The climate especially amount of rainfall can significantly affect the performance of slabs with optimized geometry if precautions are not taken in selecting the base material and subgrade/base layer separator material. A base layer containing a more open graded aggregate material that does not pump is essential for achieving the desired service life. A nonwoven geotextile must be used to prevent penetration of

the subgrade fines into the more open graded base layer. Adequate drainage is also required to avoid lowering the support stiffness and strength that could lead to premature failure.

REFERENCES

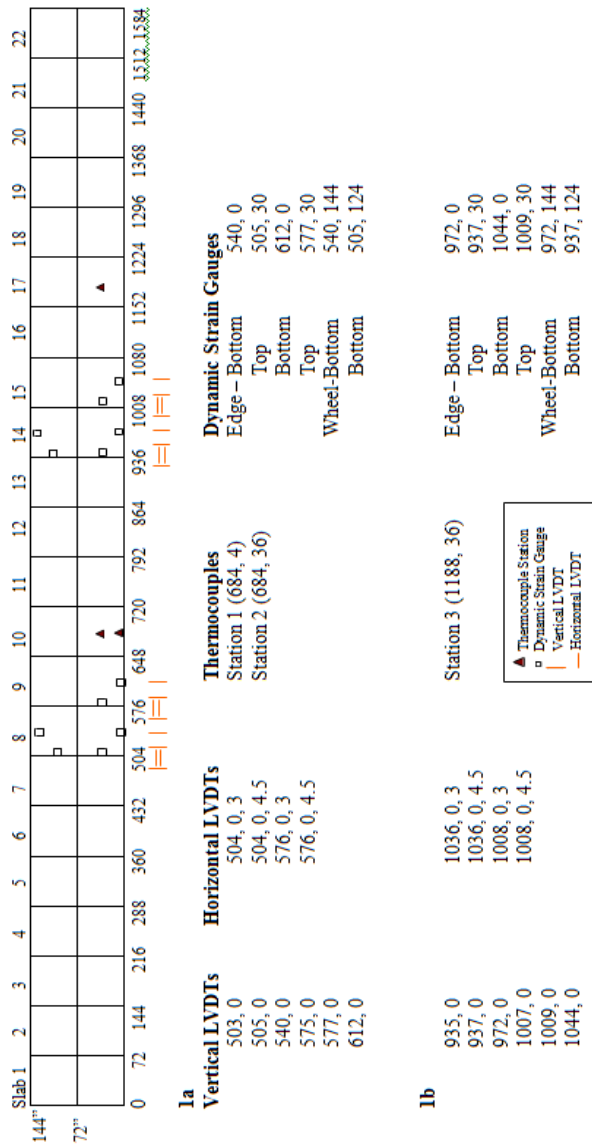
- American Concrete Pavement Association (1998), Whitetopping-State of the Practice, Publication EB210P, American Concrete Pavement Association, Skokie, IL, 1998.
- ARA, Inc. (2007) Interim Mechanistic-Empirical Pavement Design Guide Manual of Practice. Final Draft. National Cooperative Highway Research Program Project 1-37A.
- ASTM (2007) ASTM C1609-07: Standard Test Method for Flexural Performance of Fiber-Reinforced Concrete (Using Beam with Third-Point Loading). Annual Book of ASTM Standards, Section 4 Construction 02. Philadelphia, Pennsylvania: American Society for Testing and Materials International.
- Bazant ZP, Kazemi MT.(1990) Determination of fracture energy, process zone length and brittleness number from size effect, with application to rock and concrete, International Journal of Fracture 1990;44:111-131.
- Bazant ZP, Planas J. (1998) Fracture and size effect in concrete and other quasibrittle materials. Florida: CRC Press.
- Beckett, D. (1990) Comparative Tests on Plain, Fabric Reinforced and Steel Fibre Reinforced Concrete Ground Slabs. *Concrete* 24(3): 43-45.
- Caltrans (2008) Caltrans Highway Design Manual, California Department of Transportation.
- Covarrubias, J.P.T and Covarrubias, J.P.V. (2008), "TCP Design for Thin Concrete Pavements," 9th International Conference on Concrete Pavements, San Francisco, CA, 13 pp.
- Falkner, H., Huang, Z., & Teutsch, M. (1995) Comparative Study of Plain and Steel Fibre Reinforced Concrete Ground Slabs. *Concrete International* 17(1): 45-51.
- Gaedicke, C. (2009) Fracture-Based Method to Determine the Flexural Load Capacity of Concrete Slabs, Ph.D. thesis, University of Illinois, Urbana, Illinois.
- Huang, Y. H., (2004) Pavement Analysis and Design, 2nd edition, Prentice Hall, Upper Saddle River, NJ.
- Kohler, E. and Roesler, J., (2006) Accelerated Pavement Testing of Extended Life Continuously Reinforced Concrete Pavement Sections, Final Report, Transportation Engineering Series No. 141, Illinois Cooperative Highway and Transportation Series No. 289, University of Illinois, Urbana, IL, December 2006, 354 pp.
- Packard R. (1984) Thickness Design for Concrete Highway and Street Pavements. Skokie, IL: Portland Cement Association.
- Parker, F. (1974). "Steel Fibrous Concrete for Airport Pavement Applications." Technical Report 5-74-12, US Army Engineer Waterways Experiment Station, Vicksburg, MS.

- Rao, S (2005) Characterizing Built –in Curling and its Effect on Concrete Pavement Cracking, Ph.D. Thesis. University of Illinois at Urbana Champaign, Urbana IL. (2005)
- Roesler, J. R., Bordelon, A., Ioannides, A. M., Beyer, M., and Wang, D., (2008) Design and Concrete Material Requirements for Ultra-Thin Whitetopping, Final Report, Illinois Center for Transportation Series No. 08-016, University of Illinois, Urbana, IL, June 2008, 181 pp.
- Roesler, J., Lange, D., Altoubat, S., Rieder, K.-A., & Ulreich, G. (2004) Fracture of Plain and Fiber-Reinforced Concrete Slabs under Monotonic Loading. *ASCE Journal of Materials in Civil Engineering* 16(5): 452-460.
- Roesler, J.R. (2006), "Fatigue Resistance of Concrete Pavements," 6th International DUT – Workshop on Fundamental Modelling of Design and Performance of Concrete Pavements, Belgium, September 2006.
- Rollings, R. S. (1981) "Corps of Engineers Design Procedures for Rigid Airfield Pavements." Proceedings, Second International Conference on Concrete Pavement Design, Purdue University, West Lafayette, IN.
- Smith, K.D., M.J. Wade, D.G. Peshkin, L. Khazanovich, H.T. Yu, and M.I. Darter (1998). Performance of Concrete Pavements; Volume II—Evaluation of In-service Concrete Pavements. FHWA-RD-95-110, Washington, DC.
- Vandenbossche, J. M. and A.J. Fagerness. (2002) "Performance, analysis, and repair of ultrathin and thin whitetopping at Minnesota Road Research facility", *Transportation Research Record*, No. 1809, pp. 191-198.
- Vandenbossche, J.M. (2003)"Performance Analysis of Ultrathin Whitetopping Intersections on US-169: Elk River, Minnesota", *Transportation Research Record*, No. 1823, pp. 18-27.
- Vesic, A. S. and Saxena, K. (1969), "Analysis of Structural Behavior of Road Test Rigid Pavements," *Highway Research Record* No. 291, Highway Research Board, National Research Council, pp. 156-158.
- Zollinger, D. G. and Barenberg, E. J. (1989), "Proposed Mechanistic Based Design Procedure for Jointed Concrete Pavements," *Illinois Cooperative Highway Research Program - 518*, University of Illinois, Urbana, Illinois.

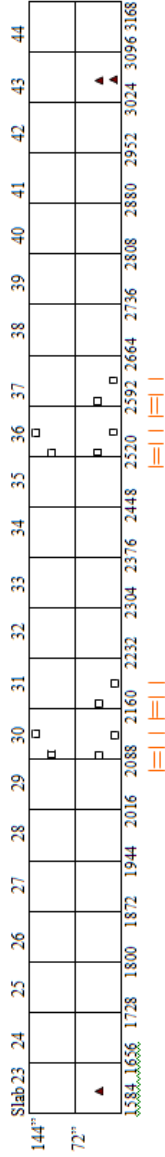
APPENDIX A

A.1 INSTRUMENTATION LAYOUT

This section is dedicated to showing the instrumentation layout for each of the sections. The triangle represents the location of where thermocouples were placed. The squares represent strain gauges and the lines are LVDTs. All of the units are in inches.



Section 2a and 2b



2a

Vertical LVDTs	Horizontal LVDTs
2087, 0	2088, 0, 3
2089, 0	2088, 0, 4, 5
2124, 0	2160, 0, 3
2159, 0	2160, 0, 4, 5
2161, 0	
2196, 0	

Thermocouples

Station 4 (1620, 36)

Dynamic Strain Gauges

Edge – Bottom 2124, 0
 Top 2089, 30
 Bottom 2196, 0
 Top 2161, 30
 Wheel-Bottom 2124, 144
 Bottom 2089, 124

2b

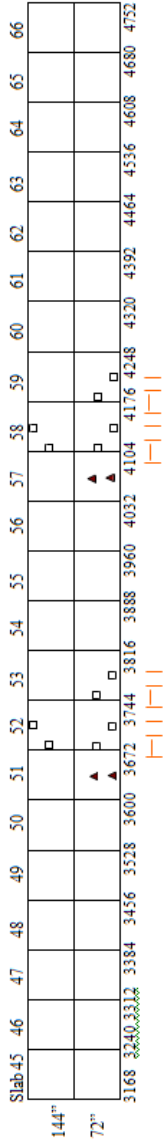
2519, 0	2520, 0, 3
2521, 0	2520, 0, 4, 5
2556, 0	2592, 0, 3
2591, 0	2592, 0, 4, 5
2593, 0	
2628, 0	

Station 5 (3060, 4)
 Station 6 (3060, 36)

Edge – Bottom 2556, 0
 Top 2521, 30
 Bottom 2628, 0
 Top 2593, 30
 Wheel-Bottom 2556, 144
 Bottom 2521, 124



Section 3a and 3b



3a

Vertical LVDTs

- 3671, 0
- 3673, 0
- 3708, 0
- 3743, 0
- 3745, 0
- 3780, 0

Horizontal LVDTs

- 3672, 0, 3
- 3672, 0, 4.5
- 3744, 0, 3
- 3744, 0, 4.5

Thermocouples

- Station 7 (3636, 4)
- Station 8 (3636, 36)

Dynamic Strain Gauges

- Edge – Bottom 3708, 0
- Top 3673, 30
- Bottom 3780, 0
- Top 3745, 30
- Wheel-Bottom 3708, 144
- Bottom 3673, 124

3b

- 4103, 0
- 4105, 0
- 4140, 0
- 4175, 0
- 4177, 0
- 4212, 0

- 4104, 0, 3
- 4104, 0, 4.5
- 4176, 0, 3
- 4176, 0, 4.5

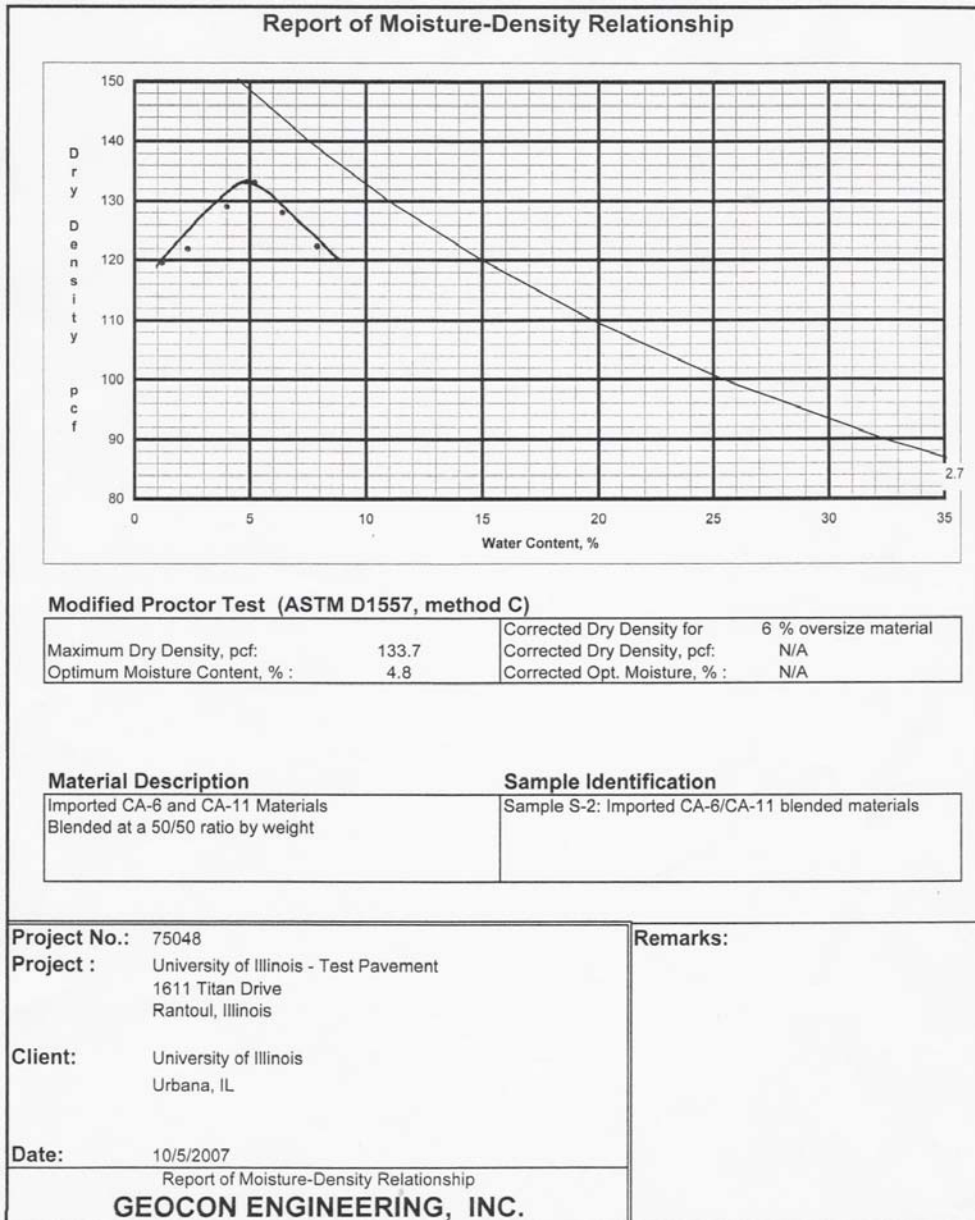
- Station 9 (4068, 4)
- Station 10 (4068, 36)

- Edge – Bottom 4140, 0
- Top 4105, 30
- Bottom 4212, 0
- Top 4177, 30
- Wheel-Bottom 4140, 144
- Bottom 4105, 124

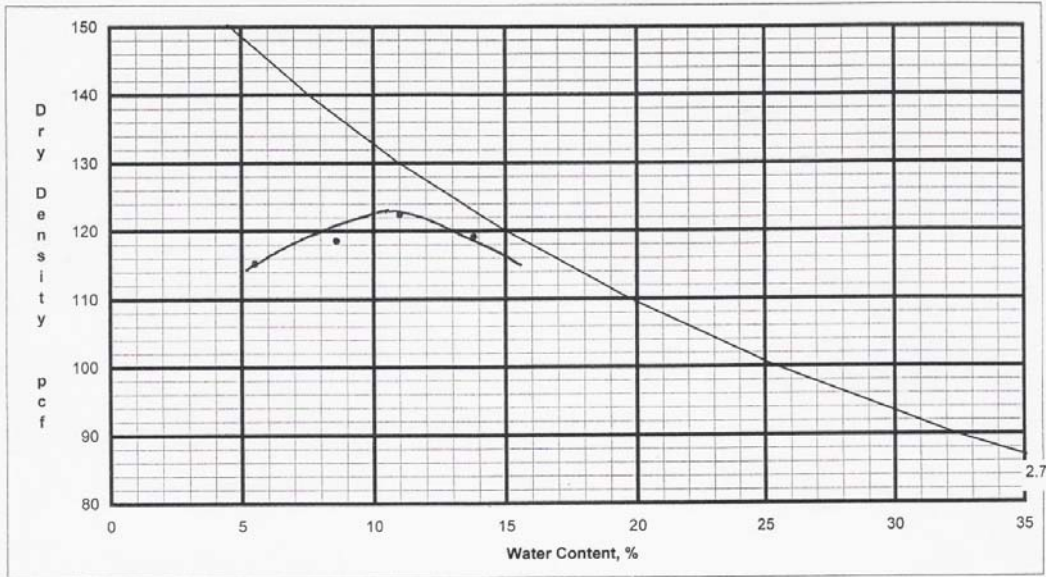


A.2 GEOTECHNICAL REPORT

The following two figures are the results of the modified proctor tests that were provided by Geocn Engineering, Inc.



Report of Moisture-Density Relationship



Modified Proctor Test (ASTM D1557, method A)

Maximum Dry Density, pcf:	122.6	Corrected Dry Density for 0 % oversize material	N/A
Optimum Moisture Content, % :	10.7	Corrected Dry Density, pcf:	N/A
		Corrected Opt. Moisture, % :	N/A

Material Description

Brown silty CLAY, trace sand

Sample Identification

Sample S-1: Imported brown silty clay fill materials

Project No.: 75048

Project : University of Illinois - Test Pavement
1611 Titan Drive
Rantoul, Illinois

Client: University of Illinois
Urbana, IL

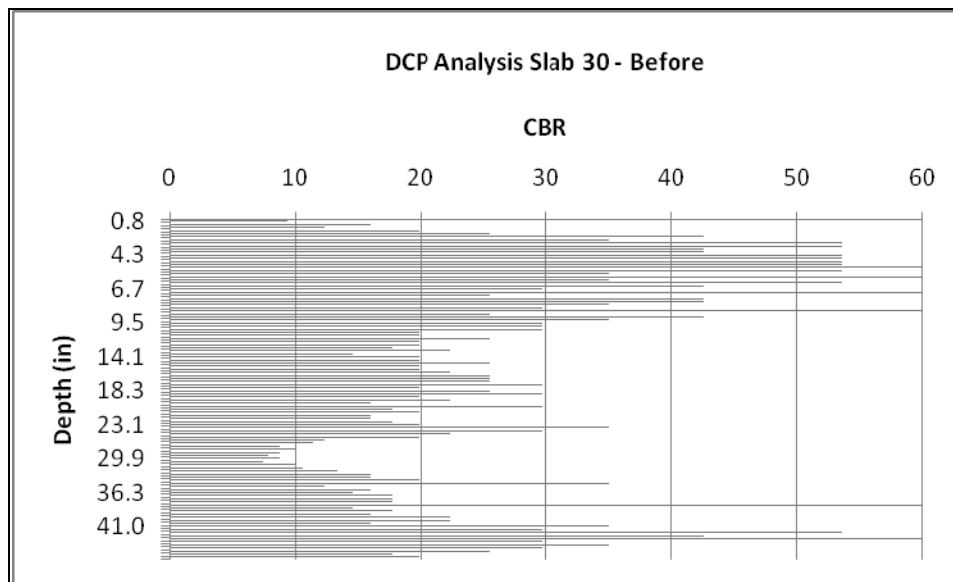
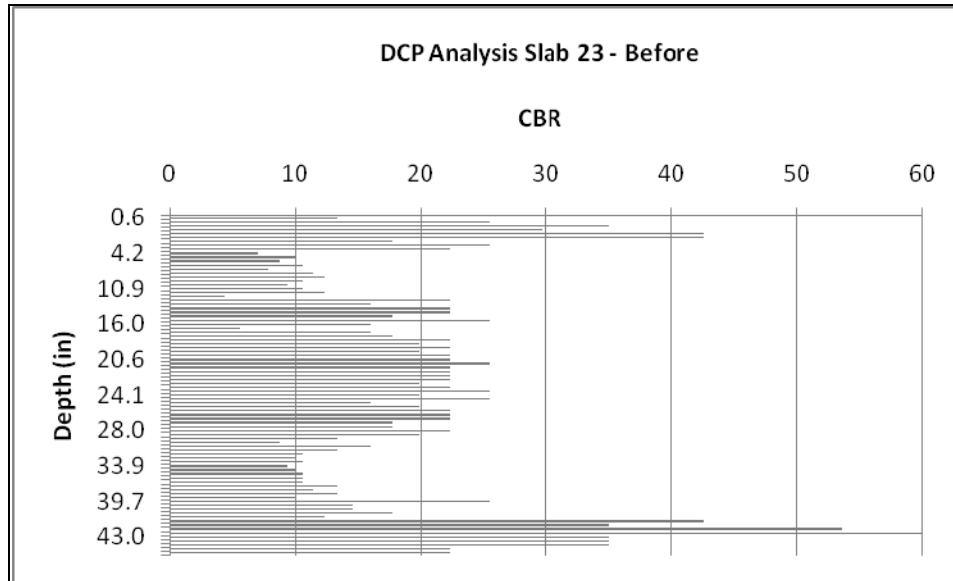
Date: 10/5/2007

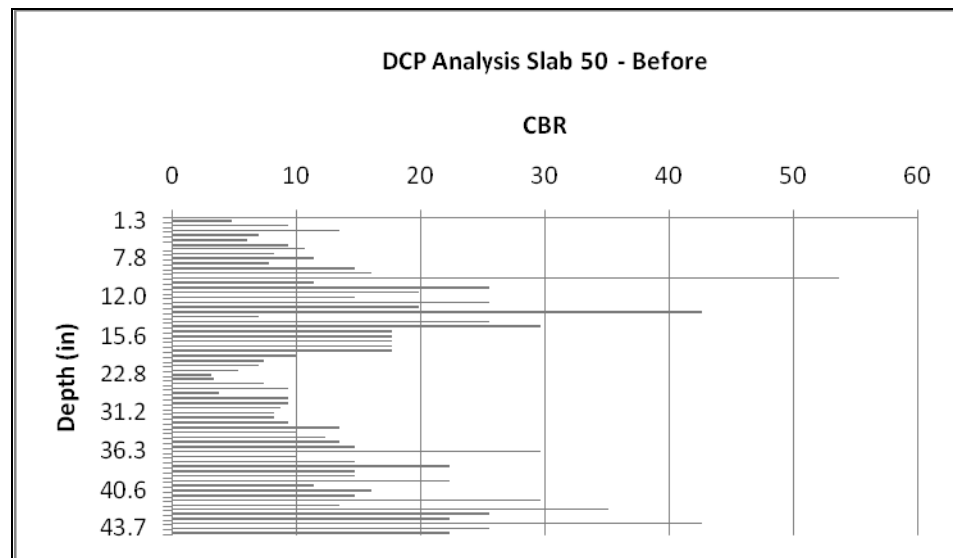
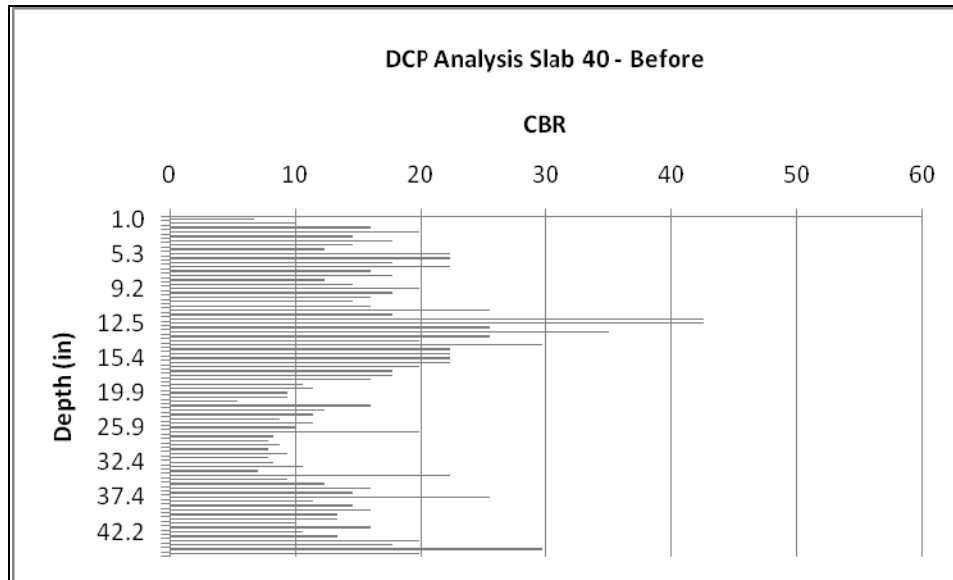
Report of Moisture-Density Relationship
GEOCON ENGINEERING, INC.

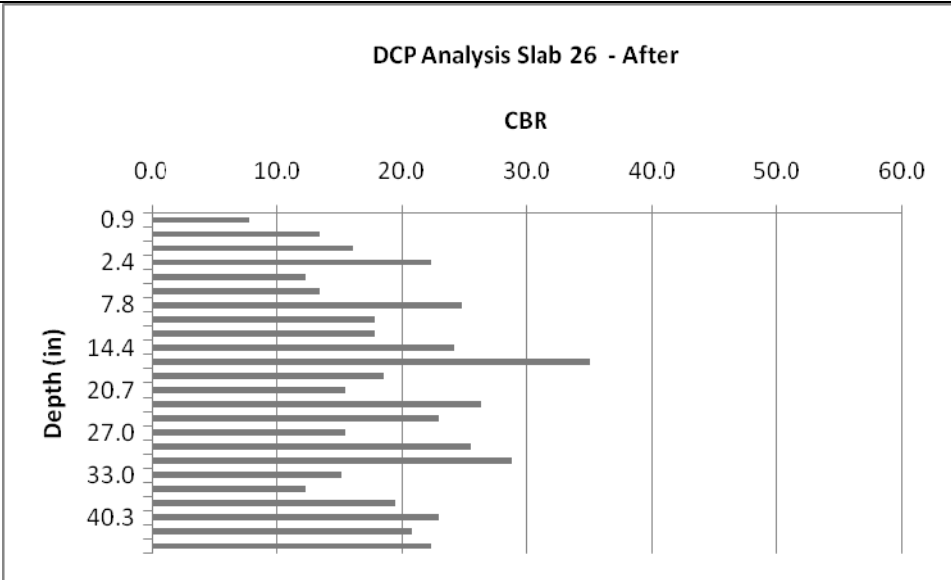
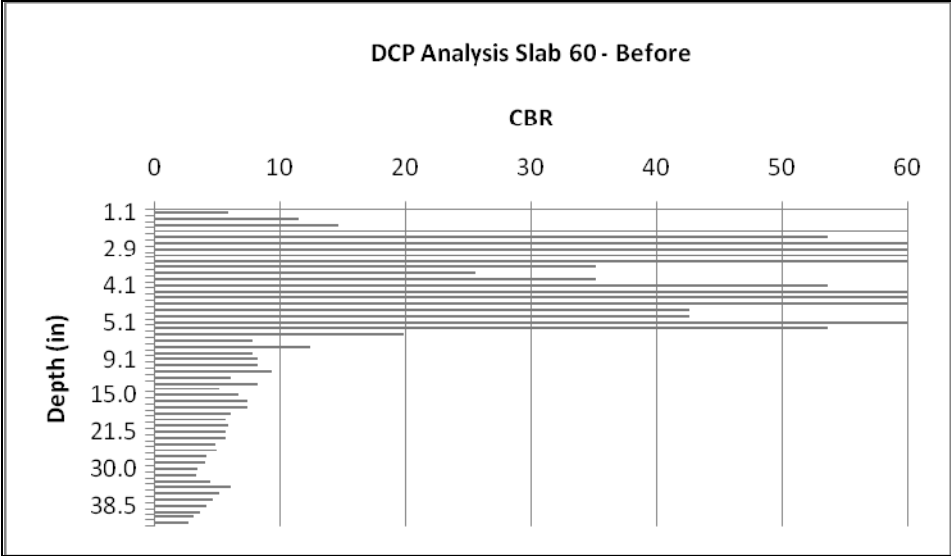
Remarks:

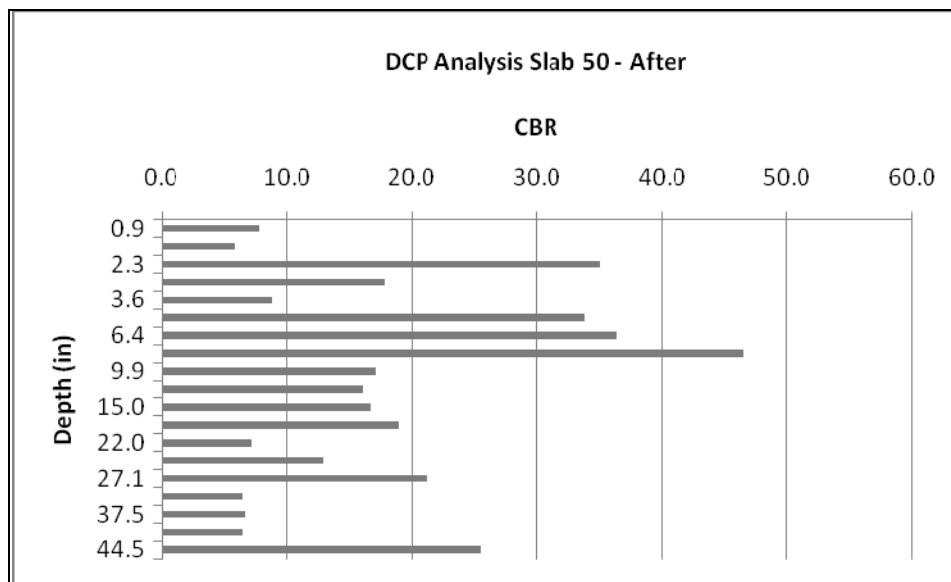
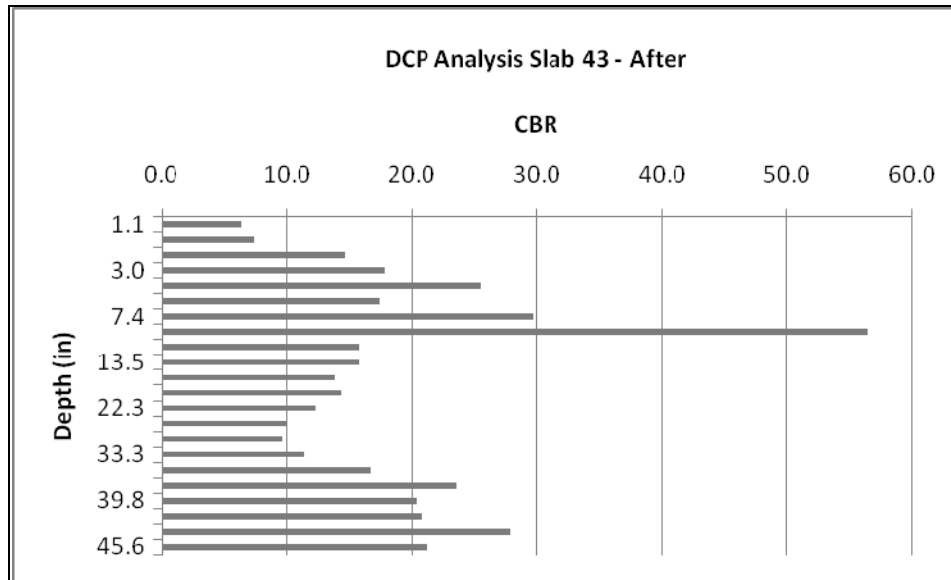
A.3 DCP ANALYSIS

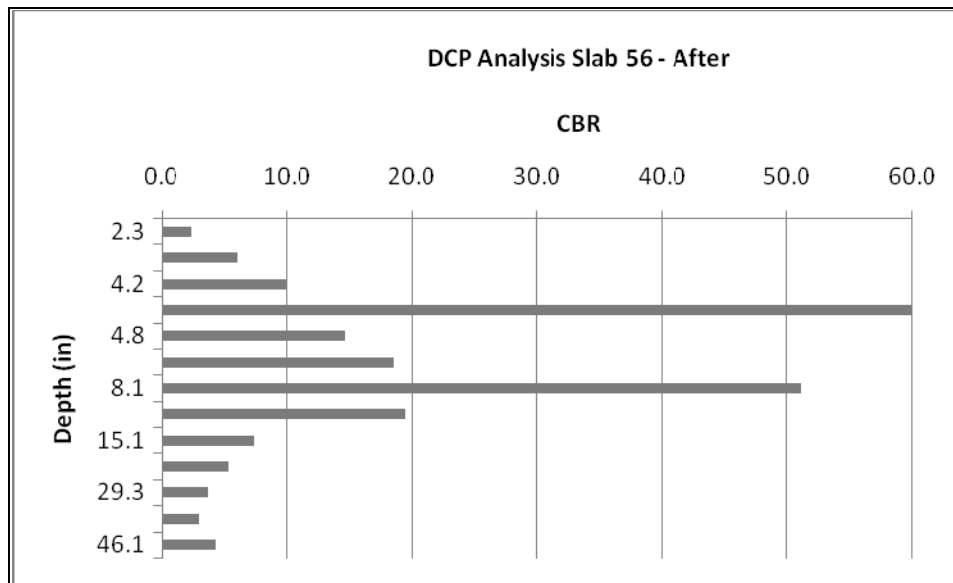
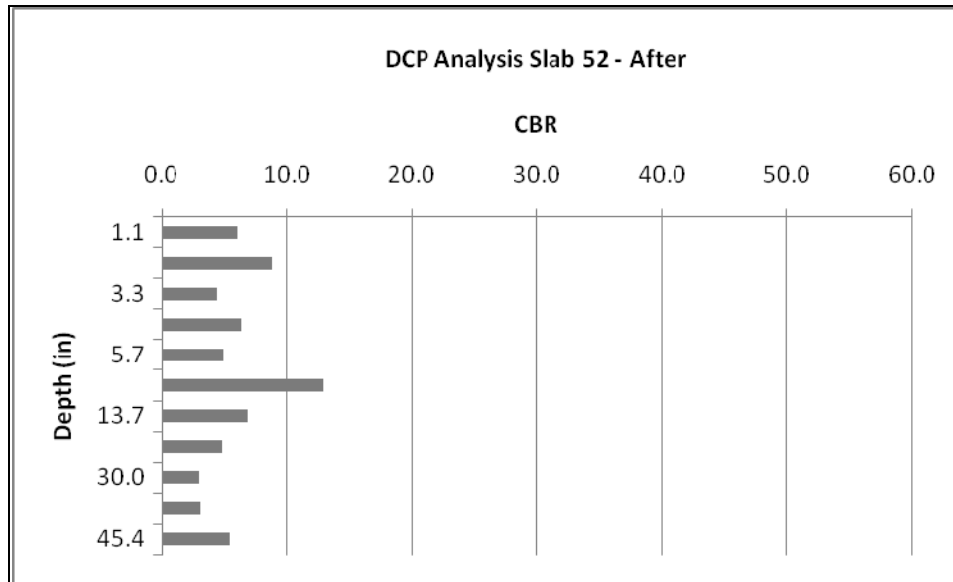
The title of each plot has the slab number which gives a reference of where the data was taken from. The annotation of before and after refers to when the test was taken. *Before* was prior to grading and placement of the granular subbase, which was when the subgrade was dry of optimum moisture. *After* refers to the DCP data being acquired after the addition of the granular subbase.

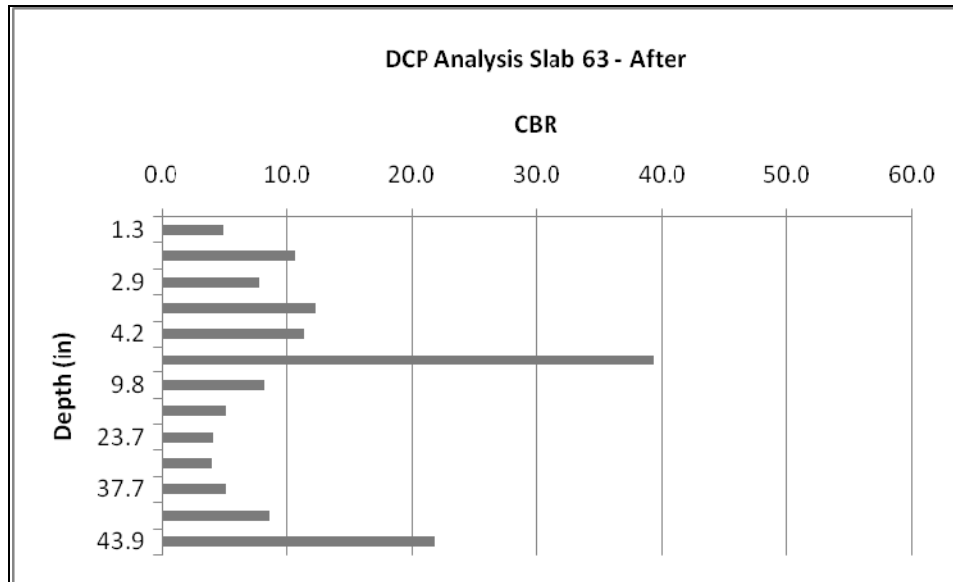












A.4 MAXIMUM THEORETICAL STRAINS

The following table is a summary of the ILLISLAB simulations that were conducted prior to construction to determine the location of the strain gauges. The table has been divided into different temperature gradients. The section refers to what pavement section is being analyzed. The highlighted areas represent the highest stress values. A temperature gradient of 20°F had the greatest influence on the bottom stresses. For the top stresses, a -20° F temperature gradient resulted in the highest stresses. It should be noted that the X is the transverse direction and Y is the longitudinal direction.

Section	Run	t/b	X					Y					
			Load X	Load Y	Critical X	Critical Y	Sig x	Load X	Load Y	Critical X	Critical Y	Sig y	
AT = 0	1a	HMA-6-15000-100	Top	144	78.1	117.8	72	-583	144	72	144	98.2	-484
	1B	HMA-4-15000-100	Top	144	78.1	114.5	72	-253	144	104.7	144	101.5	-172
	2A	AB-5000-100	Top	144	75.5	121.1	72	-161	144	72	144	101.5	-100
	2B	AB-5000-100	Top	144	75.5	117.8	72	-95	144	72	144	101.5	-55
	3A	AB-5000-100	Top	144	75.5	124.4	72	-442	144	72	144	94.9	-326
	1A	HMA-6-15000-100	Bot	132	78.1	124.4	72	-583	144	108	144	108	-484
	1B	HMA-6-15000-100	Bot	132	78.1	124.4	72	-461	144	108	144	108	-835
	2A	AB-5000-100	Bot	132	75.5	127.6	72	-253	144	108	144	108	-418
	2B	HMA-AB-15000-100	Bot	132	78.1	124.2	72	-311	144	108	144	108	-558
	3A	AB-5000-100	Bot	132	75.5	127.6	72	-726	144	108	144	108	-1139

Section	Run	t/b	X					Y					
			Load X	Load Y	Critical X	Critical Y	Sig x	Load X	Load Y	Critical X	Critical Y	Sig y	
AT = 10	1A	HMA-AB-15000-100	Top	144	78.1	111.3	72	-213	144	72	144	104.7	-180
	1B	HMA-AB-15000-100	Top	144	78.1	111.3	72	-124	144	72	144	104.7	-100
	2A	AB-5000-100	Top	144	75.5	121.1	72	-152	144	72	144	98.2	-90
	2B	HMA-AB-15000-100	Top	144	75.5	117.8	72	-209	144	72	144	101.5	-139
	3A	AB-5000-100	Top	144	75.5	127.6	72	-407	144	72	144	91.6	-289
	1A	-	-	-	-	-	-	-	-	-	-	-	
	1B	HMA-AB-15000-100	Bot	132	78.1	124.4	72	-3	144	108	144	108	-3
	2A	AB-5000-100	Bot	132	75.5	127.6	72	-259	144	108	144	108	-429
	2B	HMA-AB-15000-100	Bot	132	78.1	124.4	72	-314	144	108	144	108	-563
	3A	AB-5000-100	Bot	132	75.5	127.6	72	-754	144	108	144	108	-1189

Section	Run	t/b	X					Y					
			Load X	Load Y	Critical X	Critical Y	Sig x	Load X	Load Y	Critical X	Critical Y	Sig y	
AT = 20	1A	HMA-4-5000-100	Top	144	78.1	117.8	72	-585	144	72	144	101.5	-476
BOTTOM		HMA-4-5000-100	Top	144	78.1	114.5	72	-426	144	72	144	104.7	-347
	2A	AB-5000-100	Top	144.5	75.5	121.1	72	-144	144	72	144	98.2	-81
	2B	HMA-AB-15000-100	Top	144	78.1	114.5	72	-204	144	72	144	104.7	-133
	3A	AB-5000-100	Top	144	75.5	127.6	72	-380	144	72	144	91.6	-254
	1A	HMA-6-15000-100	Bot	132	78.1	124.4	72	-996	144	108	144	108	-1651
	1B	HMA-6-15000-100	Bot	132	78.1	124.4	72	-501	144	108	144	108	-881
	2A	AB-5000-100	Bot	132	75.5	127.6	72	-265	144	108	144	108	-440
	2B	HMA-AB-15000-100	Bot	132	78.1	124.4	72	-317	144	108	144	108	-568
	3A	AB-5000-100	Bot	132	75.5	127.6	72	-782	144	108	144	108	-1240

Section	Run	t/b	X					Y					
			Load X	Load Y	Critical X	Critical Y	Sig x	Load X	Load Y	Critical X	Critical Y	Sig y	
AT = -10	1A	-	-	-	-	-	-	-	-	-	-	-	
	1B	-	-	-	-	-	-	-	-	-	-	-	
	2A	AB-5000-100	Top	144	75.5	121.1	72	-169	144	72	144	101.5	-111
	2B	AB-5000-100	Top	144	75.5	117.8	72	-474	144	72	144	101.5	-60
	3A	AB-5000-100	Top	144	75.5	124.4	72	-474	144	72	144	94.6	-364
	1A	HMA-AB-15000-100	Bot	144	78.1	111.3	72	-167	144	72	144	104.5	-155
	1B	-	-	-	-	-	-	-	-	-	-	-	
	2A	AB-5000-100	Bot	132	75.5	127.6	72	-248	144	108	144	108	-407
	2B	HMA-AB-15000-100	Bot	132	78.1	124.4	72	-308	144	108	144	108	-553
	3A	AB-5000-100	Bot	132	75.5	127.6	72	-699	144	108	144	108	-1087

Section	Run	t/b	X					Y					
			Load X	Load Y	Critical X	Critical Y	Sig x	Load X	Load Y	Critical X	Critical Y	Sig y	
AT = -20	1A	HMA-4-5000-100	Top	144	78.1	117.8	72	-354	144	72	144	101.5	-251
	1B	HMA-4-5000-100	Top	144	78.1	114.5	72	-79	144	72	144	104.7	-3
	2A	AB-5000-100	Top	144	75.5	117.8	72	-177	144	72	144	101.5	-121
	2B	HMA-AB-15000-100	Top	144	78.1	114.5	72	-222	144	72	144	104.7	-154
	3A	AB-5000-100	Top	144	75.5	124.4	72	-503	144	72	144	98.2	-398
	1A	HMA-4-5000-100	Bot	144	78.1	124.4	72	-264	144	108	144	108	-501
	1B	HMA-4-5000-100	Bot	144	78.1	124.4	72	-189	144	108	144	108	-405
	2A	AB-5000-100	Bot	132	75.5	127.6	72	-242	144	108	144	108	-396
	2B	HMA-AB-15000-100	Bot	132	78.1	124.4	72	-305	144	108	144	108	-548
	3A	AB-5000-100	Bot	132	75.5	127.6	72	-674	144	108	144	108	-1039

The following table is a summary of the highlighted sections found in the previous table.

$\Delta T = 10$	Section	Run	t/b	Load X	Load Y	X			Y				
						Critical X	Critical Y	Sig x	Load X	Load Y	Critical X	Critical Y	Sig y
	1A	HMA-AB-15000-100	Top	144	78.1	111.3	72	-213	144	72	144	104.7	-180
$\Delta T = 20$	1B	HMA-4-5000-100	Top	144	78.1	114.5	72	-426	144	72	144	104.7	-347
$\Delta T = -20$	2A	AB-5000-100	Top	144	75.5	117.8	72	-177	144	72	144	101.5	-121
	2B	HMA-AB-15000-100	Top	144	78.1	114.5	72	-222	144	72	144	104.7	-154
	3A	AB-5000-100	Top	144	75.5	124.4	72	-503	144	72	144	98.2	-398
$\Delta T = 20$	1A	HMA-6-15000-100	Bot	132	78.1	124.4	72	-996	144	108	144	108	-1651
	1B	HMA-6-15000-100	Bot	132	78.1	124.4	72	-501	144	108	144	108	-881
	2A	AB-5000-100	Bot	132	75.5	127.6	72	-265	144	108	144	108	-440
	2B	HMA-AB-15000-100	Bot	132	78.1	124.4	72	-317	144	108	144	108	-568
	3A	AB-5000-100	Bot	132	75.5	127.6	72	-782	144	108	144	108	-1240

A.5 TABLES FOR MAGNIFICATION FACTORS

The next set of tables show the theoretical stress using Illislab at a given location along with the calculated allowable number of repetitions using the Vesic and Saxena (1969) fatigue algorithm and the magnification factor.

4 in / AC - North/South			
Distance from the edge (in)	Stress (psi)	N allow	Magnification
0	84	3.6E+09	99
1	77	5.1E+09	71
2	71	7.1E+09	51
3	66	9.7E+09	37
4	61	1.3E+10	28
5	57	1.8E+10	21
6	53	2.3E+10	16
7	50	3.0E+10	12
8	47	3.9E+10	9
9	44	5.0E+10	7
10	41	6.4E+10	6
11	39	8.1E+10	4
12	37	1.0E+11	4
13	35	1.3E+11	3
14	33	1.6E+11	2
15	31	2.0E+11	2
16	30	2.4E+11	2
17	28	3.0E+11	1
18	27	3.6E+11	1
19	25	4.4E+11	1
20	24	5.4E+11	1

6 in / AC - North/South			
Distance from the edge (in)	Stress (psi)	N allow	Magnification
0	343	1.3E+07	122
1	315	1.9E+07	86
2	289	2.6E+07	61
3	266	3.6E+07	44
4	246	5.0E+07	32
5	228	6.8E+07	24
6	212	9.0E+07	18
7	198	1.2E+08	13
8	185	1.6E+08	10
9	174	2.0E+08	8
10	163	2.6E+08	6
11	153	3.3E+08	5
12	144	4.2E+08	4
13	136	5.3E+08	3
14	129	6.7E+08	2
15	122	8.4E+08	2
16	115	1.0E+09	2
17	109	1.3E+09	1
18	103	1.6E+09	1
19	98	2.0E+09	1
20	93	2.4E+09	1

6 in. / Granular - South			
Distance from the edge (in)	Stress (psi)	N allow	Magnification
0	562	1.8E+06	69
1	526	2.4E+06	53
2	492	3.1E+06	41
3	461	4.0E+06	31
4	433	5.2E+06	24
5	406	6.7E+06	19
18	194	1.3E+08	1

6 in. / Granular - North			
Distance from the edge (in)	Stress (psi)	N allow	Magnification
0	763	5.4E+05	79
1	704	7.4E+05	57
2	651	1.0E+06	42
3	604	1.4E+06	31
4	562	1.8E+06	23
5	524	2.4E+06	18
6	491	3.2E+06	13
7	461	4.1E+06	10
8	433	5.2E+06	8
9	409	6.6E+06	6
10	386	8.3E+06	5
11	365	1.0E+07	4
12	346	1.3E+07	3
13	328	1.6E+07	3
14	312	1.9E+07	2
15	296	2.4E+07	2
16	282	2.9E+07	1
17	269	3.5E+07	1
18	256	4.3E+07	1
19	244	5.1E+07	0.8
20	233	6.2E+07	0.7

8 in /Granular South			
Distance from the edge (in)	Stress (psi)	N allow	Magnification
0	452	4.4E+06	71
1	418	6.0E+06	52
2	387	8.2E+06	38
3	359	1.1E+07	28
4	335	1.5E+07	21
5	313	1.9E+07	16
18	155	3.1E+08	1

8 in /Granular North			
Distance from the edge (in)	Stress (psi)	N allow	Magnification
0	446	4.6E+06	65
1	413	6.3E+06	48
2	383	8.5E+06	35
3	356	1.1E+07	27
4	332	1.5E+07	20
5	311	2.0E+07	15
6	292	2.5E+07	12
7	274	3.2E+07	9
8	259	4.1E+07	7
9	245	5.1E+07	6
10	232	6.4E+07	5
11	220	7.9E+07	4
12	209	9.7E+07	3
13	198	1.2E+08	3
14	189	1.4E+08	2
15	180	1.7E+08	2
16	172	2.1E+08	1
17	164	2.5E+08	1
18	157	3.0E+08	1
19	150	3.6E+08	0.8
20	144	4.3E+08	0.7

3.5 in / Granular - South			
Distance from the edge (in)	Stress (psi)	N allow	Magnification
0	1852	1.6E+04	234
1	1686	2.3E+04	161
2	1536	3.3E+04	111
3	1404	4.7E+04	77
4	1286	6.7E+04	54
5	1182	9.4E+04	39
18	474	3.6E+06	1

3.5 in / Granular - North			
Distance from the edge (in)	Stress (psi)	N allow	Magnification
0	2099	9.4E+03	111
1	1928	1.3E+04	79
2	1774	1.9E+04	57
3	1637	2.6E+04	41
4	1516	3.5E+04	30
5	1407	4.7E+04	22
6	1311	6.2E+04	17
7	1224	8.2E+04	13
8	1146	1.1E+05	10
9	1075	1.4E+05	8
10	1011	1.8E+05	6
11	952	2.2E+05	5
12	898	2.8E+05	4
13	848	3.6E+05	3
14	801	4.4E+05	2
15	758	5.5E+05	2
16	718	6.9E+05	2
17	681	8.5E+05	1
18	646	1.1E+06	1
19	614	1.3E+06	1
20	583	1.6E+06	1

